AD A 238 365

MASTER COPY KEEP THIS COPY FOR REPRODUCTION PURPOSES

REPORT DOCUMENTATION PAGE

Form Approved
OMB No 0704-0188

1. AGENCY USE ONLY (Leave blank)	2. REPORT DATE	3. REPORT TYPE AND DATES COVERED
	February 28, 1991	Final Technical Report, 1/1/88-12/31/90

4. TITLE AND SUBTITLE

Photodynamics and Physics Behind Tunable Solid-State Lasers.

5. FUNDING NUMBERS

6. AUTHOR(S)

R. R. Alfano, V. Petricevic, S. G. Demos

7. PERFORMING ORGANIZATION NAME(S) AND ADDRESS(ES)

Institute for Ultrafast Spectroscopy and Lasers
Departments of Physics and Electrical Enginnering
City College of New York
138th St. at Convent Avenue, New York, NY 10031

8. PERFORMING ORGANIZATION REPORT NUMBER

9. SPONSORING/MONITORING AGENCY NAME(S) AND ADDRESS(ES)

U. S. Army Research Office
P. O. Box 12211
Research Triangle Park, NC 27709-2211

10. SPONSORING/MONITORING AGENCY REPORT NUMBER

11. SUPPLEMENTARY NOTES

The view, opinions and/or findings contained in this report are those of the author(s) and should not be construed as an official Department of the Army position, policy, or decision, unless so designated by other documentation.

12a. DISTRIBUTION/AVAILABILITY STATEMENT

Approved for public release; distribution unlimited.

12b. DISTRIBUTION CODE

13. ABSTRACT *(Maximum 200 words)*

Research was focused in two areas:
1. Using excite-and-probe anti-Stokes Raman scattering apparatus, the nonequilibrium phonons which participate in the overall complex nonradiative decay in tunable solid-state laser crystals, were directly identified. Rise and decay behavior of different Raman-active phonon modes were measured.
2. A new laser ion, Cr^{4+} in chromium-doped forsterite was discovered, and its spectroscopic and laser characteristics were investigated.

Sixteenpapers, twelve abstracts and one patent were published during this grant.

14. SUBJECT TERMS

Nonradiative relaxation, Tunable Solid-State Lasers, Phonon Dynamics, Ultrafast Spectroscopy, Excite and Probe Raman Spectroscopy.

15. NUMBER OF PAGES

16. PRICE CODE

17. SECURITY CLASSIFICATION OF REPORT	18. SECURITY CLASSIFICATION OF THIS PAGE	19. SECURITY CLASSIFICATION OF ABSTRACT	20. LIMITATION OF ABSTRACT
UNCLASSIFIED	UNCLASSIFIED	UNCLASSIFIED	UL

PHOTODYNAMICS AND PHYSICS BEHIND TUNABLE SOLID-STATE LASERS

FINAL REPORT

AUTHORS

R. R. Alfano, V. Petricevic, S. G. Demos

DATE

February 28, 1991

U. S. ARMY RESEARCH OFFICE

CONTRACT/GRANT NUMBER

DAAL03-88-K-0014

INSTITUTION

Institute for Ultrafast Spectroscopy and Lasers
City College of The City University of New York

TABLE OF CONTENTS

1. Statement of the Problem Studied

Over the past decade, there has been a great deal of interest in tunable solid-state lasers. The extensive research focused on either finding new host materials for the trivalent chromium ion (Cr^{3+}), or finding new ions to be used in already known hosts. We have initiated a research project to investigate, using methods of conventional optical spectroscopy and picosecond time-resolved spectroscopy, new potential tunable solid-state laser materials. Very little information is available about the fundamental physical processes behind vibronic laser operation. With this in mind we have undertaken studies of the kinetics of population relaxation among the excited states of lasing ions, as well as investigations of the optical phonon dynamics using ultrafast pump-and-probe anti-Stokes Raman scattering. Most of the investigations were performed on chromium-doped forsterite, new and unique laser crystal discovered by us during the course of this research.

2. Summary of the Most Important Results

Major breakthroughs were achieved in two areas: (1) Time-resolved nonequilibrium phonon dynamics in tunable solid-state laser crystals, and (2) Discovery of a new lasing ion, tetravalent chromium (Cr^{4+}) in chromium-doped forsterite ($Cr:Mg_2SiO_4$) and studies of its spectroscopic and laser properties.

2.1 Nonequilibrium Phonon Dynamics in Tunable Solid-State Laser Crystals

Excite-and-probe anti-Stokes Raman scattering apparatus was developed to study phonon dynamics in the excited state in tunable solid-state laser materials.

Using this state-of-the-art experimental setup we have, for the first time, directly identified the nonequilibrium phonons which participate in the overall

complex nonradiative decay. By measuring the time dependence of the pump-probe Raman spectra in chromium-doped forsterite we have determined the rise and decay behavior of different Raman-active phonon modes involved in nonradiative decay.

The sample of Cr-doped forsterite was photoexcited above the Cr^{4+} lasing level by a train of 450-fs, 590-nm pump pulses and probed by a time-delayed, cross-polarized pulses of same pulse duration and wavelength. We have monitored the change in the relative intensity of anti-Stokes Raman lines due to scattering of both the pump and the probe pulses as a function of pump-probe delay. Raman spectra show that the rise and the decay dynamics are different for different phonon modes, which in turn contribute to the overall nonradiative relaxation of photoexcited ions in this crystal.

In the measured anti-Stokes Raman spectra, the 370 cm^{-1} Raman line is generated by the pump beam, while the 330 cm^{-1} and 225 cm^{-1} lines arise from Raman scattering of the probe beam. Different Raman spectra corresponding to the pump and to the probe beam are a consequence of different selection rules for the cross-polarized pump and probe beams. Measuring the ratio of the intensity of the anti-Stokes Raman lines corresponding to the probe beam and the intensity of the Raman line due to Raman scattering of the pump beam, for different pump-probe delays, a picture of the dynamics of the nonequilibrium phonons is developed. It was observed that the relative difference between the intensities of the pump and probe Raman lines in the anti-Stokes Raman spectrum changes considerably when the pump-probe delay time changes from 1 ps to 6 ps. There are differences in the rise and decay of these two modes which contribute differently to overall nonradiative decay. The two phonon modes "seen" by the probe beam exhibit an increase in the intensity ratio for the first 10 ps and a decay for the following 25 ps.

These results are an important contribution to the understanding of the underlying physics on which nonequilibrium phonons participate in the excited state nonradiative decay of photoexcited ions in crystals.

2.2 Spectroscopic and Laser Properties of chromium-doped forsterite

Measurements of the absorption, emission and excitation spectra, as well as the wavelength dependence of fluorescence lifetime provide convincing evidence that chromium ion may enter forsterite (Mg_2SiO_4) host in more than one valence states. Trivalent chromium (Cr^{3+}) enters substitutionally for divalent magnesium (Mg^{2+}) in two inequivalent octahedrally coordinated sites, while tetravalent chromium (Cr^{4+}) substitutes for Si^{4+} at tetrahedrally coordinated sites. Of the two Cr^{3+} centers, the one with mirror symmetry (C_s) is optically active due to lack of inversion symmetry and accounts for a number of features in the absorption and emission spectra. The center with inversion symmetry (C_i) is characterized with longer lifetimes that show strong temperature dependence. The absorption and emission due to transitions within the states of Cr^{4+} ion overlap with those within the states of Cr^{3+} ion. The absorption in the near infrared spectral region between 850 and 1150 nm is primarily due to transitions between the $^3A_2$ ground state and the first excited state $^3T_2$, of the Cr^{4+} ion. The four-level, vibronic mode of laser operation in Cr-doped forsterite feeds on $^3T_2 \rightarrow {}^3A_2$ transition.

Pulsed laser operation was obtained with samples rich in Cr^{4+} in a stable cavity. Pulsed laser action was observed for both the 1064-nm and 532-nm pumping. The spectra of the free-running laser radiation for both the 1064-nm and 532-nm pumping peaked at 1235 nm and had linewidth of 30 nm and 27 nm, respectively. Highest slope efficiency obtained to date is ~23% for 1064-nm pumping with an output mirror having 13% transmission at 1200 nm.

Continuous-wave laser operation was obtained using 1064-nm radiation from a cw Nd:YAG laser as a pumping source. The lasing threshold was 1.25 W of absorbed power. The measured slope efficiency was 6.8%. The spectrum of the free-running laser output peaks at 1244 nm and has a bandwidth of 12 nm.

Tunable operation of Cr:forsterite laser has been demonstrated over the 1167 - 1345 nm spectral range. A birefringent, single crystal quartz plate at Brewster's angle was used as the intracavity dispersive element. Three different output mirrors with transmission in adjacent wavelenth ranges were used to cover the range.

Maximum slope efficiency of 38 % was obtained for cw operation using 11 % transmission output mirror.

Limiting slope efficiency of the chromium-doped forsterite laser in the absence of passive losses was estimated to be >65 %.

Excited-state absorption is not a major loss mechanism in chromium-doped forsterite. The peak of the excited-state absorption is predicted at 1670 nm, far out of the tuning range.

3. List of All Publications

Articles

1. V. Petričević, S. K. Gayen, R. R. Alfano, K. Yamagishi, H. Anzai and Y. Yamaguchi, "Laser Action in Chromium-Doped Forsterite", Appl. Phys. Lett. **52**, 1040 (1988).

2. V. Petričević, S. K. Gayen and R. R. Alfano, "A New Tunable Solid-State Laser", Photonics Spectra **22** (3), 95 (1988).

3. V. Petričević, S. K. Gayen, R. R. Alfano, K. Yamagishi and K. Moriya, "Room-Temperature Vibronic Laser Action in Cr^{3+}:Mg_2SiO_4", in *Proceedings of the International Conference on Lasers '87*, 7-12 December, 1987, Lake Tahoe, Nevada , edited by F. J. Duarte , (STS Press, McLean, Virginia), pp. 423-25.

5. V. Petričević, S. K. Gayen, and R. R. Alfano, "Laser Action in Chromium-Activated Forsterite for Near-Infrared Excitation", Appl. Opt. **27**, 4162 (1988).

6. V. Petričević, S. K. Gayen, and R. R. Alfano, "Laser Action in Chromium-Activated Forsterite for Near-Infrared Excitation: Is Cr^{4+} the Lasing Ion?" Appl. Phys. Lett. **53**, 2590 (1988).

7. V. Petričević, S. K. Gayen, and R. R. Alfano, "Major Breakthrough in Tunable Solid-State Lasers", Opt. News **14** (12), 13 (1988).

8. V. Petričević, S. K. Gayen, and R. R. Alfano, "Continuous-Wave Laser Operation of Chromium-Doped Forsterite", Opt. Lett. **14**, 612, (1989).

9. V. Petričević, S. K. Gayen, and R. R. Alfano, "Near Infrared Tunable Operation of Chromium-Activated Forsterite Laser", Appl. Opt. **28**, 1609 (1989).

10. V. Petričević, S. K. Gayen, and R. R. Alfano, "Lasing and Spectroscopic Properties of Chromium-Activated Forsterite", *Advances in Laser Science-IV, Proceedings of the Fourth International Laser Science Conference* , Edited by J. L. Gole, D. F. Heller, M. Lapp, and W. C. Stwalley, 2-6 October, 1988, Atlanta, Georgia, (American Institute of Physics 1989), p. 33.

11. V. Petričević, S. K. Gayen, and R. R. Alfano, "Chromium-Activated Forsterite Laser", in *Tunable Solid-State Lasers*, Vol. 5 of the OSA Proceeding Series, M. L. Shand and H. P. Jenssen, eds. (Optical Society of America, Washington, D.C., 1989), pp. 77-84.

12. R. R. Alfano, V. Petričević, and A. Seas, "Chromium-Doped Forsterite Laser", in *Proceedings of the International Conference on Lasers '89,* December, 1989, New Orleans, Louisiana.

13. V. Petričević, A. Seas, and R. R. Alfano, "Forsterite Laser Tunes in Near-IR", Laser Focus World **26** (11),109 (1990).

14. S. K. Gayen, W. B. Wang, V. Petričević, S. G. Demos, and R. R. Alfano, "Picosecond Excite-and-probe Absorption Measurements of Nonradiative Transition Dynamics in Emerald", J. Lumin. **47**, 181 (1991).

15. V. Petričević, A. Seas, and R. R. Alfano, "Effective Gain Measurements in Chromium-Doped Forsterite", OSA Proceedings of the Advanced Solid-State Lasers Conference, March 5-7, 1990, Salt Lake City, Utah, to be published.

16. V. Petričević, A. Seas, and R. R. Alfano, "Slope Efficiency Measurements of Chromium-Doped Forsterite Laser", Opt. Lett., accepted for publication.

Abstracts & Presentations

1. S. K. Gayen, V. Petričević, R. R. Alfano, K. Yamagishi, and K. Moriya, "Spectroscopic Properties of Cr^{3+}:Mg_2SiO_4: A New Tunable Solid State Laser Crystal", Bull. Am. Phys. Soc. **33**, 810 (1988). Presented at the March Meeting of the American Physical Society, 21-25 March, 1988, New Orleans, Louisiana.

2. V. Petričević, S. K. Gayen, R. R. Alfano, K. Yamagishi, and K. Moriya, "Room-Temperature Pulsed Laser Action in Cr^{3+}:Mg_2SiO_4", Bull. Am. Phys. Soc. **33**, 811 (1988). Presented at the March Meeting of the American Physical Society, 21-25 March, 1988, New Orleans, Louisiana.

3. V. Petričević, S. K. Gayen, and R. R. Alfano, "Lasing and Spectroscopic properties of Chromium-Activated Forsterite", Bull. Am. Phys. Soc. **33**, 1626 (1988). **Invited** paper presented at the Fourth International Laser Science Conference (ILS-IV), October 2-6, 1988, Atlanta, Georgia.

4. V. Petričević, S. K. Gayen, and R. R. Alfano, "Continuous-Wave and Tunable Laser Operation of Chromium-Activated Forsterite Laser", Bull. Am. Phys. Soc. **34**, 965 (1989). Presented at the March Meeting of the American Physical Society, 20-24 March, 1989, St. Louis, Missouri.

5. S. K. Gayen, V. Petričević, and R. R. Alfano, "Spectroscopic and Quantum Electronic Properties of Chromium-Activated Forsterite", in *Quantum Electronics and Laser Science Conference, 1989 Technical Digest Series, Vol 12,* (Optical Society of America, Washington D.C. 1989) pp. 172-173, presented at the

Quantum Electronics and Laser Science (QELS) Conference, Baltimore, Maryland,April 24-28, 1989.

6. V. Petričević, S. K. Gayen, and R. R. Alfano, "A Broadly-Tunable Room-Temperature Chromium-Activated Forsterite Laser", in *Conference on Lasers and Electro-Optics, 1989 Technical Digest Series, Vol 11,* (Optical Society of America, Washington D.C. 1989) pp. 22-24, presented at the Conference on Lasers and Electro-Optics (CLEO), Baltimore, Maryland, April 24-28, 1989.

7. V. Petričević, S. K. Gayen, and R. R. Alfano, "Chromium-Activated Forsterite Laser", presented at the Topical Meeting on Tunable Solid-State Lasers, Cape Cod, May 1-3, 1989.

8. V. Petričević, S. K. Gayen, and R. R. Alfano, "Tetravalent Chromium-Doped Forsterite Laser", **Invited** paper presented at the V International Conference on Tunable Lasers, Irkutsk, USSR, 20-23 September, 1989.

9. R. R. Alfano, "A Chromium-Doped Forsterite Laser", **Plenary talk**, presented at the International Conference on Lasers '89, December 1989, New Orleans, Louisiana.

10. V. Petričević, A. Seas, S. K. Gayen, and R. R. Alfano, "Effective Gain Measurements in Chromium-Doped Forsterite", presented at the Topical Meeting on Advanced Solid-State Lasers, Salt Lake City, Utah, March 5-7, 1990.

11. A. Seas, V. Petričević, and R. R. Alfano, "Transient Gain Measurements of Nonradiative Dynamics in Chromium-Doped Forsterite (Cr^{4+}:Mg_2SiO_4)", presented at the Optical Society of America 1990 Annual Meeting, Boston, Massachusetts, November 4-9, 1990.

12. S. G. Demos, J. Buchert, and R. R. Alfano, "Nonequilibrium Phonon Dynamics in Forsterite", presented at the Optical Society of America 1990 Annual Meeting, Boston, Massachusetts, November 4-9, 1990.

4. List of All Participating Scientific Personnel

Scientific personnel involved in the research project were:

R. R. Alfano

J. Buchert

S. K. Gayen

V. Petricevic

S. G. Demos

W. B. Wang

A. Seas

Ph. D. degree awarded to V. Petricevic, Oct. 1, 1990.

5. Appendix

Reprints of all the papers already published, and preprints of papers submitted for publication are attached , and made an integral part of this report.

Articles

1. V. Petričević, S. K. Gayen, R. R. Alfano, K. Yamagishi, H. Anzai and Y. Yamaguchi, "Laser Action in Chromium-Doped Forsterite", Appl. Phys. Lett. 52, 1040 (1988).

Laser action in chromium-doped forsterite

V. Petričević, S. K. Gayen, and R. R. Alfano
Institute for Ultrafast Spectroscopy and Lasers, Photonics Application Laboratory, Departments of Physics and Electrical Engineering, The City College of New York, New York, New York 10031

Kiyoshi Yamagishi, H. Anzai, and Y. Yamaguchi
Electronic Materials Research Laboratory, Mitsui Mining and Smelting Co., Ltd., 1333-2 Haraichi, Ageo-Shi, Saitama 362, Japan

(Received 7 December 1987; accepted for publication 1 February 1988)

Room-temperature vibronic pulsed laser action in trivalent chromium-activated forsterite (Cr^{3+}:Mg_2SiO_4) is reported for the first time. The free-running laser emission is centered at 1235 nm of the broad ${}^4T_2 \rightarrow {}^4A_2$ fluorescence band, and has a bandwidth of ~22 nm.

Prompted by the successful broadly wavelength-tunable, room-temperature operation of alexandrite[1] and emerald[2,3] lasers, the surge in research activities on tunable solid-state lasers has been extensive in the 1980s.[4–17] The thrust of these research endeavors has been twofold: first to look for new host materials for the trivalent chromium ion,[7–11] and second, to search for new ions that will lase in commonly used host crystals.[4–6,12–17] These efforts have been rewarded by the successful wavelength-tunable laser operation of Cr^{3+} in a number of hosts,[7–11] by the discovery of new lasing ions trivalent titanium (Ti^{3+})[6,12,13] and divalent rhodium[16] (Rh^{2+}), as well as by the "rediscovery"[4,5,14,15,17] of tunable phonon-terminated lasers based on divalent transition metal ions Ni^{2+}, Co^{2+}, and V^{2+}. In this letter, we present the first room-temperature vibronic pulsed laser operation of Cr^{3+} in forsterite (Mg_2SiO_4).

Forsterite, like alexandrite, is a member of the olivine family of crystals. It is a naturally occurring gem. Single crystals of forsterite may be grown by the Czochralski method. A unit cell of forsterite has four formula units in an orthorhombic structure of the space group *Pbnm*.[18] The unit cell dimensions are: $a = 4.76$ Å, $b = 10.22$ Å, and $c = 5.99$ Å. The Cr^{3+} ion substitutes for the Mg^{2+} ion in two distinct octahedrally coordinated sites: one (M1) with inversion symmetry (C_i), and the other (M2) with mirror symmetry (C_s). The occupation ratio of the two sites[19] by the Cr^{3+} ion is M1:M2 = 3:2.

The single crystal of Cr^{3+}:Mg_2SiO_4 used for spectroscopic and laser action measurements was grown by the Czochralski method at the Electronic Materials Research Laboratory of the Mitsui Mining and Smelting Co., Ltd., Japan. The crystal is a 9 mm×9 mm×4.5 mm rectangular parallelepiped with the three mutually orthogonal axes oriented along the *b*, *c*, and *a* crystallographic axes of the crystal. The crystal contains 0.04 at. % of Cr^{3+} ions, which is equivalent to a chromium ion concentration of 6.9×10^{18} ions/cm^3.

The room-temperature fluorescence and absorption spectra of Cr^{3+}:Mg_2SiO_4 for E||*b* crystallographic axis are shown in Fig. 1. The fluorescence spectrum of Cr^{3+}:Mg_2SiO_4 was excited by the 488-nm radiation from an argon-ion laser and recorded by a germanium photodiode detector lock-in amplifier combination at the end of a 0.25-m monochromator equipped with a 1000-nm blazed grating. The room-temperature spectrum is a broad band covering the wavelength range 700–1400 nm. The room-temperature fluorescence lifetime is 15 μs.

The absorption spectrum was taken with a Perkin–Elmer Lambda-9 spectrophotometer along the 4.5-mm path length of the sample. It is characterized by two broad bands centered at 740 and 460 nm attributed to the ${}^4A_2 \rightarrow {}^4T_2$ and ${}^4A_2 \rightarrow {}^4T_1$ absorptive transitions, respectively, of the Cr^{3+} ion. The broad, weak absorption band between 850 and 1150 nm is not observed in the excitation spectrum.[20] This indicates that the origin of this absorption is not transitions in Cr^{3+} ion, but in some other impurity ions, e.g., Fe^{3+} in the host crystal.[21] It is evident from Fig. 1 that this background absorption overlaps a significant spectral region of Cr^{3+}:Mg_2SiO_4 emission, and inhibits laser action in that region.

The experimental arrangement for investigating the laser action[22] in Cr^{3+}:Mg_2SiO_4 is shown schematically in Fig. 2. The sample is placed at the center of a stable resonator formed by two 30-cm-rad mirrors placed 20 cm apart. The mirrors were dielectric coated to transmit the 532-nm pump beam, and to have high reflectivity in the 1150–1250 nm spectral range. The reflectivity of the back mirror M_1 is 99.9%, while that of the output mirror M_2 is ~98% for normal incidence over the specified wavelength range. It is

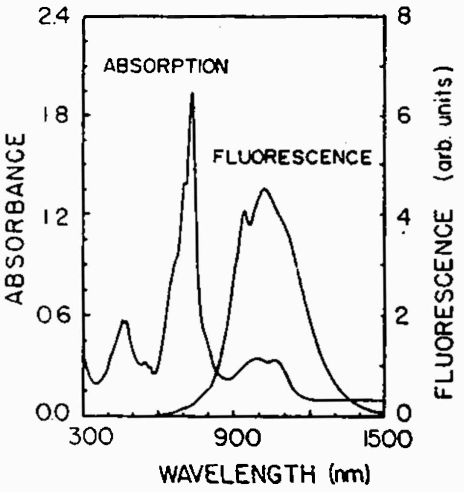

FIG. 1. Absorption and fluorescence spectra of Cr^{3+}:Mg_2SiO_4 at room temperature. Both the spectra were taken for E||*b* axis and excitation along *a* axis. The thickness of the sample along *a* axis is 4.5 mm.

 0003-6951/88/131040-03$01.00

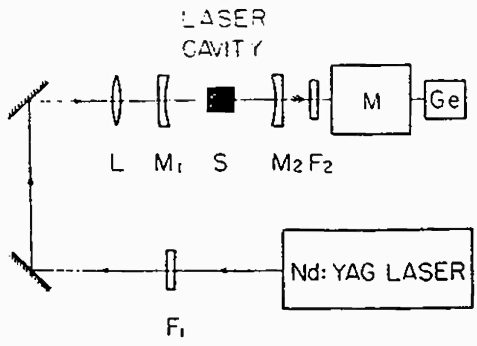

FIG. 2. Schematic diagram of the experimental arrangement for investigating laser action in $Cr^{3+}:Mg_2SiO_4$. (Key: F_1 = 1060-nm blocking filter, F_2 = 532-nm blocking infrared transmitting filter, M_1 = back mirror, M_2 = output mirror, L = lens, S = sample, Ge = germanium photodiode detector, M = monochromator.)

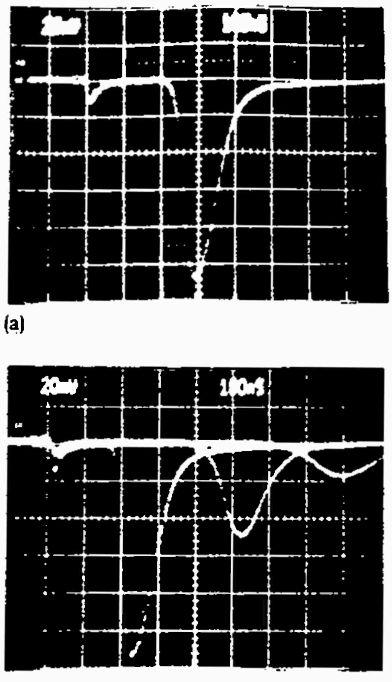

FIG. 3. Temporal profile and delay with respect to the pump pulse of the $Cr^{3+}:Mg_2SiO_4$ laser pulse: (a) a single pulse for pump energy 1.7 times the threshold energy; and (b) three pulses for pump energies near (right), twice (middle), and 2.4 times (left) the threshold energy. The narrow pulse at the extreme left of both the oscilloscope traces is the leakage of the pump pulse. For this measurement the monochromator was removed and filters were adjusted to allow a small leakage of pump pulse. The time and voltage scales are 100 ns/div and 20 mV/div, respectively.

to be noted that this spectral region does not correspond to the peak of the fluorescence spectrum, but was chosen so that the background absorption is minimal. The sample was longitudinally pumped by frequency-doubled 532-nm, 10-ns full width at half maximum (FWHM) pulses from a Q-switched Nd:YAG laser (Quanta Ray DCR-1) operating at a 10-Hz repetition rate. The spatial profile of the pump pulse was a doughnut, characteristic of an unstable cavity. The pump beam was linearly polarized along the b axis and propagated along the a axis of the sample. It was focused 3 cm before the sample by a 25-cm focal length lens. The radius of the pump beam at the center of the sample is $\sim 600\,\mu$m. The output from the laser cavity was analyzed by a 0.25-m monochromator and monitored by a germanium photodiode detector. The output of the detector was displayed on a fast oscilloscope. No dispersive element was placed in the cavity and the laser operated in a free-running pulsed mode.

Pulsed laser operation was readily obtained for pumping at or above the lasing threshold of 2.2 mJ. A single output laser pulse was obtained, implying a gain-switched operation which is a consequence of pump-pulse duration being shorter than the lasing-level lifetime. The amplitude and duration of the laser pulse varied, as expected, with the pulse-to-pulse energy fluctuation of the pump laser. The output was extremely sensitive even to a small misalignment of the cavity, or insertion of a glass plate (8% loss) in the cavity.

The temporal profile of the $Cr^{3+}:Mg_2SiO_4$ laser pulse is shown in Fig. 3(a), and fluctuations in its amplitude, duration, and delay with respect to the pump pulse are displayed in Fig. 3(b). The temporal duration (FWHM) of the output laser pulse varied from 200 ns at the threshold to 100 ns at 2.4 times the threshold energy. The delay between the peak of the pump pulse and the peak of the $Cr^{3+}:Mg_2SiO_4$ laser pulse also varied, as expected, with pump-pulse energy, from 700 ns at the threshold to 200 ns at 2.4 times the threshold energy. This indicates that the laser cavity is highly lossy, and several hundred round trips are required to build up the laser oscillation in the cavity.

The laser threshold and slope efficiency were measured for the cavity used in this experiment and the data are displayed in Fig. 4. The laser oscillation starts to build up at an absorbed input energy of 2.2 mJ. The measured slope efficiency of 1.4% is rather low, and indicates large losses in the cavity. These losses include $\sim 13\%$ reflection loss from the uncoated sample surfaces, scattering from inhomogeneities in the crystal, and a large mismatch between the size of the pump beam and the $Cr^{3+}:Mg_2SiO_4$ cavity modes in the sample.

The spectrum of $Cr^{3+}:Mg_2SiO_4$ laser is shown in Fig. 5, for an absorbed pump energy of 3.4 mJ. The spectrum peaks at 1235 nm and has a bandwidth (FWHM) of 22 nm. The wide spectrum of the laser output can be used to pro-

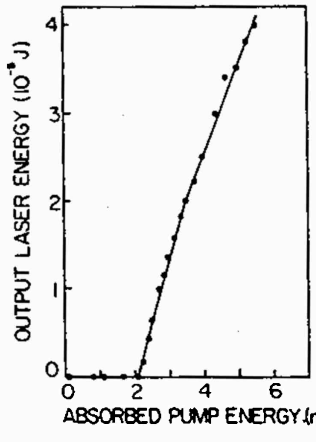

FIG. 4. Output energy of $Cr^{3+}:Mg_2SiO_4$ laser as a function of input energy.

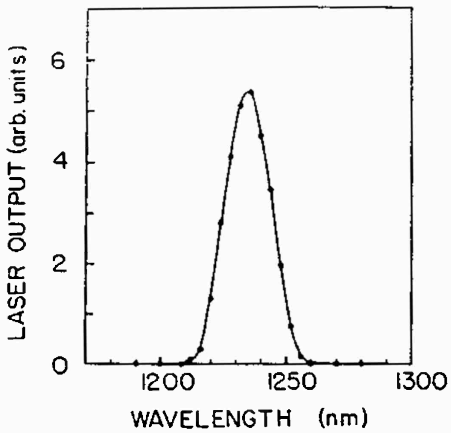

FIG. 5. Spectrum of free-running $Cr^{3+}:Mg_2SiO_4$ laser.

duce femtosecond pulses. The spectral range is limited at the high-energy end by the mirror transmission and the impurity absorption, while at the low-energy end by the mirror transmission as well as by the decrease in fluorescence intensity. Using different sets of mirrors, laser action in the 1.1–1.3 μm spectral range can be obtained.

In summary, pulsed laser operation has been obtained in $Cr^{3+}:Mg_2SiO_4$ at room temperature. The laser emission is centered at 1235 nm and has a bandwidth of $\sim$22 nm. The spectral range for laser emission is expected to extend from 850 to 1300 nm if the parasitic impurity absorption may be minimized by improved crystal growth technique, making it one of the most widely tunable solid-state lasers in this spectral region. The large fluorescence bandwidth of the crystal promises ultrashort pulse generation through mode-locked operation. The fluorescence lifetime of 15 μs is suitable for effective energy storage and high-power Q-switched operation.

We would like to acknowledge Professor Roger Dorsinville for helpful discussions and Teruo Hiruma for help and support. The research is supported by National Aeronautics and Space Administration, Army Research Office, Hamamatsu Photonics, and City College of New York Organized Research.

[1]J. C. Walling, O. G. Peterson, H. P. Jenssen, R. C. Morris, and E. Wayne O'Dell, IEEE J. Quantum Electron. **QE-16**, 1302 (1980) and references therein.
[2]M. L. Shand and J. C. Walling, IEEE J. Quantum Electron. **QE-18**, 1829 (1982).
[3]J. Buchert, A. Katz, and R. R. Alfano, IEEE J. Quantum Electron. **QE-19**, 1477 (1983).
[4]P. F. Moulton, IEEE J. Quantum Electron. **QE-21**, 1582 (1985).
[5]P. F. Moulton, IEEE J. Quantum Electron. **QE-18**, 1185 (1982).
[6]P. F. Moulton, J. Opt. Soc. Am. B **3**, 125 (1986) and references therein.
[7]B. Struve, G. Huber, V. V. Laptev, J. A. Scherbakov, and Y. V. Zharikov, Appl. Phys. B **28**, 235 (1982).
[8]U. Brauch and U. Dürr, Opt. Commun. **49**, 61 (1984).
[9]H. P. Jenssen and S. T. Lai, J. Opt. Soc. Am. **3**, 115 (1986).
[10]W. Kolbe, K. Petermann, and G. Huber, IEEE J. Quantum Electron. **QE-21**, 1596 (1985).
[11]S. T. Lai, B. H. T. Chai, M. Long, and R. C. Morris, IEEE J. Quantum Electron. **QE-22**, 1931 (1986).
[12]G. M. Loiacono, M. F. Shone, G. Mizell, R. C. Powell, G. J. Quarles, and B. Elouadi, Appl. Phys. Lett. **48**, 622 (1986).
[13]A. I. Alimpiev, G. V. Bukin, V. N. Matrosov, E. V. Pestryakov, V. P. Solntsev, V. I. Trunov, E. G. Tsvetkov, and V. P. Chebotaev, Sov. J. Quantum Electron. **16**, 579 (1986).
[14]U. Brauch and U. Dürr, Opt. Commun. **55**, 35 (1985).
[15]W. Knierim, A. Honold, U. Brauch, and U. Dürr, J. Opt. Soc. Am. B **3**, 119 (1986) and references therein.
[16]R. C. Powell, G. J. Quarles, J. J. Martin, C. A. Hunt, and W. A. Sibley, Opt. Lett. **10**, 212 (1985).
[17]P. F. Moulton and A. Mooradian, Appl. Phys. Lett. **35**, 838 (1979).
[18]J. R. Smyth and R. M. Hazen, Am. Mineral. **58**, 588 (1973).
[19]L. V. Bershov, J. M. Gaite, S. S. Hafner, and H. Rager, Phys. Chem. Minerals **9**, 95 (1983).
[20]K. Yamagishi (unpublished).
[21]W. A. Runciman, D. Sengupta, and J. T. Gourley, Am. Mineral. **58**, 451 (1973).
[22]R. R. Alfano, V. Petričević, and S. K. Gayen, U.S. Patent pending.

2. V. Petričević, S. K. Gayen and R. R. Alfano, "A New Tunable Solid-State Laser", Photonics Spectra **22** (3), 95 (1988).

TECHNOLOGY Trends

A New Tunable Solid-State Laser

BY V. PETRICEVIC, S. K. GAYEN AND R. R. ALFANO

The eighties have been a decade of rapid development for tunable solid-state lasers[1] with progress reaching the point where tunable solid-state lasers are making headway in the marketplace and attracting the financial community's interest. In the area of laser applications, interest in tunable solid-state lasers stems from their many advantages over dye lasers. These include wide wavelength tunability,

A new tunable solid-state laser of chromium-activated forsterite offers wide tunability and a variety of applications.

compactness, long operational lifetime, rigidity and ease of handling — all of which make them highly reliable and extremely suitable for spaceborne remote sensing, ranging, lidar and optical communication applications.

Tunable solid-state lasers also have a high potential for medical applications in eye surgery, cutting tissues, treating birthmarks and removing kidney stones. Industrial applications include on-line pollutant-emission monitoring and fiber optic communications along with basic scientific research.

In this article, we will introduce a new tunable solid-state laser system: Chromium-activated forsterite (Cr^{3+}:Mg_2SiO_4), which has the potential for tunability from 850-1400nm — one of the most widely tunable laser systems in this spectral region. Chromium-based crystals that are known to lase, cover a spectral range of 700-1100nm. The first laser, ruby, operates only at a well defined wavelength of 694.3nm. Four different hosts are necessary to cover the 700-1100nm range. The Cr^{3+}:Mg_2SiO_4 system extends the range further into the infrared and shows promise of covering most of the range and beyond.

We have observed pulsed laser action in Cr^{3+} at room temperature.[2] The emission is centered at 1235nm, and has a bandwidth (FWHM) of 22nm. In the following sections, we will introduce the characteristics of the host crystal, present the basic spectroscopic properties of the system, describe the laser experiments and measurements, and point out the possibilities of the system.

Forsterite, like alexandrite, is a member of the olivine family of crystals and is a naturally occurring gem. The crystal appears different when looked at from different directions. Along the [100] axis it appears to have a bluish hue, along [010] it appears violet, while along the [001] axis it looks greenish.

Single crystals of Cr^{3+}:Mg_2SiO_4 may be grown by the Czochralski method. The crystal is easy to grow, and large crystals (several centimeters long and about a centimeter in diameter) are readily grown. The single crystal of Cr^{3+}:Mg_2SiO_4 used for spectroscopic and laser action measurements presented in this article was grown by the Czochralski method at the Electronic Materials Research Laboratory of the Mitsui Mining and Smelting Co. Ltd., in Japan. The crystal is a 9mm × 9mm × 4.5mm rectangular parallelepiped with the three mutually orthogonal axes oriented along the b, c and a crystallographic axes of the crystal. The crystal contains 0.04 atomic percentage of Cr^{3+} ions, which is equivalent to a chromium-ion concentration of 6.9×10^{19} ions/cm^3.

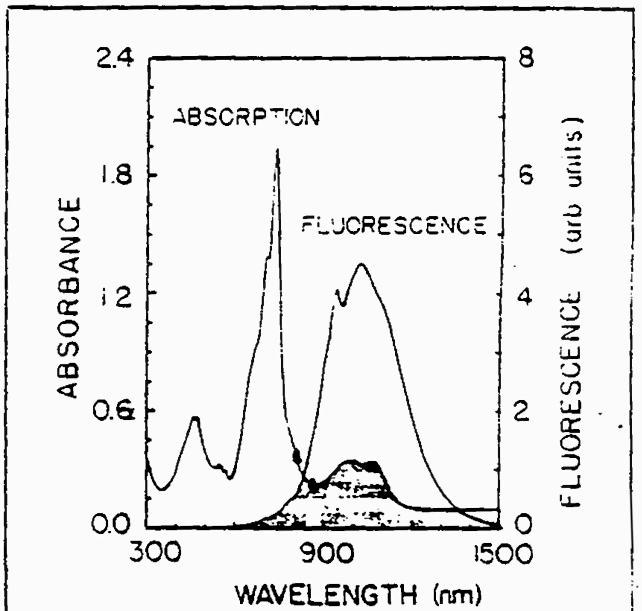

Figure 1.
Absorption and fluorescence spectra of Cr^{3+}:Mg_2SiO_4 at room temperature.

The room-temperature fluorescence and absorption spectra of Cr^{3+}:Mg_2SiO_4 for E ∥ b crystallographic axis are shown in Figure 1. The fluorescence spectrum was excited by the 488nm radiation from an argon-ion laser and recorded by a germanium photodiode detector-lock-in-amplifier combination at the end of a 0.25m monochromator equipped with a 1000nm blazed grating. The room-temperature spectrum is a broad band covering 700-1400nm. The room-temperature fluorescence lifetime is 15μsec. The absorption spectrum is characterized by two broad bands centered at 740nm and 460nm attributed at the $^4A_2 \rightarrow {}^4T_2$ and $^4A_2 \rightarrow {}^4T_1$ absorption transitions, respectively, of the Cr^{3+} ion. The broad weak absorption band between 850-1150nm is not observed in the excitation spectrum. This indicates that the origin of this absorption is not transitions in the Cr^{3+} ion, but in some other impurity ions, e.g., Fe^{3+} in the host crystal.[3] It is evident from Figure 1 that this background absorption overlaps a significant spectral region of Cr^{3+}:Mg_2SiO_4 emissions and inhibits laser action in that region. Both the emission and absorption spectra of such systems depend strongly on the polarization of the incident light

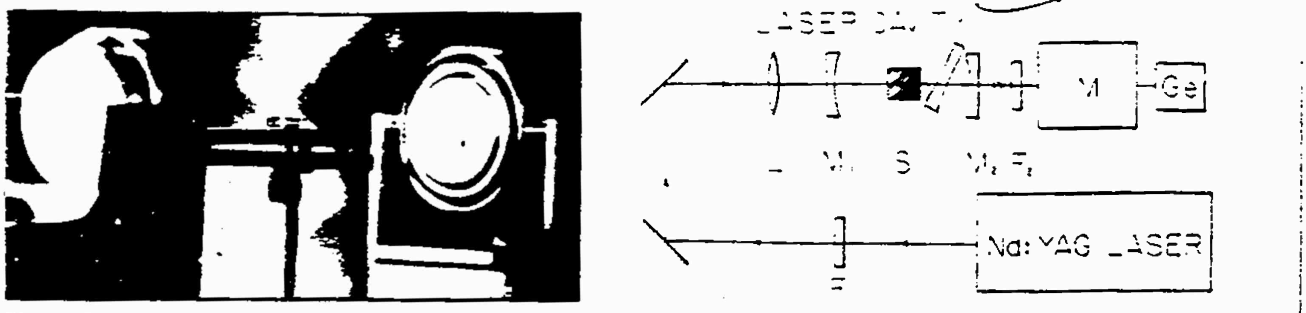

Figure 2.
A photograph of the laser cavity (left), and a schematic of the experimental arrangement for investigating laser action in Cr Mg$_2$SiO$_4$. Key: F_1 = 1060nm blocking filter. F_2 = 532nm blocking infrared transmitting filter. M_1 = back mirror. M_2 = output mirror. L = lens. S = sample. Ge = germanium photodiode detector. M = monochromator

and the orientation of the crystallographic axes in the sample.

Laser action

The experimental arrangement for investigating the laser action in Cr^{4+}:Mg$_2$SiO$_4$ is shown in Figure 2(a), and drawn schematically in Figure 2(b). The sample is placed at the center of a stable resonator formed by two 30cm-radius mirrors placed 20cm apart. The mirrors were dielectric coated to transmit the 532nm pump beam, and to have high reflectivity in the 1150-1250nm spectral range. It should be noted that this spectral region does not correspond to the peak of fluorescence spectrum, but was chosen to minimize background absorption.

The sample was longitudinally pumped by frequency-doubled 532nm, 10ns (FWHM) pulses from a Q-switched Nd:YAG laser (Quanta Ray DCR-1) operating at a 1 repetition rate. The pump beam was linearly polarized along the b axis and propagated along the a axis of the sample. It was focused 3cm before the sample by a 25cm-focal-length lens. The radius of the pump beam at the center of the sample is ~600μm. The output from the laser cavity was analyzed by a 0.25m monochromator, monitored by a germanium photodiode detector and dis-

ADVERTISEMENT

MORE NEW PRODUCTS FROM PULNIX

ASYNCHRONOUS RESET, VARIABLE SHUTTER AND INTEGRADABLE CCD

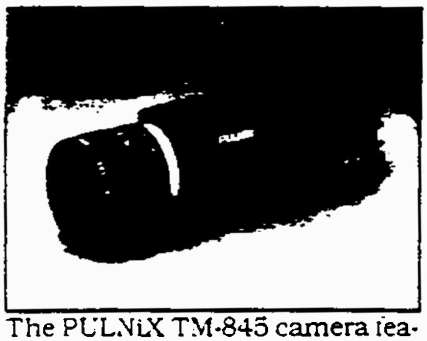

The PULNiX TM-845 camera features a high resolution (800 × 492 pixel) frame transfer CCD imager. The TM-845 offers both variable, asynchronous shuttering and random image integration in an extremely small (1.25" × 1.75" × 5.50" camera. Sync is internal/external.

Options include an external shutter control and a Peltier cooling attachment for optimum imaging in the integration mode. A CCIR version (TM-865) will be available soon.

REMOTE IMAGER CCD CAMERA

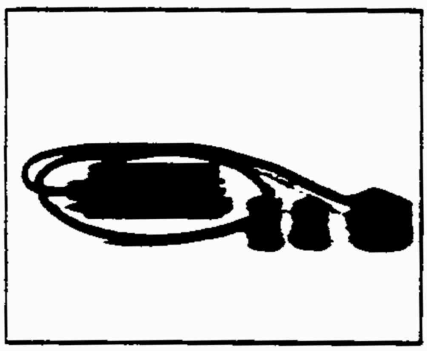

The PULNiX TM-540R remote imager CCD camera permits mounting of the lens/imager assembly within a very confined area. The 510 × 492 pixel imager is attached to the main camera module by a 48" flexible cable which carries all video and power. The TM-540R comes standard with 48" remote (84" maximum distance); shorter distances are available by custom order.

To facilitate mounting, different versions of the imager module are offered. The TM-540R uses C-mount or special miniature lenses and accepts external sync.

played on a fast oscilloscope. No dispersive element was placed in the cavity and the laser operated in a free-running pulsed mode.

Pulsed laser operation was readily obtained for pumping at or above the lasing threshold energy of 2.2mJ. A single output laser pulse was obtained, implying a gain-switched operation, a consequence of pump-pulse duration being shorter than the lasing-level lifetime.

The spectrum peaks at 1235nm and has a bandwidth FWHM) of 25nm. The measured slope efficiency is ~1.5 percent for the cavity configuration described above. With an optimized cavity, we expect the slope efficiency to increase substantially. We have observed laser action in this crystal for E ∥ a and c axes as well. This appears to be a unique property of this system, since most of the systems, including alexandrite, lase in only one preferred direction.

The chromium-activated forsterite system has a high potential to be a very useful and practical laser system in optical communications and ranging. The spectral range for laser emission is expected to extend from 850-1400nm if the parasitic impurity absorption can be minimized by improving the crystal growth technique. The output at the low-energy end of this laser is of particular importance for transmission through optical fibers and eye-safe ranging. The large fluorescence bandwidth promises ultrashort pulse generation through mode-locked operation. Since large crystals can be readily grown, the system may be used as an amplifier medium in the near infrared region as well.

Acknowledgment

We would like to acknowledge Mr. Teruo Hiruma of Hamamatsu Photonics KK for help and support, and K. Yamagishi, H. Anzai and Y. Yamaguchi of Mitsui Mining and Smelting Company for providing us with the crystals. The research is supported by National Aeronautics and Space Administration, Army Research Office, Hamamatsu Photonics KK and City College of New York Organized Research.

References

1. Esterowitz, L. and N. Barnes (1987). *Topical Meeting on Tunable Solid State Lasers*. October 1987, Williamsburg, Va.
2. Petricevic, V., S.K. Gayen, R.R. Alfano, K. Yamagishi, and K. Moriya (1987). Laser Action in Chromium-Doped Forsterite. *International Conference on Lasers '87*. December 1987, Lake Tahoe, Nev.; and R.R. Alfano, V. Petricevic and S.K. Gayen, U.S. Patent pending.
3. Smythe, J.R. and R.M. Hazen (1973). *American Mineralogist*. 58:588.
4. Runciman, W.A., D. Sengupta and J.T. Gourley (1973). *American Mineralogist*. 58:451.

Meet the authors

The authors are associated with the Institute for Ultrafast Spectroscopy and Lasers (IUSL) and Photonics Laboratory (PAL) of the City College of New York. Vladimir Petricevic is a graduate student in electrical engineering, Swapan Kumar Gayen is a research associate at IUSL, and Robert R. Alfano is a Distinguished Professor of Science and Engineering, director of IUSL and PAL, and a member of *Photonics Spectra*'s advisory board.

3. V. Petričević, S. K. Gayen, R. R. Alfano, K. Yamagishi and K. Moriya, "Room-Temperature Vibronic Laser Action in Cr^{3+}:Mg_2SiO_4", in *Proceedings of the International Conference on Lasers '87,* 7-12 December, 1987, Lake Tahoe, Nevada , edited by F. J. Duarte , (STS Press, McLean, Virginia), pp. 423-25.

ROOM TEMPERATURE VIBRONIC LASER ACTION IN $Cr^{3+}:Mg_2SiO_4$

V. Petričević, S. K. Gayen and R. R. Alfano
Institute for Ultrafast Spectroscopy and Lasers
Photonics Application Laboratory
Departments of Physics and Electrical Engineering
The City College of New York
New York, NY 10031
and
Kiyoshi Yamagishi and Kazuo Moriya
Electronic Materials Research Laboratory
Mitsui Mining and Smelting Co. Ltd.
1333-2 Haraichi, Ageo-Shi
Saitama 362, Japan

Abstract

Room temperature vibronic laser action in trivalent chromium ion-doped forsterite ($Cr^{3+}:Mg_2SiO_4$) is reported for the first time. The free running pulse laser emission is centered at 1235 nm of the broad $^4T_2 \rightarrow {}^4A_2$ fluorescence band with a bandwidth of ~ 22 nm. The spectral range for laser emission is expected to cover the 800-1350 nm range if the parasitic absorption may be minimized, making it one of the most widely tunable solid state lasers.

In this paper we present the first room temperature vibronic pulsed laser operation of Cr^{3+}-doped forsterite ($Cr^{3+}:Mg_2SiO_4$). Forsterite is a naturally occurring gem[1,2] which can be grown by the Czochralski method.[1] The single crystal of $Cr^{3+}:Mg_2SiO_4$ used for spectroscopic and laser action measurements was grown at the Electronic Materials Research Laboratory of the Mitsui Mining and Smelting Co., Ltd., Japan. The crystal is a 9 mm x 9 mm x 4.5 mm rectangular parallelepiped with the three mutually orthogonal axes oriented along the b, c and a crystallographic axes of the crystal. The crystal contains 0.04 at.% of Cr^{3+} ions, which is equivalent to a chromium ion concentration of 6.9×10^{18} ions/cm^3.

The room-temperature fluorescence and absorption spectra of $Cr^{3+}:Mg_2SiO_4$ for $\vec{E} \parallel b$ crystallographic axis are shown in Fig. 1. The fluorescence spectrum of $Cr^{3+}:Mg_2SiO_4$ was excited by the 488-nm radiation from an argon-ion laser and recorded by a germanium photodiode detector-lock-in-amplifier combination at the end of a 0.25-m monochromator equipped with a 1000-nm blazed grating. The room-temperature spectrum is a broad band covering the wavelength range 700-1400 nm. The room-temperature fluorescence lifetime is 15 μs.

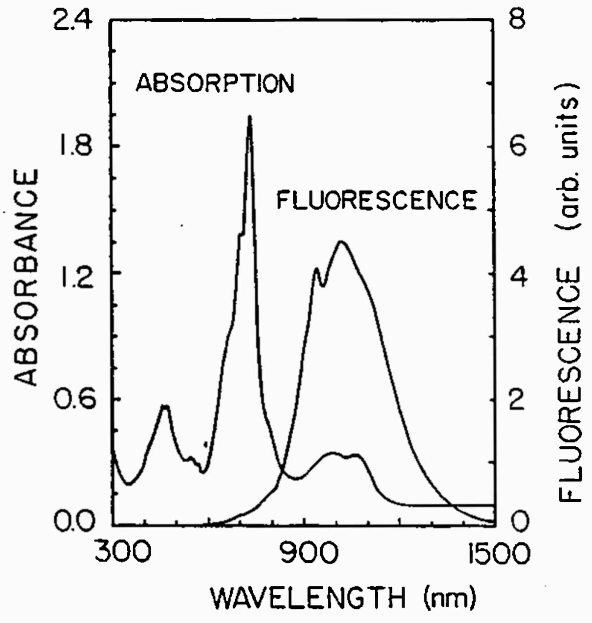

Fig. 1 Absorption and fluorescence spectra of $Cr^{3+}:Mg_2SiO_4$ at room temperature. Both the spectra were taken for $\vec{E} \parallel$ b-axis and excitation along a-axis. The thickness of the sample along a-axis is 4.5 mm.

The absorption spectrum was taken with a Perkin-Elmer Lambda-9 spectrophotometer along the 4.5-mm path length of the sample. It is characterized by two broad bands centered at 740 nm and 460 nm attributed to the $^4A_2 \rightarrow {}^4T_2$ and $^4A_2 \rightarrow {}^4T_1$ absorptive transitions, respectively, of the Cr^{3+} ion. The broad, weak absorption band between 850-1150 nm is not observed in the excitation spectrum.[3] This indicates that the origin of this

absorption is not transitions in Cr^{3+} ion, but in some other impurity ions, e.g., Fe^{3+} in the host crystal.[5] It is evident from Fig. 1 that this background absorption overlaps a significant spectral region[5] of $Cr^{3+}:Mg_2SiO_4$ emission, and inhibits laser action in that region.

The experimental arrangement for investigating the laser action[6] in $Cr^{3+}:Mg_2SiO_4$ consisted of a stable resonator formed by two 30-cm-radius mirrors placed 20 cm apart. The mirrors were dielectric coated to transmit the 532-nm pump beam, and to have high reflectivity in the 1150-1250 nm spectral range. The reflectivity of the back mirror is 99.9%, while that of the output mirror is ~ 98% for normal incidence over the specified wavelength range. It is to be noted that this spectral region does not correspond to the peak of the fluorescence spectrum, but was chosen so that the background absorption is minimal. The sample was longitudinally pumped by frequency-doubled 532-nm, 10-ns full-width-at-half-maximum (FWHM) pulses from a Q-switched Nd:YAG laser (Quanta Ray DCR-1) operating at a 10-Hz repetition rate, employing an unstable resonator configuration. The pump beam was linearly polarized along the b axis and propagated along the a axis of the sample. It was focused 3 cm before the sample by a 25-cm-focal-length lens. The radius of the pump beam at the center of the sample is ~ 600 μm. The output from the laser cavity was analyzed by a 0.25-m monochromator and monitored by a germanium photodiode detector. The output of the detector was displayed on a fast oscilloscope. No dispersive element was placed in the cavity and the laser operated in a free-running pulsed mode.

Pulsed laser operation was readily obtained for pumping at or above the lasing threshold of 2.2 mJ. A single output laser pulse was obtained, implying a gain-switched operation which is a consequence of pump-pulse duration being shorter than the lasing-level lifetime. The amplitude and duration of the laser pulse varied, as expected, with the pulse-to-pulse energy fluctuation of the pump laser. The temporal duration (FWHM) of the output laser pulse varied from 200 ns at the threshold to 100 ns at 2.4 times the threshold energy. The delay between the peak of the pump pulse and the peak of the $Cr^{3+}:Mg_2SiO_4$ laser pulse also varied with pump-pulse energy, from 700 ns at the threshold to 200 ns at 2.4 times the threshold energy. This indicates that the laser cavity is highly lossy, and several hundred round trips are required to build up the laser oscillation in the cavity.

The laser threshold and slope efficiency were measured for the cavity used in this experiment and the data is displayed in Fig. 2. The laser oscillation starts to build up at an absorbed input energy of 2.2 mJ. The measured slope efficiency of 1.4% is rather low, and indicates large losses in the cavity. These losses include ~ 13% reflection loss from the uncoated sample surfaces, scattering from inhomogeneties in the crystal, and a large mismatch between the size of the pump beam and the $Cr^{3+}:Mg_2SiO_4$ cavity modes in the sample.

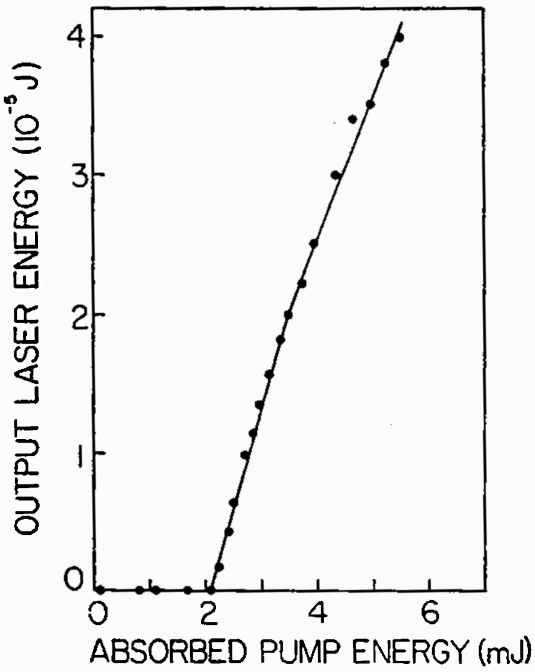

Fig. 2 The output energy of $Cr^{3+}:Mg_2SiO_4$ laser as a function of input energy.

The spectrum of $Cr^{3+}:Mg_2SiO_4$ laser is shown in Fig. 3, for an absorbed pump energy of 3.4 mJ. The spectrum peaks at 1235 nm and has a bandwidth (FWHM) of 22 nm. The spectral range is limited at the high energy end by the mirror transmission and the impurity absorption, while at the low energy end by the mirror transmission as well as by the decrease in fluorescence intensity.

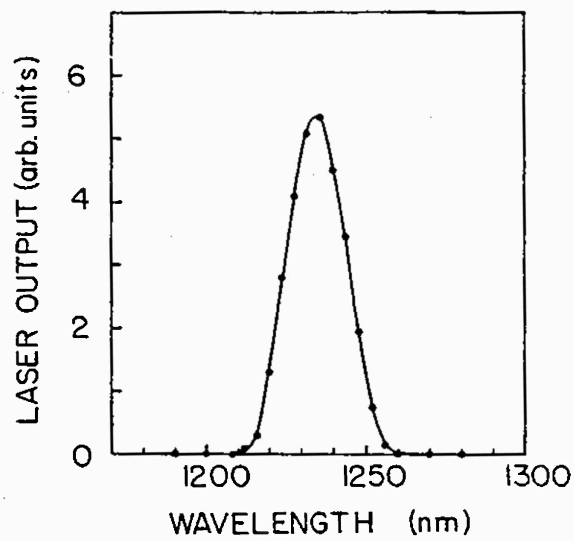

Fig. 3 The spectrum of free-running $Cr^{3+}:Mg_2SiO_4$ laser for the resonator configuration described in the text.

In summary, pulsed laser operation has been obtained in $Cr^{3+}:Mg_2SiO_4$ at room temperature. The laser emission is centered at 1235 nm and has a bandwidth of ~ 22 nm. The spectral range for laser emission is expected to extend from 850-1300 nm if the parasitic absorption may be minimized by improved crystal growth technique, making it one of the most widely tunable solid state lasers in this spectral region. The large fluorescence bandwidth of the crystal promises ultrashort pulse generation through mode locked operation.

The research is supported by National Aeronautics and Space Administration, Army Research Office, Hamamatsu Photonics KK and CCNY Organized Research.

References

1. J. R. Smyth and R. M. Hazen, American Mineralogist 58, 588 (1973).
2. L. V. Bershov, J. M. Gaite, S. S. Hafner, and H. Rager, Phys. Chem. Minerals 9, 95 (1983).
3. K. Yamagishi, unpublished.
4. W. A. Runciman, D. Sengupta, and J. T. Gourley, American Mineralogist 58, 451 (1973).
5. V. Petričević, S. K. Gayen, R. R. Alfano and K. Moriya, "Spectroscopic Properties of Trivalent-Chromium-Ion-Doped Forsterite: A new Potential Tunable Laser Crystal", Paper PD-8, presented at the Topical Meeting on Tunable Solid State Lasers, Williamsburg, Virginia, Oct. 26-28, 1987; and Tunable Solid State Laser Technical Digest Series, 1987 vol. 20, p. PD-8.
6. R. R. Alfano, V. Petričević and S. K. Gayen, U.S. Patent pending.

5. V. Petričević, S. K. Gayen, and R. R. Alfano, "Laser Action in Chromium-Activated Forsterite for Near-Infrared Excitation", Appl. Opt. **27**, 4162 (1988).

Reprinted from Applied Optics, Vol. 27, page 4162, October 15, 1988

Laser action in chromium-activated forsterite for near infrared excitation

V. Petricevic, S. K. Gayen, and R. R. Alfano

CUNY-City College, Institute for Ultrafast Spectroscopy & Lasers, New York, New York 10031.
Received 8 August 1988.
Sponsored by Govind P. Agrawal, AT&T Bell Laboratories.
0003-6935/88/204162-02$02.00/0.

Recently, we reported[1-3] room-temperature pulsed laser action in chromium-activated forsterite ($Cr:Mg_2SiO_4$). The free-running laser output was centered at 1235 nm with a spectral bandwidth (full width at half-maximum, FWHM) of 22 nm. The laser emission was stimulated by the 532-nm excitation of the green-red absorption band of the system. The crystal is characterized by a shallow absorption band spanning the 850–1200-nm wavelength range, which overlaps a significant portion of the emission spectrum and was previously thought to inhibit laser action in that region. In this communication, laser action in chromium-doped forsterite for 1064-nm excitation of this band is reported. The near infrared absorption thus turns out to be effective in populating the initial level of the lasing transition.

The absorption and fluorescence characteristics of Cr:forsterite in the near infrared spectral region are shown in Fig. 1. The room-temperature absorption spectrum is a double-humped band covering the 850–1200-nm wavelength range. The room-temperature fluorescence spectrum extends from 1000 to 1400 nm and peaks at 1140 nm. At liquid nitrogen temperature both the spectra show a sharp zero-phonon line at 1093 nm followed by elaborately structured vibrational sidebands. A detailed analysis of the vibrational sidebands is out of the scope of the present paper and will be presented in a future publication. The fluorescence lifetime is 15 μs at room temperature and 20 μs at liquid nitrogen temperature.

The cavity arrangement used for obtaining laser action in $Cr:Mg_2SiO_4$ has been described elsewhere.[1] An identical arrangement was used in this measurement, except that the separation between the front and the back mirrors was 40 cm, and the pump beam was focused 5 cm in front of the sample by a 50-cm focal-length lens. The fundamental and second harmonic emissions from a Q-switched Nd:YAG laser (Quanta Ray DCR-1) operating at a 10-Hz repetition rate were used for excitation of the near infrared and visible bands, respectively. Pulsed laser action was readily observed for both the 1064- and 532-nm pumping at or above the respective thresholds. To switch from one pump wavelength to the other, one merely had to change a filter in the beam path to transmit the desired wavelength and block the other. The amplitude and duration of the $Cr:Mg_2SiO_4$ laser

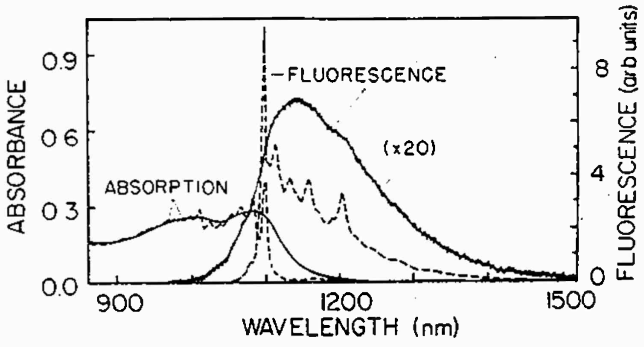

Fig. 1. Near infrared absorption spectrum and fluorescence spectrum for 1064-nm excitation of $Cr:Mg_2SiO_4$ at room temperature (solid line) and liquid-nitrogen temperature (broken line) for $E \| b$ axis. The crystal contains 0.04 at.% of Cr ions and has a thickness of 4.5 mm along the excitation direction.

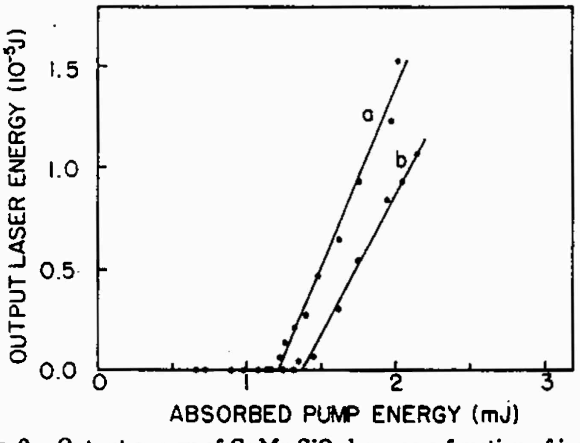

Fig. 2. Output energy of $Cr:Mg_2SiO_4$ laser as a function of input energy for (a) 1064-nm pumping, and (b) 532-nm pumping.

Table I. Properties of Laser Emission for the Two Excitation Wavelengths

Property	Value at the excitation wavelength	
	1064 nm	532 nm
Lasing threshold (absorbed energy)	1.25 mJ	1.37 mJ
Slope efficiency	1.8%	1.4%
Spectral bandwidth (FWHM)	25 nm	22 nm
Center wavelength	1235 nm	1235 nm

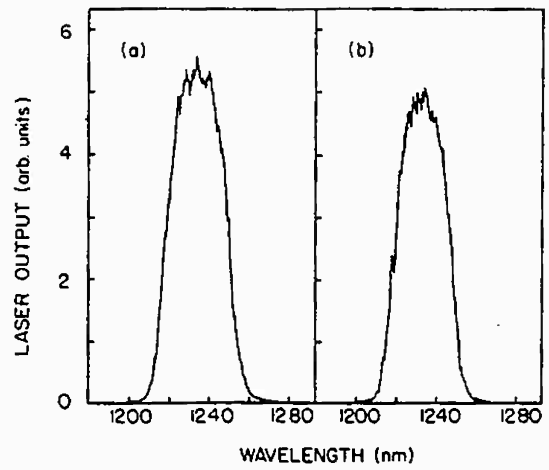

Fig. 3. Spectra of free running $Cr:Mg_2SiO_4$ laser for (a) 1064-nm pumping and (b) 532-nm pumping.

pulse, as well as its delay with respect to the pump pulse, varied as expected with the pulse-to-pulse energy fluctuation of the pump pulses. However, for a similar level of excitation and within the time resolution of the experiment, there was no appreciable difference in the delay between the pump pulse and the output laser pulse for the two pump wavelengths. The laser thresholds and slope efficiencies for the two excitation wavelengths, 1064 and 532 nm, are shown in Fig. 2. The spectra of the free-running laser for pumping at 1064 and 532 nm are displayed in Figs. 3(a) and (b), respectively. Table I summarizes and compares the characteristics of laser emission for the two excitation wavelengths.

The close similarity of laser parameters clearly indicates that the infrared band is responsible for laser action for both the 532- and 1064-nm excitations. For 532-nm pumping there is a fast transfer of excitation from the levels directly pumped to the lasing level. Chromium-activated forsterite thus has the useful property that it can be pumped by the fundamental of Nd:YAG or Nd:glass lasers, and no frequency doubling is necessary. A detailed understanding of the spectroscopic properties that lead to this behavior of this system is an interesting problem and will be presented in an upcoming publication.

We thank K. Yamagishi of Mitsui Mining and Smelting Co. of Japan for providing us the $Cr:Mg_2SiO_4$ crystals used in this study. The research is supported by National Aeronautics and Space Administration, Army Research Office, and City College of New York Organized Research.

Note added in proof: We obtained cw laser action in chromium-activated forsterite pumping with 1064-nm cw radiation from a Nd:YAG laser. Using a single plate birefringent filter in pulsed mode, tuning over 1167–1270 nm range has also been demonstrated.

References

1. V. Petricevic, S. K. Gayen, R. R. Alfano, K. Yamagishi, H. Anzai, and K. Yamaguchi, "Laser Action In Chromium-Doped Forsterite," Appl. Phys. Lett. **52**, 1040 (1988).
2. V. Petricevic, S. K. Gayen, R. R. Alfano, K. Yamagishi, and K. Moriya, "Room-Temperature Vibronic Laser Action in $Cr^{3+}:Mg_2SiO_4$," in *Proceedings, International Conference on Lasers '87*, 7–12 Dec. 1987, Lake Tahoe, NV (to be published).
3. V. Petricevic, S. K. Gayen, and R. R. Alfano, "A New Tunable Solid-State Laser," Photonics Spectra **22**(3), 95 (1988).

6. V. Petričević, S. K. Gayen, and R. R. Alfano, "Laser Action in Chromium-Activated Forsterite for Near-Infrared Excitation: Is Cr^{4+} the Lasing Ion?" Appl. Phys. Lett. **53**, 2590 (1988).

Laser action in chromium-activated forsterite for near-infrared excitation: Is Cr^{4+} the lasing ion?

V. Petričević, S. K. Gayen, and R. R. Alfano
Institute for Ultrafast Spectroscopy and Lasers, Departments of Physics and Electrical Engineering, City College of New York, New York, New York 10031

(Received 9 May 1988; accepted for publication 18 October 1988)

Room-temperature pulsed laser action has been obtained in chromium-activated forsterite ($Cr:Mg_2SiO_4$) for excitation of the near-infrared absorption band of the system by the 1064 nm radiation from a Nd:YAG laser. The characteristics of laser emission are similar to those observed for 532 nm pumping. It is suggested that the laser action is due to a "center" other than the trivalent chromium (Cr^{3+}), presumably the tetravalent chromium (Cr^{4+}).

Recently, we reported[1-3] room-temperature pulsed laser action in chromium-activated forsterite ($Cr:Mg_2SiO_4$). The free-running laser output was centered at 1235 nm with a spectral bandwidth of 22 nm. The laser emission was stimulated by the 532 nm excitation of the green-red absorption band of the system. This absorption band, together with the one in the blue spectral region, originates from transitions between crystal-field-split states of the Cr^{3+} ion. The origin of the shallow absorption band spanning the 850–1200 nm wavelength range has not been determined with any certainty, and was tentatively attributed to other impurity ions.[3] This absorption band overlaps a significant portion of the emission band of the system and inhibits laser action in that region. Identical absorption band has been observed in gadolinium scandium gallium garnet crystals codoped with trivalent chromium and neodymium ions ($GSGG:Nd^{3+}, Cr^{3+}$).[5-7] The chromium ion in this crystal acts as an efficient sensitizer of Nd^{3+} emission, resulting in about a factor of two improvement in lasing efficiency relative to the Nd^{3+}:YAG crystal.[8,9] The near-infrared absorption acts as a significant loss mechanism for Nd^{3+} emission in codoped GSGG crystal and impedes the full potential of the sensitization process. The "center" responsible for this infrared absorption has been considered to be a nuisance, and efforts have been made to get rid of this center by improving the crystal growth technique, or annealing the crystal in reducing atmosphere.[10] In this letter we report for the first time on laser action in chromium-doped forsterite pumped by 1064 nm radiation and present evidence that in chromium-doped forsterite the near-infrared active "center" is responsible for laser action. Absorption, emission, and lasing properties of this "center" are presented. We suggest that the center may be a Cr^{4+} ion in a tetrahedral site.

The absorption and fluorescence spectra of the center in the near-infrared spectral region are shown in Figs. 1 and 2, respectively. The room-temperature absorption spectrum is a double-humped band covering the 850–1200 nm wavelength range. The room-temperature fluorescence spectrum extends from 1000 to 1400 nm and peaks at 1140 nm. At liquid-nitrogen temperature both the spectra show a sharp zero-phonon line at 1093 nm followed by elaborately structured vibrational sidebands. A detailed analysis of the vibrational sidebands is out of the scope of the present letter and will be presented in a future publication. The fluorescence lifetime is 15 μs at room temperature and 20 μs at liquid-nitrogen temperature.

The cavity arrangement used for obtaining laser action in $Cr:Mg_2SiO_4$ has been described elsewhere.[1] An identical arrangement was used in this measurement, except that the separation between the front and the back mirrors was 40 cm, and the pump beam was focused 5 cm in front of the sample by a 50 cm focal length lens. The fundamental and the second-harmonic emissions from a Q-switched Nd:YAG laser (Quanta Ray DCR-1) operating at a 10 Hz repetition rate were used for excitation of the near infrared and the visible bands, respectively. Pulsed laser action was readily observed for both the 1064 nm and the 532 nm pumping at or above the respective thresholds. To switch from one pump wavelength to the other, one merely had to change a filter in the beam path to transmit the desired wavelength and block the other. The amplitude and duration of the $Cr:Mg_2SiO_4$ laser pulse, as well as its delay with respect to the pump pulse, varied, as expected, with the pulse-to-pulse energy fluctuation of the pump pulses. However, for a similar level of excitation and within the time resolution of the experiment, there was no appreciable difference in the delay between the pump pulse and the output laser pulse for the two pump wavelengths. The laser thresholds and slope efficiencies for the two excitation wavelengths, 1064 and 532 nm, are shown in Fig. 3. The spectra of the free-running laser for pumping at 1064 and 532 nm are displayed in Figs. 4(a) and 4(b), respectively. Table I summarizes and compares

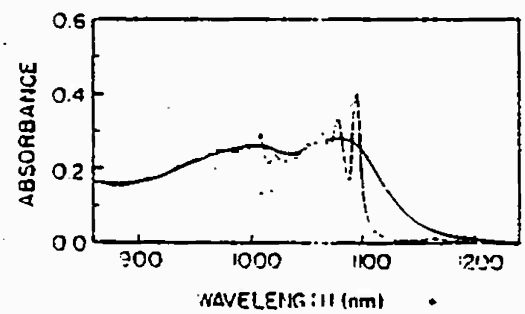

FIG. 1. Near-infrared absorption spectra of $Cr:Mg_2SiO_4$ at room temperature (solid line) and liquid-nitrogen temperature (broken line) for $E \| b$ axis. The crystal contains 0.04 at. % of Cr ions and has a thickness of 4.5 mm along the excitation direction.

 0003-6951/88/522590-03$01.00

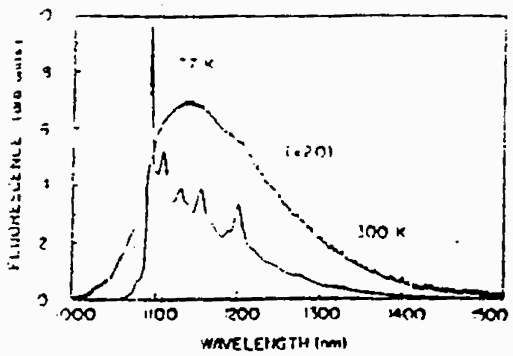

FIG. 2. Near-infrared fluorescence spectra of $Cr:Mg_2SiO_4$ at room temperature and liquid-nitrogen temperature for 1064 nm excitation.

the characteristics of laser emission for the two excitation wavelengths.

The data presented so far clearly indicate that the same center is active in laser action for both the 532 nm and 1064 nm excitations. For the 532 nm pumping there is a fast transfer of excitation from the levels directly pumped to the lasing level. The absorption at 532 nm and for that matter, the entire red-green band has been attributed to $^4A_2 \rightarrow {}^4T_2$ transitions in Cr^{4+} ion.[1,10] If that is the case, then the CR^{4+} ions act as a sensitizer, rapidly and efficiently transferring energy to the lasing center. However, the lasing center itself may have a higher lying absorption band that overlaps the Cr^{3+} absorption in the red-green spectral region. Similar contributions to absorption in this spectral region have indeed been suggested for Cr^{4+} in GSGG,[11] and for isoelectronic V^{3+} in corundum.[12] The growth of population in the lasing level for 532 nm pumping will then be due to vibrational nonradiative transitions which are very fast.[13] Probably, both the interband nonradiative transitions, and the $CR^{3+} \rightarrow$ lasing center energy transfer are effective in populating the lasing level for excitation in the visible. However, for the 1064 nm pumping, the lasing band is directly populated.

The key question that remains to be answered is, what is the origin of this lasing center. Trivalent chromium enters the forsterite crystal in two distinct sites, one with mirror ($M2$) and the other with inversion ($M1$) symmetry. Generally, the ions in the mirror sites are optically active. The

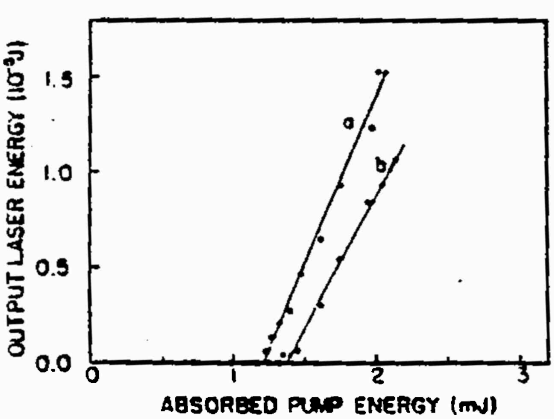

FIG. 3. Output energy of $Cr:Mg_2SiO_4$ laser as a function of input energy for (a) 1064 nm pumping and (b) 532 nm pumping.

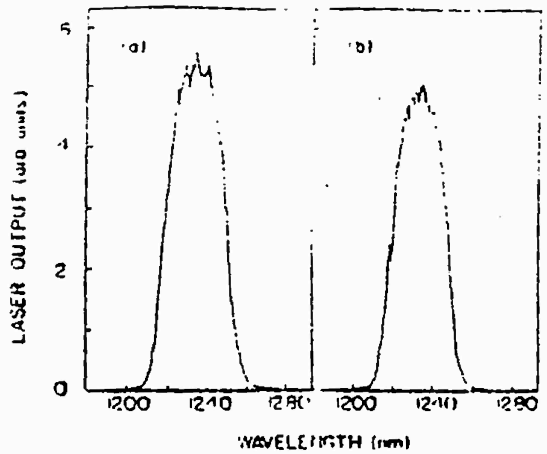

FIG. 4. Spectra of free-running $Cr:Mg_2SiO_4$ laser for (a) 1064 nm pumping and (b) 532 nm pumping.

polarized absorption spectra of chromium-activated forsterite have been analyzed[10] in terms of Tanabe–Sugano formalism,[14] and no infrared absorption band is predicted for Cr^{4+} ions in mirror sites. For Cr^{4+} ions in inversion sites, even ligand field-induced electric-dipole transitions are not possible. Dynamic interaction with lattice vibrations may result in transitory reduction of inversion symmetry, making transitions possible. However, such transitions are very weak and slow, as seen for Cr^{3+} ions in inversion sites in alexandrite, where the fluorescence lifetime is ~ 60 ms.[15] The measured lifetime of 15 μs is too short for transitions within the states of a Cr^{3+} ion in inversion site. It is highly unlikely that the infrared absorption is due to the Cr^{3+} ions in inversion site.

Impurities other than chromium could be another possibility. Trivalent iron (Fe^{3+}) is a commonly occurring impurity in olivines, and exhibits a similar absorption band in the near infrared. However, the low-temperature spectrum of iron in olivine does not show the sharp-line structure as observed in chromium-activated forsterite.[4] Chemical analysis of the sample did not indicate sufficient iron content to account for the observed absorption either.

A similar 850–1200 nm absorption band observed[5–7] in Nd,Cr:GSGG was first assumed[6] to be due to Cr^{2+}, and finally has been attributed to Cr^{4+} centers.[5] This band appears only in Cr-activated GSGG crystals and never in undoped or only Nd-doped crystals. The absorption coefficient of the band depends on the crystal growth condition and has been observed[6] to vary over three orders of magnitude from a high of 2 cm^{-1} down to 1×10^{-3} cm^{-1} at 1061 nm, the

TABLE I. Properties of laser emission for the two excitation wavelengths.

Property	Value at the excitation wavelength of 1064 nm	532 nm
Lasing threshold (absorbed energy)	1.25 mJ	1.37 mJ
Slope efficiency	1.8%	1.4%
Spectral bandwidth (FWHM)	30 nm	27 nm
Center wavelength	1235 nm	1235 nm

wavelength for Nd laser emission. After a series of careful tests for impurities[5] and analytical chemistry studies,[5] these authors established a correlation between the strength of this absorption and the level of divalent calcium impurity in the sample. Divalent calcium appears as an impurity in scandium oxide, the starting material for growing GSGG. Also, to promote the growth of garnet crystals a small amount of calcium oxide is sometimes added to the melt. The working hypothesis here is that the Ca^{2+} causes Cr^{3+} to change to Cr^{4+}, and the Cr^{4+} ion on a tetrahedral site is responsible for the near-infrared absorption in question. In view of the similarities between the near-infrared absorption band in GSGG and forsterite, we tentatively assign the center in forsterite to Cr^{4+} ion as well. The role of Ca^{2+} is presumably played by Mg^{2+} in forsterite.[16] Substitution for Si^{4+} in tetrahedrally coordinated sites is less frequent but possible,[17] and may lead to tetrahedrally coordinated chromium ions in forsterite. Another possible identity of the lasing center may be the divalent chromium ion (Cr^{2+}) substituting for Mg^{2+} in the inversion ($M1$) site. It has been indicated that in distorted coordination sites, like the forsterite $M1$ site, Cr^{2+} may occur and be stable.[18,19] According to the prediction of the crystal field theory such a center may account for the observed infrared absorption. The exact identification of the lasing center in chromium-activated forsterite still remains an interesting problem for further investigation.

Note added in proof. We have obtained cw laser action in chromium-activated forsterite by pumping the crystal with 1064 nm radiation from a cw Nd:YAG laser. By using a single-plate birefringent filter in pulsed mode, tuning over 1167–1345 nm has also been demonstrated.

We would like to acknowledge Dr. Alex Pertica, and Dr. John Caird of Lawrence Livermore National Laboratory for suggesting that the infrared absorption may be due to transitions in Cr^{4+}, and Dr. Roger Belt for providing a Cr,Nd:GSGG crystal and for helpful discussions. We thank K. Yamagishi of Mitsui Mining and Smelting Co. of Japan for providing us the Cr:Mg_2SiO_4 crystals used in this study. The research is supported by the Army Research Office, National Aeronautics and Space Administration, and City College of New York Organized Research. Note: The submission date of this manuscript shows the priority of who obtained laser action in forsterite with the 1064 nm pumping first.

[1] V. Petričević, S. K. Gayen, R. R. Alfano, K. Yamagishi, H. Anzai, and K. Yamaguchi, Appl. Phys. Lett. 52, 1040 (1988).
[2] V. Petričević, S. K. Gayen, R. R. Alfano, K. Yamagishi, and K. Moriya, *Proceedings of the International Conference on Lasers '87*, 7–12 December 1987, Lake Tahoe, Nevada, edited by T. J. Duarte (STS, McLean, VA, 1988), pp. 423–425.
[3] V. Petričević, S. K. Gayen, and R. R. Alfano, Photonics Spectra 22 (3), 95 (1988).
[4] W. A. Runciman, D. Sengupta, and J. T. Gourlev, Am. Mineral. 58, 451 (1973); 59, 630 (1974); R. G. Burns, Am. Mineral. 59, 625 (1974).
[5] J. A. Caird, M. D. Shinn, T. A. Kirchoff, L. K. Smith, and R. E. Wilder, Appl. Opt. 25, 4294 (1986).
[6] J. A. Caird, W. F. Krupke, M. D. Shinn, L. K. Smith, and R. E. Wilder, in *Technical Digest, Conference on Lasers and Electrooptics* (Optical Society of America, Washington, D.C., 1984), paper TUR3, p. 232.
[7] M. I. Demchuk, E. V. Zharikov, A. M. Zabaznov, I. A. Manichev, V. P. Mikhailov, A. M. Prokhorov, A. P. Shkadarevich, A. F. Chernyakovskii, I. A. Shcherbakov, and K. V. Yumashev, Sov. J. Quantum Electron. 17, 266 (1987).
[8] E. V. Zharikov, N. N. Il'ichev, V. V. Laptev, A. A. Malyutin, V. G. Ostroumov, P. P. Pashinin, A. S. Pimenov, V. A. Smirnov, and I. A. Shcherbakov, Sov. J. Quantum Electron. 13, 82 (1983).
[9] E. Reed, IEEE J. Quantum Electron. QE-21, 1625 (1985).
[10] H. Rager and G. Weiser, Bull. Mineral. 104, 603 (1981).
[11] A. Pertica and J. A. Caird (private communications).
[12] D. S. McClure, J. Chem. Phys. 36, 2757 (1962).
[13] S. K. Gayen, W. B. Wang, V. Petričević, and R. R. Alfano, Appl. Phys. Lett. 49, 437 (1986).
[14] S. Sugano, Y. Tanabe, and H. Kamimura, *Multiplets of Transition-Metal Ions in Crystals* (Academic, New York, 1970).
[15] J. C. Walling, O. G. Peterson, H. P. Jenssen, R. C. Morris, and E. W. O'Dell, IEEE J. Quantum Electron. QE-16, 1302 (1980).
[16] This view is also shared by Dr. Roger Belt of Airtron, who has grown GSGG crystals extensively.
[17] L. V. Bershov, J. M. Gaite, S. S. Hafner, and H. Rager, Phys. Chem. Minerals 9, 95 (1983).
[18] B. E. Scheetz and W. B. White, Contr. Mineral. Petrol. 37, 221 (1972).
[19] R. G. Burns, Contr. Mineral. Petrol. 51, 213 (1975).

7. V. Petričević, S. K. Gayen, and R. R. Alfano, "Major Breakthrough in Tunable Solid-State Lasers", Opt. News **14** (12), 13 (1988).

Optics News

About the cover . . .

"Optics in 1988," our annual overview of the field, represents many of the principle advances in optics over the past year. While not meant to be all-inclusive, we have tried to highlight accomplishments in all areas, from classical geometric optics to modern quantum optics. Cover courtesy of CLARK DUNBAR/UNIPHOTO.

FEATURES

DEPARTMENTS

OPTICS NEWS, Volume 14, No. 12. Second-class postage paid at Woodbury, N.Y., and additional mailing offices.

OPTICS NEWS (USPS 121950, ISSN 0098-907X, CODEN ONEWDU) is published monthly by the Optical Society of America, 1816 Jefferson Place, N.W., Washington, D.C. 20036; telephone (202) 223-8130. Annual subscription, $70. Membership in the Optical Society of America includes $4 from membership dues to be applied to a subscription to OPTICS NEWS. Send all remittances and correspondence about subscriptions, undelivered copies, and changes of address to Optics News Subscription Fulfillment, c/o American Institute of Physics, 500 Sunnyside Blvd., Woodbury, N.Y. 11797. POSTMASTER: Send form 3579 to same address.

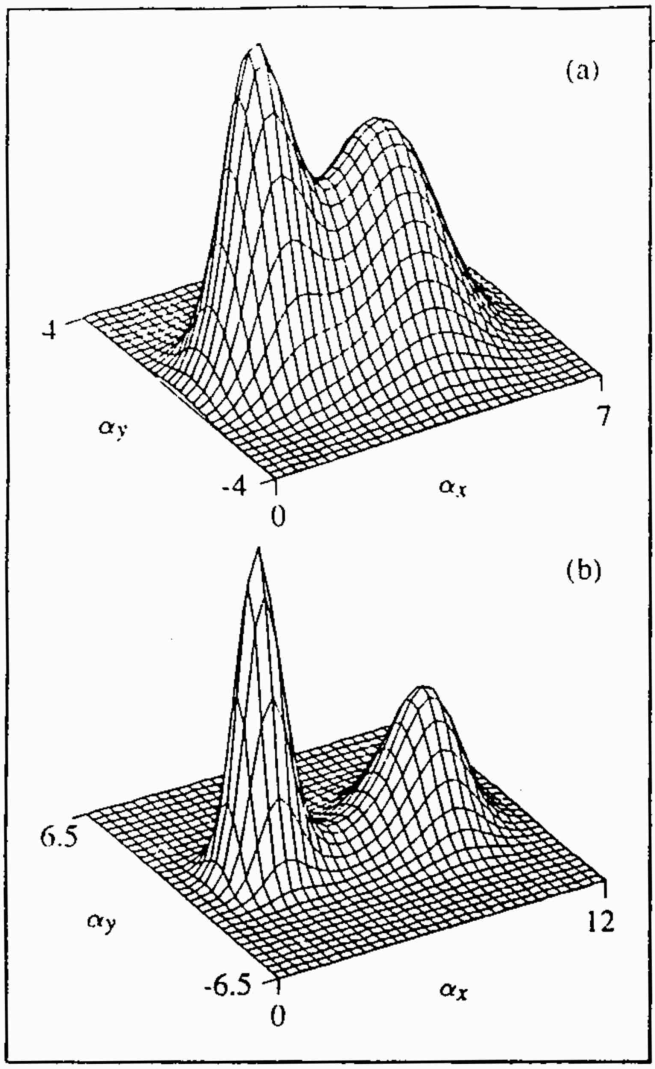

Bimodal Q distributions for the intracavity field in single-atom intracavity resonance fluorescence. The strength of the quantum fluctuations is inversely proportional to the size of the system, measured by the number of cavity photons needed to saturate the atomic transition. Figures (a) and (b) are plotted for saturation photon numbers of one and five, respectively.

side a cavity. Much attention has been paid to enhanced and inhibited spontaneous emission rates. Actually, cavity effects are much more diverse, even for the simplest configuration of a single atom transition. With cavity and atomic loss included, the quantum dynamics of this coupled system depend on the relative sizes of three parameters: the atomic decay rate, the cavity decay rate, and the coupling strength between the cavity mode and the atomic transition. Work at the University of Arkansas seeks to reach a global understanding of these dynamics.[2-4-6]

Free-space behavior is recovered if the atom-field coupling strength is much smaller than the atomic and cavity decay rates. When it is not, the quantum statistics can differ markedly from free-space resonance fluorescence. A notable example of the possible behavior is the existence, verified by Craig Savage at the Optical Sciences Center,[5] of bimodal states of the intracavity field. This is a single-atom version of absorptive optical bistability. Intracavity resonance fluorescence, therefore, provides a quantized version of a dissipative nonlinear dynamical system. It can be used to study the relationship between linear microscopic quantum mechanics and macroscopic nonlinearity, including the important questions that surround the subject of quantum chaos.

REFERENCES

1. D.F. Walls and P. Zoller, Phys. Rev. Lett., 47, 709 (1981).
2. P.R. Rice and H.J. Carmichael, J. Opt. Soc. A. B, 5, 1661 (1988).
3. B.R. Mollow, Phys. Rev. 188, 1969 (1969).
4. P.R. Rice and H.J. Carmichael, IEEE J. Quantum Electron. QE 24, 1351 (1988).
5. C.M. Savage and H.J. Carmichael, IEEE J. Quantum Electron. QE 24, 1495 (1988).
6. P.R. Rice and H.J. Carmichael, in preparation.

LASERS

MAJOR BREAKTHROUGH IN TUNABLE SOLID-STATE LASERS

V. PETRICEVIC, S.K. GAYEN, AND R.R. ALFANO
INSTITUTE FOR ULTRAFAST SPECTROSCOPY AND LASERS
PHOTONICS APPLICATION LABORATORY
DEPARTMENTS OF PHYSICS AND ELECTRICAL ENGINEERING
THE CITY COLLEGE OF NEW YORK
NEW YORK, N.Y.

Chromium-doped forsterite ($Cr:Mg_2SiO_4$) is a new member[1-4] of the expanding family of tunable solid-state lasers.[5-7] Forsterite is a member of the olivine family of crystals and like alexandrite, and emerald is a naturally occurring gem. Laser action in Cr:forsterite has been obtained for excitation by both the fundamental (1064 nm) and the second harmonic (532 nm) radiation from a Q-switched Nd:YAG laser. The laser emission peaks at 1235 nm, and to date has been tuned over the 1167–1270 nm wavelength range. In this review, a description of the spectroscopic and laser properties of forsterite laser crystal is presented.

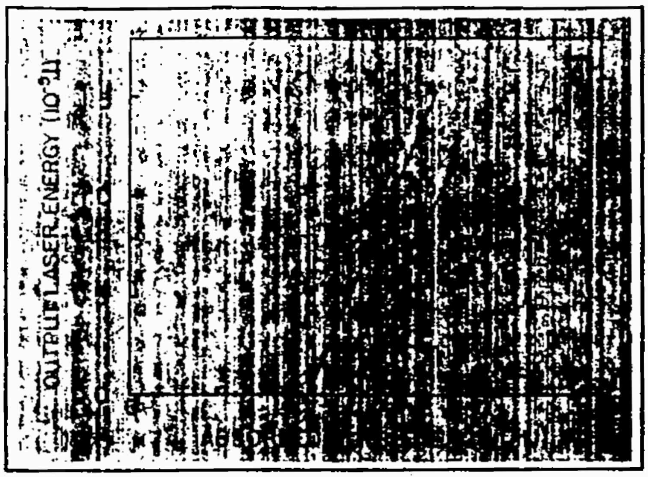

Output energy of $Cr:Mg_2SiO_4$ laser as a function of input energy for (a) 1064 nm pumping, and (b) 532 nm pumping.

The room-temperature absorption spectrum of the crystal is characterized by three bands.[1] For excitation with light polarized along the b-axis of the crystal, these bands span the 360–520 nm, 600–800 nm, and 850-1200 nm range. The 600 to 800 nm band changes dramatically with the polarization of the incident light, while the other two bands exhibit little significant change. The room-temperature fluorescence spectrum extends from 600-1400 nm.

At liquid nitrogen temperature, the fluorescence spectrum breaks up into three components and exhibits sharp line structures. The behavior of the fluorescence spectrum gives an indication that more than one center may be involved in the absorption and emission of radiation in this crystal. This is further substantiated by the wavelength-dependent fluorescence life-time of the crystal. The room-temperature fluorescence lifetime for emission around 701 nm is 75 μsec while for emission in the lasing region it is 15 μsec.

Since the absorption spectrum of the crystal overlaps with a significant portion of the emission spectrum, laser action was obtained only in the infrared end, where the absorption losses are minimum. The sample was placed at the center of a stable resonator formed by two 30 cm radius mirrrors. The mirrors were dielectric coated to transmit the 532 nm and 1060 nm pump beams, and to have high reflectivity in the 1150–1250 nm spectral range. Details of the cavity configuration have been presented elsewhere.[1,3]

The sample was longitudinally pumped both by the 1064 nm fundamental, and the 532 nm second-harmonic radiation from a Q-switched Nd:YAG laser. Pulsed laser action was readily obtained for both the 1064 nm and the 532 nm pumping at or above the respective thresholds. The laser thresholds and slope efficiencies for the two excitation wave-lengths, 1064 nm and 532 nm, are shown in the figure. The table summarizes and compares the characteristics of laser emission for the two excitation wavelengths.

To date, continuous tuning of the Cr:forsterite laser has been obtained over the 1167–1270 nm spectral range. A single-plate birefringent filter is used as a dispersive element in the laser cavity. Continuous wave laser operation was achieved using a chopped cw Nd:YAG radiation.

The forsterite crystals were provided by K. Yamagishi of Mitsui Mining and Smelting Co. of Japan. The research is supported by Army Research Office, National Aeronautics and Space Administration, Hamamatsu Photonics KK, and City College of New York Organized Research.

REFERENCES

1. V. Petricevic, S.K. Gayen, R.R. Alfano, K. Yamagishi, H. Anzai and K. Yamaguchi, Appl. Phys. Lett. 52, 1040 (1988).
2. V. Petricevic, S.K. Gayen, R.R. Alfano, K. Yamagishi, and K. Moriya, "Room-temperature vibronic laser action in $Cr^{4+}:Mg_2SiO_4$". Proceedings of the International Conference on Lasers '87, F. Duarte, Ed., McLean, Va. (STS), 1987, pp. 423–425.
3. V. Petricevic, S.K. Gayen, and R.R. Alfano, Photonics Spectra 22 (3), 95 (1988).
4. V. Petricevic, S.K. Gayen, and R.R. Alfano, Appl. Optics (to be published).
5. W.F. Krupke and G. Huber, Ed., J. Opt. Soc. Am. B, 3, 81–157 (1986), Special issue on Solid-State Laser Materials.
6. R.L. Byer, Ed., IEEE J. Quantum Electron. QE-21, 1567–1638 (1985), Special issue on Tunable Solid-State Lasers.
7. W.F. Krupke, M.L. Shand and L. Esterowitz, Ed., IEEE J. Quantum Electron. QE-24, 881-1228 (1988), Special issue on Solid-State Lasers.

ROOM-TEMPERATURE OPERATION OF THE Co: MgF_2 LASER

D. Welford and P.F. Moulton
Schwartz Electro-Optics Inc.
Concord, Mass.

The Co:MgF_2 laser is a continuously tunable source for the mid-IR covering, to date, the wavelength region from 1500 to 2300 nm at cryogenic temperature and 1750 to 2500 nm at room temperature. Laser operation was first demonstrated by Johnson et al.[1] using flashlamp excitation. Later work by Moulton resulted in the development of both cw[2] and pulsed Q-switched[3] operation using laser excitation. However, until recently, liquid-nitrogen[2,3] or thermoelectric[4] cooling were required for efficient operation. This year, we reported the first room-temperature, pulsed, normal-mode operation of the Co:MgF_2 using laser excitation.[5] At a 10-Hz pulse-repetition-rate

8. V. Petričević, S. K. Gayen, and R. R. Alfano, "Continuous-Wave Laser Operation of Chromium-Doped Forsterite", Opt. Lett. **14**, 612, (1989).

Continuous-wave laser operation of chromium-doped forsterite

V. Petričević, S. K. Gayen,* and R. R. Alfano

Institute for Ultrafast Spectroscopy and Lasers, Departments of Physics and Electrical Engineering, The City College of New York, New York, New York 10031

Received September 21, 1988; accepted March 12, 1989

Room-temperature continuous-wave laser action in chromium-activated forsterite ($Cr:Mg_2SiO_4$) has been achieved for longitudinal pumping in a nearly concentric cavity by the 1064-nm radiation from a cw Nd:YAG laser. The laser emission is centered at 1244 nm and has a spectral bandwidth of 12 nm. An output-power slope efficiency of 6.8% is measured. The effective emission cross section is estimated to be $\sim 1.1 \times 10^{-19}$ cm^2.

Chromium-doped forsterite ($Cr:Mg_2SiO_4$), a new member of the family of tunable solid-state lasers,[1] is emerging as a useful, important, and practical laser system for operation in the near-infrared spectral region. Recently we reported room-temperature pulsed laser action in this crystal for both 532- and 1064-nm pumping.[2-5] The laser emission peaks at 1235 nm and is continuously tunable over the 1167–1345-nm spectral range.[6] Successfully operated tunable solid-state lasers such as alexandrite,[7] emerald,[8] Cr:GSGG,[9] and other chromium-based crystals,[1] together with $Ti^{3+}:Al_2O_3$,[10] span quite a different spectral range of 660–1090 nm. Chromium-activated forsterite is unique since it extends the spectral range further into the near infrared to 1345 nm. The most remarkable feature of the operating wavelength range of Cr:forsterite is that it lies near 1276 nm, a wavelength of zero material dispersion. The practical implication for optical communications is that the material dispersion will be minimal for a source that emits in the vicinity of this wavelength and hence would permit the maximum information capacity of the fiber to be exploited. This laser's spectral range also makes it suitable for eye-safe ranging and remote sensing.

Consequently, the cw operation of such a promising source of coherent radiation in the near infrared is of technological importance. Although a number of chromium-activated lasers have been operated in the cw mode, none covers the spectral range spanned by the Cr:forsterite laser. Successful pulsed operation does not ensure cw lasing either, as has been found for Nd:glass lasers. Room-temperature cw operation of a laser material, on the other hand, opens up the possibilities of the laser's being used in various oscillator and amplifier configurations. In this Letter we report, for the first time to our knowledge, the room-temperature cw laser operation of chromium-doped forsterite in the near-infrared spectral region.

The experimental arrangement used for obtaining cw laser action in Cr:forsterite is shown schematically in Fig. 1. The sample was placed at the center of a nearly concentric cavity formed by two 5-cm-radius mirrors. The input mirror was dielectric coated to transmit 70% of the 1064-nm pump beam and to have a reflectivity of 99.9% over the 1200–1400-nm wavelength range. The output mirror was similarly coated to have a reflectivity of 99% for the 1175–1250-nm range and to transmit 20% of 1064-nm pump beam.

The single crystal of Cr:forsterite used in this study was grown by the Czochralski method at the Electronic Materials Research Laboratory of the Mitsui Mining and Smelting Company, Ltd., Japan. The crystal is a 6 mm × 6 mm × 30 mm rectangular parallelepiped with the three mutually orthogonal axes oriented along the *a*, *b*, and *c* crystallographic axes of the crystal. It contains 2.8×10^{18} chromium ions per cubic centimeter. The 6 mm × 6 mm end faces of the crystal were broadband antireflection coated, such that the reflectivity over the 1050–1250-nm spectral range was less than 0.5%. The sample was sandwiched between two copper blocks to facilitate dissipation of heat.

The 1064-nm radiation from a cw Nd:YAG laser (Spectra-Physics Model 3460) was focused by a 75-mm focal-length lens to pump the sample longitudinally along its 30-mm path length. The pump beam propagated along the *c* axis and was linearly polarized along the *b* axis of the crystal. The beam was chopped at a duty factor (i.e., the ratio of the interval for which the beam is blocked to that for which the beam is open) of 9:1 to reduce heating effects. When the pump beam was not chopped, the Cr:forsterite laser operated at a 40% reduced power level, indicating the effect due to local heating. The measurements reported here were taken with a fixed cavity length corresponding to a cavity mode waist of 75 μm. The

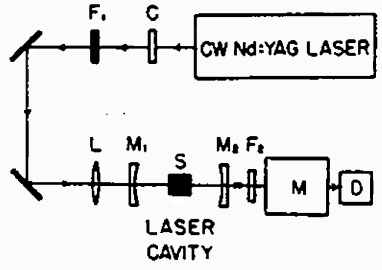

Fig. 1. Schematic diagram of the experimental arrangement for investigating cw laser action in Cr:forsterite: C, light chopper; F_1, variable neutral-density filter; L, focusing lens; M_1, input mirror; M_2, output coupler; S, sample; F_2, 1064-nm cutoff, Cr:forsterite laser light-transmitting filter; M, monochromator; D, germanium or PbS detector.

0146-9592/89/120612-03$2.00/0

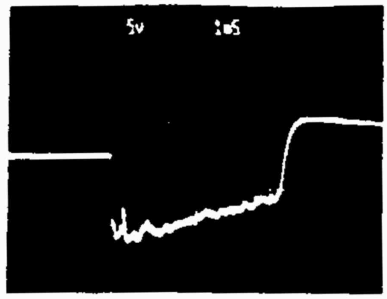

Fig. 2. Temporal behavior of the cw Cr:forsterite laser emission over the entire duration of the pump pulse (scale: 1 msec/cm).

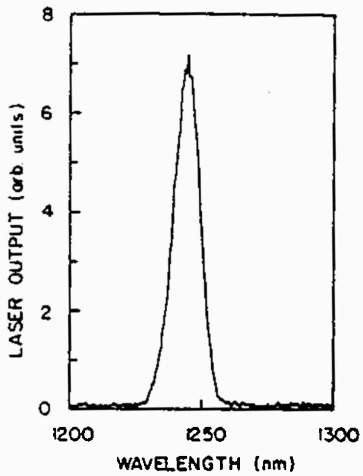

Fig. 3. Spectrum of the free-running cw Cr:forsterite laser.

waist of the pump beam at the center of the sample was 70 μm.

The transmitted 1064-nm light was blocked by cut-off filters. The output of the Cr:forsterite laser was monitored either by a slow PbS detector or by a fast germanium photodiode. A set of calibrated neutral density filters was used for output-power slope efficiency measurement. The spectrum of the free-running laser was recorded by a photodiode–lock-in-amplifier combination at the end of a 0.25-m monochromator equipped with a 1000-nm blazed grating.

Quasi-cw laser operation was readily obtained for pumping above the lasing threshold of 1.25 W of absorbed power. The laser output is polarized along the *b* axis of the crystal. The crystal could be pumped by a beam polarized along the *a* axis, but the emission would still be polarized along the *b* axis. The time evolution of laser output is displayed in the oscilloscope trace shown in Fig. 2.

The spectrum of free-running cw Cr:forsterite laser is shown in Fig. 3 for an absorbed pump power of 3 W. The spectrum looks similar to that for the pulsed mode; however, the peak is shifted from 1235 to 1244 nm and the bandwidth reduces to 12 nm compared with 25 nm for the pulsed case. The shift of the center wavelength is attributed to the transmission characteristics of the output coupler used in the cw lasing experiment. The reduction in spectral bandwidth indicates that a laser medium has to be driven harder for cw operation than for pulsed operation.

The cw output power of the Cr:forsterite laser as a function of the absorbed pump power was measured for the cavity used in this experiment, and the data are displayed in Fig. 4. The laser oscillation starts to build up at an absorbed input power of 1.25 W. The measured slope efficiency is 6.8%.

The experimentally obtained values of the absorbed pump power at the threshold and the slope efficiency together with known mirror reflectivities may be used to estimate a number of key laser parameters. The slope efficiency η is given by[11]

$$\eta = (\lambda_p T)/\lambda_L (T + L), \tag{1}$$

where T is the total transmission of the cavity mirrors and L is the cavity loss. Using the data in Fig. 4, we obtain a value of 12.7% for L. This value of L should be compared with the absorption losses of ~9% measured with a Perkin-Elmer Lambda 9 spectrophotometer. The disagreement between the two values indicates that additional small loss mechanisms, e.g., excited-state absorption and nonradiative relaxation, are operative as well.

The threshold pump power depends on the cavity losses and the effective emission cross section. An expression relating these parameters for a longitudinally pumped laser[12] has been developed and is readily applicable to the present system and experimental conditions:

$$P_t = \frac{\pi E_p w_L^2 (L + T)(a^2 + 1)}{4\sigma\tau[1 - \exp(-\alpha l)]}, \tag{2}$$

where P_t is the incident threshold pump power; σ is the effective emission cross section; E_p is the energy of a pump photon; w_L is the radius of the laser cavity mode in the crystal; a is the ratio w_p/w_L, where w_p is the pump-beam radius; τ is the lasing state lifetime; α is the pump-beam absorption coefficient; and l is the length of the crystal. We estimate a value of 1.1×10^{-19} cm^2 for the effective emission cross section, using the measured threshold pump power (absorbed), $P_t[1 - \exp(-\alpha L)]$ of 1.25 W, the beam waist parameters

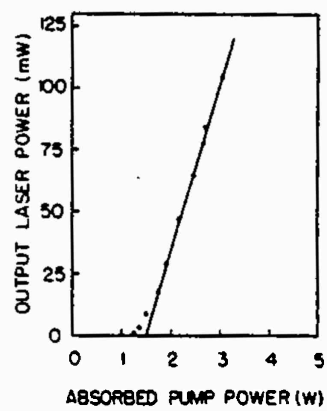

Fig. 4. Output power of the cw Cr:forsterite laser as a function of absorbed pump power.

Table 1. Properties of cw Emission from a Cr:Forsterite Laser

Property	Value
Lasing wavelength (center)	1244 nm
Spectral bandwidth (FWHM)	12 nm
Lasing threshold (absorbed power)	1.25 W
Slope efficiency, η	6.8%
Threshold inversion density, N_t	2×10^{17} cm^{-3}
Effective emission cross section	1.1×10^{-19} cm^2

quoted above, and a room-temperature fluorescence lifetime τ of $\sim$15 μsec. The value of the emission cross section may also be determined from the radiative lifetime and the emission line shape. The radiative lifetime in this calculation was approximated by the fluorescence lifetime. However, care must be taken to choose the fluorescence lifetime and line shape to be used. This caution is warranted from the realization that in Cr:forsterite more than one center is optically active. In our earlier publications[2-4] we attributed the entire emission in Cr:forsterite to radiative transitions within the states of the Cr^{3+} ion. However, our subsequent investigations revealed that the emission in the 1050–1400-nm range is the Stokes-shifted fluorescence corresponding to the 850–1200-nm absorption band. It is these absorption and emission bands that are effective in laser action in Cr:forsterite.[5,13] These absorption and emission bands are attributed to transitions within the states of a second center other than Cr^{3+}, which has tentatively been identified as tetravalent-chromium ion (Cr^{4+}). The details of the spectroscopic properties of Cr:forsterite, and the role played by the two centers, are interesting and intriguing. However, they are outside the scope of this Letter and will be presented in a forthcoming publication.

Both the emission line shape and the fluorescence lifetime used in emission cross-section calculation were measured by exciting the 850–1200-nm absorption band of the sample by 1064-nm radiation, thus ensuring that only the emission from Cr^{4+} ions is taken into account. The emission spectrum thus obtained has been reported elsewhere[5,13] and hence is not repeated here. The value of the emission cross section was calculated by approximating the fluorescence spectrum mentioned above by a center wavelength and an emission linewidth. The fluorescence lifetime for 1064-nm excitation is 15 μsec, which is the value used for the radiative lifetime.

The value of the emission cross section obtained from the emission lifetime and line shape is 3.3×10^{-19} cm^2, a factor of 3 larger than that estimated from the cw lasing threshold condition, Eq. (2). This large discrepancy may arise from two factors. First, there may be substantial nonradiative relaxation, which will imply that fluorescence lifetime is not a good approximation for the radiative lifetime used in the calculation. Second, excited-state absorption may be operative. The presence of such loss mechanisms has also been suggested from the discrepancy in the values of cavity loss discussed above.

From the emission cross section and threshold pump power, we estimate the threshold population inversion density from the threshold condition[11]:

$$2\sigma N_t l = L + T. \tag{3}$$

A value of 2×10^{17} cm^{-3} for the population inversion is calculated. The key cw laser parameters are summarized in Table 1.

The successful cw lasing of Cr:forsterite together with its large fluorescence bandwidth promises high-repetition-rate mode-locked operation (e.g., by synchronous pumping) for generating ultrashort pulses in the near infrared. Since large crystals may be readily grown, various types of oscillator and amplifier design are now possible.

We thank K. Yamagishi, H. Anzai, and Y. Yamaguchi of Mitsui Mining and Smelting Company, Japan, for providing us the crystal used in this measurement. The research is supported by the U.S. Army Research Office, the National Aeronautics and Space Administration, and City College of New York Organized Research.

* Present address, Department of Physics and Engineering Physics, Stevens Institute of Technology, Hoboken, New Jersey 07030.

References

1. For a list of tunable solid-state lasers see J. A. Caird, S. A. Payne, P. R. Staver, A. J. Ramponi, L. L. Chase, and W. F. Krupke, IEEE J. Quantum Electron QE-24, 1077 (1988), and references therein.
2. V. Petričević, S. K. Gayen, R. R. Alfano, K. Yamagishi, H. Anzai, and Y. Yamaguchi, Appl. Phys. Lett. 52, 1040 (1988).
3. V. Petričević, S. K. Gayen, and R. R. Alfano, Photon. Spectra 22(3), 95 (1988).
4. V. Petričević, S. K. Gayen, R. R. Alfano, K. Yamagishi, and K. Moriya, in *Proceedings of the International Conference on Lasers '87*, F. J. Duarte, ed. (STS, McLean, Va., 1988), p. 423.
5. V. Petričević, S. K. Gayen, and R. R. Alfano, Appl. Opt. 27, 4162 (1988).
6. V. Petričević, S. K. Gayen, R. R. Alfano, Appl. Opt. 28, 1610 (1989).
7. J. C. Walling, O. G. Peterson, H. P. Jenssen, R. C. Morris, and E. W. O'Dell, IEEE J. Quantum Electron. QE-16, 1302 (1980).
8. M. L. Shand and J. C. Walling, IEEE J. Quantum Electron. QE-18, 1829 (1982); J. Buchert, A. Katz, and R. R. Alfano, IEEE J. Quantum Electron. QE-19, 1477 (1983).
9. B. Struve, G. Huber, V. V. Laptev, I. A. Shcherbakov, and E. V. Zharikov, Appl. Phys. B 30, 117 (1983).
10. P. F. Moulton, J. Opt. Soc. Am B 3, 125 (1986).
11. H. G. Danielmeyer, in *Lasers*, A. K. Levine and A. DeMaria, eds. (Dekker, New York, 1975), Vol. IV.
12. P. F. Moulton, IEEE J. Quantum Electron. QE-12, 1582 (1985).
13. V. Petričević, S. K. Gayen, and R. R. Alfano, Appl. Phys. Lett. 53, 2590 (1988).

9. V. Petričević, S. K. Gayen, and R. R. Alfano, "Near Infrared Tunable Operation of Chromium-Activated Forsterite Laser", Appl. Opt. **28,** 1609 (1989).

Reprinted from Applied Optics

Near infrared tunable operation of chromium doped forsterite laser

V. Petricevic, S. K. Gayen, and R. R. Alfano

When this work was done all authors were with City University of New York, City College, Institute for Ultrafast Spectroscopy and Lasers, New York, New York 10031; S. K. Gayen is now with Stevens Institute of Technology, Department of Physics & Engineering Physics, Hoboken, New Jersey 07030.

Received 1 December 1988.
0003-6935/89/091609-03$02.00/0.

Tunable, room temperature pulsed laser operation of a chromium-doped forsterite laser for 1064-nm pumping is reported. Using different sets of mirrors and a single birefringent plate as the intracavity wavelength selecting element, tunability over the 1167–1345-nm spectral range has been demonstrated.

The practical utility of a vibronic solid state laser is determined, to a great extent, by the wavelength range over which it can be tuned effectively. Laser emission in the infrared is of technological importance for eye safe ranging, remote sensing, and optical communication. A number of chromi-

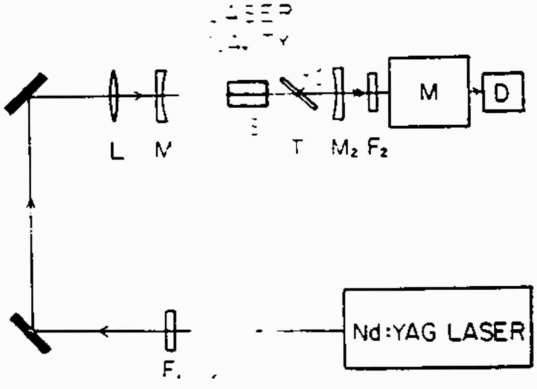

Fig. 1. Schematic diagram of the experimental arrangement used for wavelength tuning the Cr:forsterite laser: F_1 = 1064-nm transmitting, visible blocking filter, F_2 = pump beam blocking, laser output transmitting filter; L = focusing lens, M_1 = back mirror; M_2 = output mirror; S = sample; T = birefringent plate tuning element; M = monochromator, and D = detector.

um-based tunable solid state lasers,[1] together with a $Ti^{3+}:Al_2O_3$ laser,[2] span a spectral range of 660–1090 nm. A chromium-activated forsterite laser[3–7] is unique since it extends the tuning range further into the near infrared to 1345 nm. The most important feature of the tuning range of the Cr:forsterite laser is that it lies around 1276 nm, a wavelength referred to in the literature[8] as the "wavelength of zero material dispersion." We recently reported both the pulsed and the cw laser operation of this crystal at room temperature.[3–7] In this Letter, we present the continuously tunable operation of this laser over the 1167–1345-nm spectral range.

The room temperature fluorescence spectrum of Cr:forsterite covers the 680–1400-nm wavelength range. Laser operation has been obtained in the low energy infrared end of this fluorescence band.[3–5] The absorption spectrum overlaps most of the high energy end including the peak of the fluorescence spectrum and inhibits laser action in that region.[3,4] The tunable operation to be presented here thus spans only a fraction of the fluorescence spectrum.

The experimental arrangement used for wavelength tuning the Cr:forsterite laser is shown schematically in Fig. 1. The sample (S) was placed at the center of a stable cavity formed by two 30-cm radius mirrors placed 45 cm apart. The input mirror (M_1) was dielectric coated to transmit the 1064-nm pump beam and to have a high reflectivity of 99.9% in the 1150–1250-nm range, which decreased to 98.5% at 1270 nm. Three different mirrors were used as output couplers (M_2). The first mirror (output coupler A) had a reflectivity of 98% for the 1200–1300-nm range, the reflectivity of the second mirror (output coupler B) varied from 99% at 1150 nm to 87% at 1200 nm, while that of the third (output coupler C) varied from 99.8% at 1150 nm to 90% at 1200 nm. The left and center curves presented in Fig. 2 were taken with the first two of these output couplers. The tuning curve on the right was obtained with another pair of mirrors: the input mirror which had high transmission for the 1064-nm pump beam and reflectivity of 99.9% in the 1275–1375-nm range and the output mirror (output coupler D), whose reflectivity varied from 96% at 1275 nm to 94.5% at 1375 nm with a maximum of 97% at 1320 nm.

The dispersive element used for frequency tuning the Cr:forsterite laser output was a single birefringent crystalline quartz plate provided by Apollo Lasers, Inc. The plate was a 30- × 31.75-mm rectangle, 513.4 μm thick, with the optic axis in the plane of the plate and parallel to the 30-mm side. The plate was inserted in the cavity at the Brewster angle with respect to the cavity axis, which is also the ray axis. The tuning of the laser output was effected by rotating the tilted plate about an axis perpendicular to its surface.

The single crystal of Cr:forsterite used in this study was grown by the Czochralski method at the Electronic Materials Research Laboratory of the Mitsui Mining & Smelting Co., Ltd., Japan. The crystal is a 6- × 6- × 30-mm rectangular parallelepiped with three mutually orthogonal axes oriented along the a, b, c, crystallographic axes of the crystal. The chromium-ion concentration in the crystal is 2.8×10^{18} cm^{-3}. The 6- × 6-mm endfaces of the crystal are broadband antireflection coated, such that reflectivity over the 1050–1250-nm spectral range was <0.5%.

The sample was longitudinally pumped by the fundamental 1064-nm, 10-ns full width at half-maximum (FWHM) pulses from a Q-switched Nd:YAG laser (Quanta-Ray DCR-1) operating at a 10-Hz repetition rate. The spatial profile of the pump pulse was a Gaussian. The pump beam was linearly polarized along the a-axis and propagated along the c-axis of the sample. The 1064-nm beam was focused into the center of the sample by a 50-cm focal length lens. The waist of the cavity mode at the sample was ~225 μm. The position of the focusing lens was adjusted to optimize the overlap between the pump beam spot size and the cavity mode waist monitored by maximizing the laser output. The laser output was analyzed by a 0.25-m monochromator equipped with a 1000-nm blazed grating and monitored by a fast germanium photodiode.

The first proof of wavelength tunability was that for four different output couplers, A, B, C, and D free-running laser outputs were centered at 1235, 1200, 1192, and 1250 nm, respectively.

With the birefringent plate inserted in the cavity, smooth tuning was obtained and the result is displayed in Fig. 2.

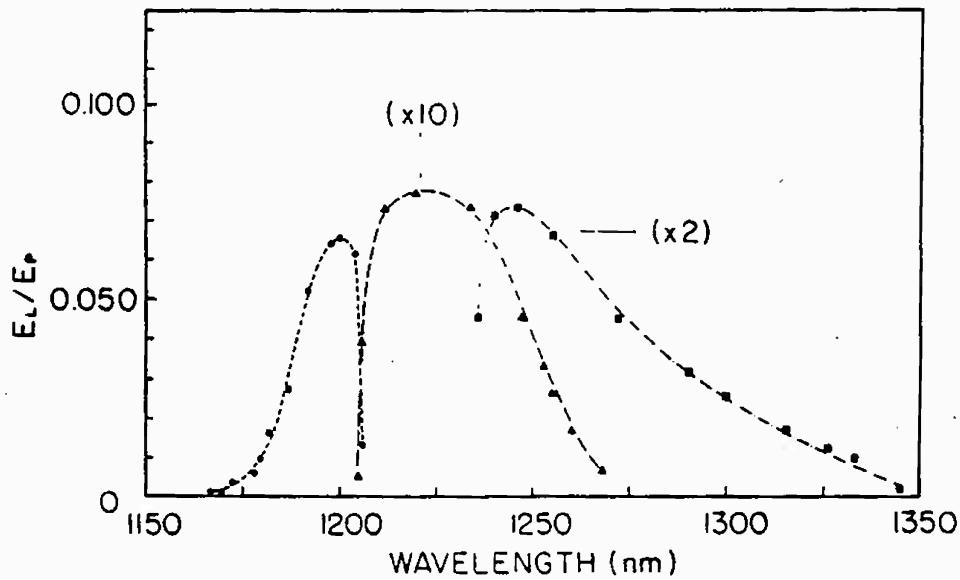

Fig. 2. Ratio of Cr:forsterite laser output (E_L) to the absorbed pump energy (E_p) as a function of wavelength. The curve in the center was taken with output coupler A, the one to the left with output coupler B, and the curve to the right with a set of mirrors coated for the 1275–1375-nm range. The transmission characteristics of the mirrors and output couplers are described in the text.

The center curve taken with output coupler A shows the ratio of the output laser energy to the absorbed input energy as a function of wavelength, spanning the 1205–1268-nm spectral range. At the peak of the tuning curve at 1220 nm, the output laser pulse energy is ~7 μJ/pulse for an input absorbed energy of 0.9 mJ/pulse.

The tuning curve on the left covering 1167–1206 nm was obtained with output coupler *B* described earlier in the text. The laser output peaks at 1200 nm with an energy per pulse of 125 μJ for an absorbed input pulse energy of 1.9 mJ. This order of magnitude larger output power for this output coupler is attributed to its higher transmission (13% at 1200 nm) compared with that for output coupler *A* (<2% over the tuning range). The free-running output slope efficiencies for the two output couplers, 21% for Coupler *B* compared with 4% for coupler *A*, also reflect the same behavior. The lasing threshold of 317 μJ for output coupler *B* is a factor of ~3.5 higher than that for coupler *A* which is expected since the cavity with coupler *B* is lossier than the one with output coupler *A*, and is consistent with the respective output slope efficiencies. The tuning curve on the right was obtained using a pair of mirrors coated for the 1275–1375-nm range. It covers the 1236–1345-nm range. The output peaks at 1245 nm with an energy per pulse of 85 μJ for an absorbed pump energy of 2.4 mJ. The free-running output slope efficiency for this pair of mirrors was 12% with a lasing threshold of 0.27 mJ. It should be noted that we have obtained similar tunable operation for 532-nm and 630-nm pumping as well.

In summary, we have demonstrated continuously tunable operation of a Cr:forsterite laser over the 1167–1345-nm spectral range. At the peak of the tuning curve at 1200 nm an output of 125 μJ/pulse is obtained, with an output to absorbed input energy ratio of 6.6%. A maximum output slope efficiency of ~21% has been obtained so far.

We would like to acknowledge K. Yamagishi, M. Anzai, and Y. Yamaguchi of Mitsui Mining & Smelting Co. for growing the forsterite crystal, Ralph Page of Apollo Lasers, Inc. for providing us with the birefringent plate used as the tuning element in this study, and Y. Budansky for technical help. The research is supported by Army Research Office and National Aeronautics and Space Administration.

References

1. For a list of tunable solid state lasers see J. A. Caird, S. A. Payne, P. R. Staver, A. J. Ramponi, L. L. Chase, and W. F. Krupke, "Quantum Electronic Properties of the $Na_3Ga_2Li_3F_{12}:Cr^{3+}$ Laser," IEEE J. Quantum Electron. **QE-24**, 1077 (1988) and references therein.
2. P. F. Moulton, "Spectroscopic and Laser Characteristics of $Ti:Al_2O_3$," J. Opt. Soc. Am. B **3**, 125–133 (1986).
3. V. Petricevic, S. K. Gayen, R. R. Alfano, K. Yamagishi, H. Anzai, and Y. Yamaguchi, "Laser Action in Chromium-Doped Forsterite," Appl. Phys. Lett. **52**, 1040 (1988).
4. V. Petricevic, S. K. Gayen, and R. R. Alfano, "A New Tunable Solid-State Laser," Photonics Spectra **22**(3), 95 (1988).
5. V. Petricevic, S. K. Gayen, R. R. Alfano, K. Yamagishi, and K. Moriya, "Room Temperature Vibronic Laser Action in $Cr^{3+}:Mg_2SiO_4$," in *Proceedings of the International Conference on Lasers '87*, F. J. Duarte Ed. (STS, McLean, VA, 1988), p. 423.
6. V. Petricevic, S. K. Gayen, and R. R. Alfano, "Laser Action in Chromium-Activated Forsterite for Near Infrared Excitation," Appl. Opt. **27**, 4162–4163 (1988).
7. V. Petricevic, S. K. Gayen, and R. R. Alfano, "Continuous-Wave Laser Operation of Chromium-Doped Forsterite," Opt. Lett. *14*, June 1 (1989), to be published.
8. J. Gowar, *Optical Communication Systems* (Prentice-Hall, London, 1984), pp. 48–53.

10. V. Petričević, S. K. Gayen, and R. R. Alfano, "Lasing and Spectroscopic Properties of Chromium-Activated Forsterite", *Advances in Laser Science-IV, Proceedings of the Fourth International Laser Science Conference* , Edited by J. L. Gole, D. F. Heller, M. Lapp, and W. C. Stwalley, 2-6 October, 1988, Atlanta, Georgia, (American Institute of Physics 1989), p. 33.

CONFERENCE PROCEEDINGS **191**

OPTICAL SCIENCE AND ENGINEERING SERIES 10

RITA G. LERNER
SERIES EDITOR

ADVANCES IN LASER SCIENCE–IV

PROCEEDINGS OF THE FOURTH INTERNATIONAL LASER SCIENCE CONFERENCE

ATLANTA, GA 1988

EDITORS:

JAMES L. GOLE, PROGRAM CHAIR
GEORGIA INSTITUTE OF TECHNOLOGY

DONALD F. HELLER, PROGRAM VICE-CHAIR
LIGHT AGE, INC., MT. BETHEL, NEW JERSEY

MARSHALL LAPP, CONFERENCE CHAIR
SANDIA NATIONAL LABORATORIES AND
LAWRENCE LIVERMORE NATIONAL LABORATORIES

WILLIAM C. STWALLEY, ADMINISTRATIVE VICE-CHAIR
UNIVERSITY OF IOWA

AIP
American Institute of Physics New York

LASER AND SPECTROSCOPIC PROPERTIES OF CHROMIUM-ACTIVATED FORSTERITE

V. Petričević, S. K. Gayen* and R. R. Alfano
Institute for Ultrafast Spectroscopy and Lasers
Departments of Physics and Electrical Engineering
City College of New York
New York, NY 10031

Abstract

Room-temperature pulsed laser action has been obtained in chromium-activated forsterite ($Cr:Mg_2SiO_4$) for both 532-nm and 1064-nm pumping. Free running laser emission in both cases is centered at 1235 nm and has bandwidth of ~ 30 nm. Slope efficiency as high as 22% has been measured. Using different sets of output mirrors and a single birefringent plate as the intracavity wavelength-selecting element tunability over the 1167-1268 nm spectral range has been demonstrated. Continuous-wave laser operation at room temperature has been obtained for 1064-nm pumping from a cw Nd:YAG laser. The output power slope efficiency is 6.3%. The gain cross section is estimated to be 1.1×10^{-19} cm^2. Spectroscopic studies suggest that the laser action is due to a 'center' other than the trivalent chromium (Cr^{3+}), presumably the tetravalent chromium (Cr^{4+}) in a tetrahedrally coordinated site.

I. INTRODUCTION

Recently, we have reported room-temperature pulsed laser action in chromium-doped forsterite ($Cr:Mg_2SiO_4$) for both 532-nm and 1064-nm excitation.[1-4] Laser emission is continuously tunable over the 1167-1268 nm spectral range,[5] with a potential for extending the tuning range beyond 1300 nm. This wavelength range is of great importance in optical communication and eye-safe ranging. The large bandwidth of the laser emission promises generation of ultrashort pulses through mode-locked operation. Large crystals of chromium-doped forsterite can be grown by Czochralski method, which means that this crystal has a potential to be used as an amplifier medium in the near infrared. Furthermore, the successful cw laser operation[6] of Cr forsterite has the practical implication that various types of laser and amplifier designs are possible.

On the other hand, spectroscopy of chromium-doped forsterite is very unusual and intriguing. It is the first chromium-activated laser crystal, to our knowledge, where the tetravalent chromium ion (Cr^{4+}) in a tetrahedral site is presumably responsible for laser action in the near infrared.[7]

In this paper we review the lasing and spectroscopic properties of this new and important tunable solid-state laser crystal.

II. CRYSTAL PROPERTIES AND SPECTROSCOPY

Forsterite is a member of the olivine family of crystals. A unit cell of forsterite has four formula units in an orthorhombic structure of the space group Pbnm. The unit cell's dimensions are: a=4.76Å, b=10.22Å, and c=5.99Å. The Cr^{3+} ion substitutes for the Mg^{2+} ion in two distinct octahedrally coordinated sites: one (M1) with inversion symmetry (C_i) and the other (M2) with mirror symmetry (C_s). The occupation ratio of the two sites by the Cr^{3+} ion is M1:M2=3:2.

Both the single crystals of $Cr:Mg_2SiO_4$ used for spectroscopic and laser experiments were grown by the Czochralski method at the Electronic Materials Research Laboratory of the Mitsui Mining and Smelting Co., Ltd., Japan. The first crystal, referred to as sample 1 hereafter, is a 9mmx9mmx4.5mm rectangular parallelepiped with the three mutually orthogonal axes oriented along the b, c, and a crystallographic axes of the crystal. It contains 0.04 at . % of Cr ions which is equivalent to a chromium ion concentration of 6.9×10^{18} ions/cm^3. The second crystal (sample 2) is a 6mmx6mmx30mm rectangular parallelepiped with the three mutually orthogonal axes oriented along the a, b, c, crystallographic axes of the crystal. It contains 2.8×10^{18} chromium ions per cm^3. The 6mmx6mm faces of the crystal were broad-band anti-reflection coated, such that the reflectivity over the 1050-1250 nm spectral range is less than 0.5%.

The room-temperature fluorescence and absorption spectra of $Cr:Mg_2SiO_4$ taken with sample 1 for E||b axis are shown in Fig. 1.

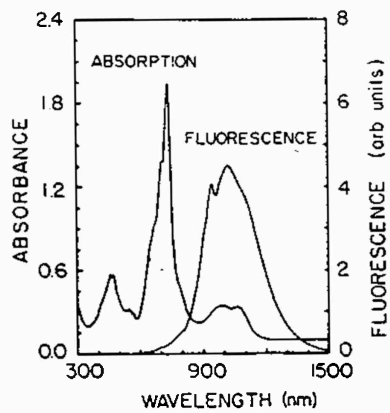

Fig. 1. Absorption and fluorescence spectra of $Cr:Mg_2SiO_4$ at room temperature. Both the spectra were taken for E||b axis and excitation along a axis. The thickness of the sample along a axis is 4.5 mm.

The room-temperature fluorescence is a broad band covering the wavelength range from 680-1400 nm. The absorption spectrum is characterized by two broad bands centered at 740 nm and 460 nm, attributed to the $^4A_2 \rightarrow {}^4T_2$ and $^4A_2 \rightarrow {}^4T_1$ transitions, respectively, of the Cr^{3+} ion. The broad, weak absorption band spanning the 850-1200 nm range is similar to the one observed in chromium-doped GSGG[8] and is attributed to transitions between states in another 'center', presumably the tetravalent Cr^{4+} ion in a tetrahedral site. This

absorption band overlaps a significant portion of $Cr:Mg_2SiO_4$ emission, and inhibits laser action in that region.

The absorption and fluorescence spectra of the 'center' in the near infrared spectral region are shown in Fig. 2. The room-temperature absorption spectrum is a double-humped band covering the 850-1200 nm wavelength range. The room-temperature fluorescence spectrum, excited by 1064-nm radiation from a cw Nd:YAG laser extends from 1000-1400 nm and peaks at 1140 nm. At liquid nitrogen temperature both the spectra show a sharp zero-phonon line at 1093 nm followed by elaborately structured sidebands. The fluorescence lifetime is 15 μs at room-temperature and 20 μs at liquid nitrogen temperature.

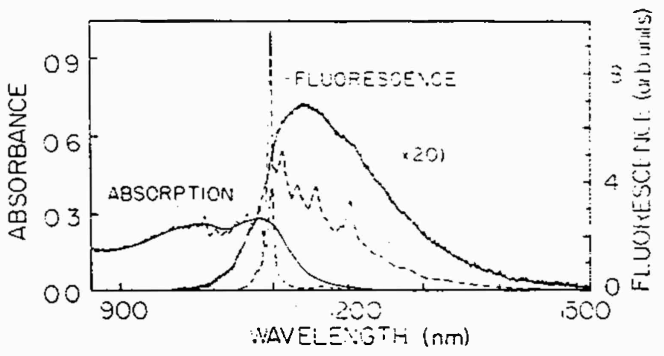

Fig. 2. Near infrared absorption and fluorescence spectra of $Cr:Mg_2SiO_4$ for 1064-nm excitation at room temperature (solid line) and liquid-nitrogen temperature (broken line) for E||b axis.

III. PULSED LASER ACTION

The first laser experiments were conducted with sample 1 in a stable cavity. Details of the cavity arrangement have been described elsewhere.[1] The fundamental and the second harmonic emissions from a Q-switched Nd:YAG laser operating at a 10-Hz repetition rate were used for excitation of the near-infrared and the visible bands, respectively. Pulsed laser action was observed for both the 1064-nm and the 532-nm pumping[6,7] at or above the respective thresholds of 1.25 mJ and 1.37 mJ of absorbed energy. The amplitude and duration of the $Cr:Mg_2SiO_4$ laser pulse, as well as its delay with respect to the pump pulse, varied with the pulse-to-pulse energy fluctuation of the pump pulses. However, for similar level of excitation and within the time resolution of the experiment, there was no appreciable difference in the delay between the pump pulse and the output laser pulse for the two pump wavelengths. The spectra of the free-running Cr:forsterite laser for both 1064-nm and 532-nm pumping peaked at 1235 nm and had FWHM of 30 nm and 27 nm, respectively. These facts clearly indicate that the same 'center' is active in laser action for both the 532-nm and 1064-nm excitations. For 532-nm pumping there is a fast transfer of excitation from the levels directly pumped to the lasing level. In case of 1064-nm pumping, the lasing level is directly populated. The output power slope efficiencies were 1.8%

for 1064-nm pumping and 1.4% for 532-nm pumping, indicating high losses in the cavity.

To improve the laser performance by reducing the losses anti-reflection-coated sample 2 was used, and care was taken to overlap the pump beam and cavity mode accurately. The sample was longitudinally pumped by the fundamental 1064-nm, 10-ns pulses from a Q-switched Nd:YAG laser in a cavity similar to that used earlier. An output power slope efficiency of 22% was obtained using an output coupler having 87% reflectivity over the lasing region.

IV. TUNABLE OPERATION OF FORSTERITE LASER

Tunable operation of Cr:forsterite laser has been obtained over the 1167-1268 nm spectral range.[5] A single birefringent crystalline quartz plate was inserted in the cavity at Brewster's angle with respect to the cavity axis as the intracavity wavelength-selective element. Smooth tuning over the 1167-1268 nm spectral range was obtained by rotating the tilted plate about an axis perpendicular to its surface and the result is displayed in Fig. 3.

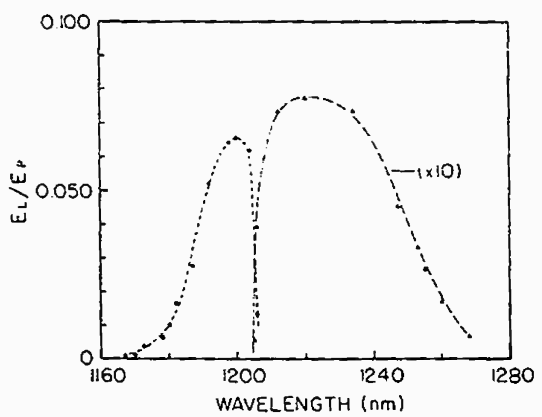

Fig. 3. The ratio of Cr:forsterite laser output (E_L) to the absorbed pump energy (E_p) as a function of wavelength. The curve to the right was taken with an output coupler having 98% reflectivity for 1200-1300 nm range, and one to the left with an output coupler with reflectivity that varied from 99% at 1150 nm to 87% at 1200 nm.

At the peak of the tuning curve at 1220 nm, the output laser energy is ~ 7 μJ/pulse for an absorbed pump energy of 0.9 mJ/pulse. Similar tunable operation has been obtained for 532-nm pumping as well.

IV. CW LASER OPERATION

To obtain cw laser action in Cr:forsterite, sample 2 was placed at the center of a nearly concentric cavity formed by two 5-cm radius mirrors. The output mirror had ~ 1% transmission for the 1175-1250 nm range. The 1064-nm radiation from a cw Nd:YAG laser was focused

by a 75-mm focal length lens to longitudinally pump the sample along the 30-mm path length. The pump beam propagated along the c axis and was linearly polarized along the b axis of the crystal. The pump beam was chopped at a duty factor of 9:1 to reduce heating effects. When the pump beam was not chopped, the Cr:forsterite laser operated at 40% reduced power, indicating the effect due to local heating.

Quasi-cw laser operation was readily obtained for pumping above the lasing threshold of 1.25 W of absorbed power. The spectrum of the free-running cw Cr:forsterite laser peaks at 1244 nm and has a bandwidth of 12 nm.

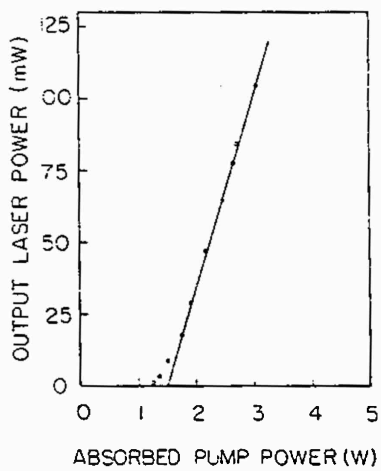

Fig. 4. Output power of the cw Cr:forsterite laser as a function of absorbed pump power.

The cw output power of the Cr:forsterite laser as a function of the absorbed pump power is displayed in Fig. 4. The measured slope efficiency is 6.8%. The experimentally obtained values of the absorbed pump power at the threshold and the slope efficiency together with known mirror reflectivities have been used to estimate a number of key laser parameters. The round-trip cavity loss is estimated to be 12.7%. The effective emission cross section is $1.1\times10^{-19}cm^2$, and threshold inversion density is $2\times10^{17}cm^{-3}$. Important laser and spectroscopic properties of Cr:forsterite are summarized in Table 1.

TABLE 1 Spectroscopic and laser properties of Cr:forsterite

Property	Value
Major pump bands	850-1200 nm, 600-850 nm, and 350-550 nm
Fluorescence band	680-1400 nm
Room temperature fluorescence lifetime	15 μs
Cr-ion concentration	~ 7×10^{18} ions/cm^3
Lasing wavelength (center)	1235 nm (pulsed) 1244 nm (cw)
Spectral bandwidth	~ 30 nm (pulsed) ~ 12 nm (cw)
Slope efficiency	22% (pulsed) 6.8% (cw)
Tuning range	1167-1268 nm
Effective emission cross section	1.1×10^{-19}cm^2

V. ACKNOWLEDGEMENTS

We would like to acknowledge K. Yamagishi, H. Anzai and Y. Yamaguchi of Mitsui Mining and Smelting Co., Japan for providing us the crystals used in these measurements. The research is supported by Army Research Office, National Aeronautics and Space Administration, and City College of New York Organized Research.

*Present Address: Department of Physics and Engineering Physics, Stevens Institute of Technology, Hoboken, New Jersey 07030.

REFERENCES

1. V. Petričević, S. K. Gayen, R. R. Alfano, K. Yamagishi, H. Anzai, and Y. Yamaguchi, Appl. Phys. Lett. 52, 1040 (1988).
2. V. Petričević, S. K. Gayen, and R. R. Alfano, Photonics Spectra 22(3), 95 (1988).
3. V. Petričević, S. K. Gayen, R. R. Alfano, K. Yamagishi and K. Moriya, in Proceedings of the International Conference on Lasers '87, F. J. Duarte, Ed., STS, McLean, VA(1988), p. 423.
4. V. Petričević, S. K. Gayen, and R. R. Alfano, Appl. Opt. 27, 4126 (1988).
5. V. Petričević, S. K. Gayen, R. R. Alfano, Appl. Opt. (submitted).
6. V. Petričević, S. K. Gayen, R. R. Alfano, Optics Lett. (submitted).
7. V. Petričević, S. K. Gayen, R. R. Alfano, Appl. Phys. Lett. (to be published).
8. J. A. Caird, M. D. Shinn, T. A. Kirchoff, L. K. Smith, and R. E. Wilder, Appl. Opt. 25, 4294 (1986).

11. V. Petričević, S. K. Gayen, and R. R. Alfano, "Chromium-Activated Forsterite Laser", in *Tunable Solid-State Lasers*, Vol. 5 of the OSA Proceeding Series, M. L. Shand and H. P. Jenssen, eds. (Optical Society of America, Washington, D.C., 1989), pp. 77-84.

Reprinted from the

OSA Proceedings on

Tunable Solid State Lasers

Edited by Michael L. Shand and Hans P. Jenssen

Volume 5

Proceedings of the OSA Topical Meeting
on Tunable Solid State Lasers,
May 1–3, 1989,
North Falmouth, Cape Cod, Massachusetts

Optical Society of America
1816 Jefferson Place, N.W. • Washington, DC 20036

Chromium-Activated Forsterite Laser

V. Petricevic
Institute for Ultrafast Spectroscopy and Lasers, Departments of Physics and Electrical Engineering, City College of New York, New York, New York 10031

S. K. Gayen
Department of Physics and Engineering Physics, Stevens Institute of Technology, Hoboken, New Jersey 07030

R. R. Alfano
Institute for Ultrafast Spectroscopy and Lasers, Departments of Physics and Electrical Engineering, City College of New York, New York, New York 10031

Abstract

Spectroscopic, quantum electronic and laser characteristics of chromium-doped forsterite ($Cr:Mg_2SiO_4$) are presented. Spectroscopic data suggest that the lasing center in chromium-doped forsterite is tetravalent chromium ion (Cr^{4+}), not the common trivalent chromium (Cr^{3+}).

Introduction

Chromium-doped forsterite ($Cr:Mg_2SiO_4$) laser has emerged as an important member of the ever growing family of tunable solid state lasers based on chromium ion as the lasing center.[1-3] Both pulsed[1] and continuous-wave[4] laser operation have been obtained for 532-nm, 629-nm, and 1064-nm pumping, and the tuning range now covers the 1167 - 1345 nm range.[5] This wavelength range covers the region of minimum material dispersion for optical fibers. Together with the chromium-based lasers tabulated by Caird et al.[2], and more recently developed chromium-doped crystals of Ca-gallogermanate structure,[3] lasers based on chromium ion as the active center now span the broad spectral range of 695 - 1345 nm. The most interesting and distinguishing feature of laser action in $Cr:Mg_2SiO_4$ is that the lasing ion is not trivalent chromium (Cr^{3+}), as is the case with the rest of the chromium-based lasers. Available experimental data suggest that the active ion is tetravalent chromium (Cr^{4+}). In this paper, we present spectroscopic results which indicate that the lasing ion is Cr^{4+} and review the properties of laser action in this crystal.

Spectroscopic Properties

Forsterite is a member of the olivine family of crystals and is a naturally occurring gem. Single crystals of chromium-doped forsterite have been grown successfully using the Czochralski method,[6] as well as the laser-heated pedestal growth (LHPG) technique.[7] The general features of the absorption and emission spectra of Cr:forsterite grown by the two methods are similar. The spectroscopic properties distinctly depend on the growth atmosphere. In this work, we present measurements performed with Czochralski-grown crystals.

Earlier spectroscopic work[8] on chromium-doped forsterite was based on the assumption that only trivalent chromium (Cr^{3+}) substitutes for the octahedrally coordinated Mg^{2+} ions in Mg_2SiO_4 host. There are two inequivalent Mg^{2+} sites in forsterite, one with mirror symmetry (C_s) and the other with inversion symmetry (C_i). Trivalent chromium ion enters the mirror and the inversion site in a ratio of 3:2. The existence of Cr^{3+} ions in the two sites in the ratio given above has been verified by

1-55752-111-5/89/$2.00

EPR and ENDOR measurements as well.[9,10] Our recent spectroscopic measurements indicate that, in addition to Cr^{3+} ions in those sites, tetrahedrally coordinated Cr^{4+} ions are also present in the Czochralski-grown forsterite. Similar conclusions have been reached for crystals grown by LHPG method as well.[7]

The relative concentration of Cr^{3+} and Cr^{4+} ions in Mg_2SiO_4 depends on the growth atmosphere. By growing the crystal in a reducing atmosphere the relative concentration of Cr^{4+} ions can be reduced and that of Cr^{3+} increased. We will compare measurements on crystals grown under standard conditions with those grown in reducing atmosphere, and attempt to identify the contributions from different centers.

The absorption spectrum of $Cr:Mg_2SiO_4$ grown under standard conditions (referred to as sample 1, henceforth), for different orientation of the crystal are shown in Fig. 1.

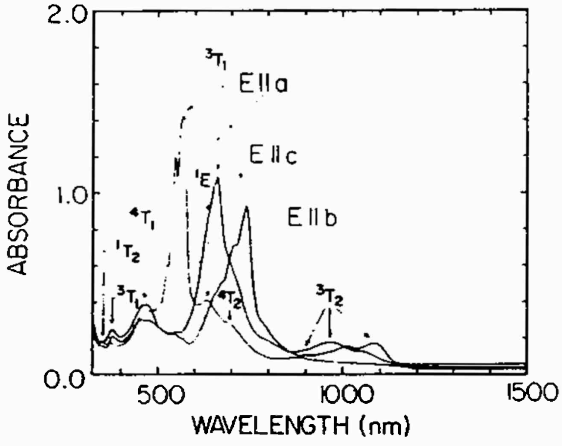

Fig. 1 Room temperature absorption spectrum of $Cr:Mg_2SiO_4$ grown under standard conditions for all three crystal orientations.

The spectrum is characterized by three broad absorption bands spanning the near ultraviolet to near infrared spectral regions. At liquid nitrogen temperature, the near infrared absorption band spanning the 850 - 1150 nm range shows a sharp zero-phonon line followed by an elaborately structured sideband. The absorption spectra depend strongly on the polarization of the incident radiation with respect to the crystallographic axes of the host. In particular, the peak position of the strongest band in the red-green spectral region shifts considerably with the polarization. Smaller shift has been observed in the near infrared region as well.

To distinguish between the contributions from Cr^{3+} and Cr^{4+} ions to the absorption spectra, we have complemented the absorption spectrum in Fig. 1 by the spectrum of sample 2, shown in Fig. 2.

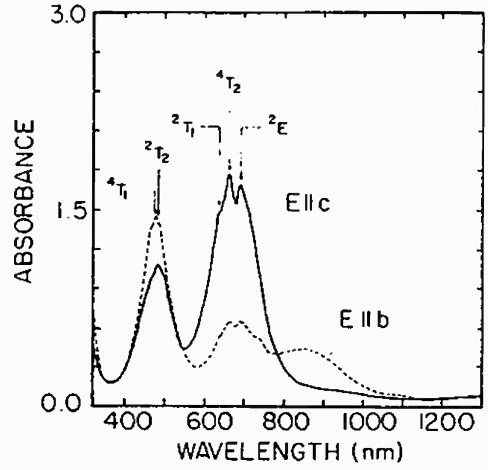

Fig. 2 Room temperature absorption spectrum of $Cr:Mg_2SiO_4$ grown in a reducing atmosphere for two different crystal orientations.

Sample 2 was grown in a reducing atmosphere and contains mostly Cr^{3+} ions as compared to sample 1 which has both the Cr^{3+} and Cr^{4+} centers. The near infrared absorption band is almost missing in the spectrum of sample 2, which implies that the band is due to transitions within the states of Cr^{4+} ion. We attribute this band to absorptive transitions from the $^3A_2$ ground state of the Cr^{4+} ion to the $^3T_2$ state.

For the visible and the near ultraviolet absorption the contributions from the two valence states cannot be distinguished so easily. The absorption due to Cr^{3+} and Cr^{4+} ions overlap in these spectral regions. To gain further insight, we have analyzed both the spectra in terms of Tanabe-Sugano formalism.[11] We have taken Cr^{3+} to be in octahedrally coordinated sites and Cr^{4+} to be in tetrahedrally coordinated sites. Comparison of the predicted values of

tetrahedral Cr^{4+} and octahedral Cr^{3+} in forsterite with the measured values are presented in Tables 1 and 2, respectively. The values of crystal field parameter Dq and Raccah parameters B and C are also listed. The transition assignments in Figs. 1 and 2 follow from this analysis.

TABLE 1: Energy Levels of Cr^{4+}:Mg_2SiO_4

Transition	Energy (cm^{-1}) Measured	Predicted
$^3A_2 \rightarrow {}^3T_2$	9,150	(9,150)
$^3A_2 \rightarrow {}^3T_1$	15,430	15,150
$^3A_2 \rightarrow {}^1E$	15,875	16,245
$^3A_2 \rightarrow {}^3T_1$	26,810	26,800
$^3A_2 \rightarrow {}^1T_2$	28,735	28,700
$^3T_2 \rightarrow {}^3A_2$	8,750	(8,750)

Predicted values are based on Tanabe-Sugano diagram for tetrahedral Cr^{4+} with parameters: B=970 cm^{-1}, C=3,980 cm^{-1}, and Dq=915 cm^{-1}. For bands whose position vary with the polarization of the incident light, average position (the centroid of three bands marked $^3T_1$ in Fig. 1, for example) is taken for this analysis.

TABLE 2: Energy Levels of Cr^{3+}:Mg_2SiO_4

Transition	Energy (cm^{-1}) Measured	Predicted
$^4A_2 \rightarrow {}^4T_2$	15,100	(15,100)
$^4A_2 \rightarrow {}^2E$	14,450	14,600
$^4A_2 \rightarrow {}^2T_1$	15,380	15,300
$^4A_2 \rightarrow {}^2T_2$	21,050	21,300
$^4A_2 \rightarrow {}^4T_{1a}$	21,500	21,780
$^4A_2 \rightarrow {}^4T_{1b}$	33,780	33,940
$^4T_2 \rightarrow {}^4A_2$	11,100	(11,100)
$^2E \rightarrow {}^4A_2$	14,450	14,600

Predicted values are based on the Tanabe-Sugano diagram for octahedral Cr^{3+} with parameters: B=695 cm^{-1}, C=3,130 cm^{-1}, and Dq=1,510 cm^{-1}.

The Tanabe-Sugano diagrams, with transitions indicated, are presented in Figs. 3 and 4.

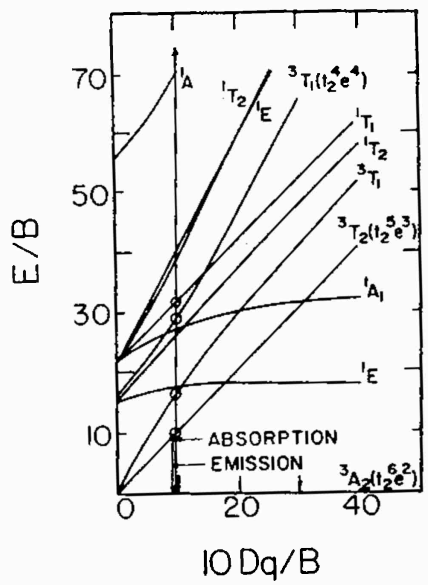

Fig. 3 Tanabe-Sugano diagram for Cr^{4+} in tetrahedral coordination. The values Dq=915 cm^{-1} and B=970 cm^{-1} were used to assign transitions shown in Fig. 1 and listed in Table 1.

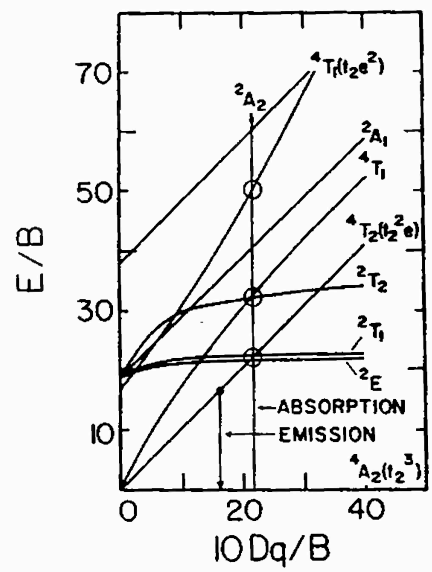

Fig. 4 Tanabe-Sugano diagram for Cr^{3+} in octahedral coordination. The values Dq=1510 cm^{-1} and B=695 cm^{-1} were used to assign transitions shown in Fig. 2 and listed in Table 2.

The polarization dependence of the absorption spectra may be explained in terms of lower site symmetry of

chromium ions invoking the polarization selection rules. A detailed analysis of polarization dependence of spectral properties will be presented in a forthcoming publication.

The fluorescence spectra of Cr:forsterite taken for the Cr^{4+}-rich sample (sample 1) are shown in Figs. 5 and 6, and that of sample 2 (mostly Cr^{3+}-containing) in Fig. 7.

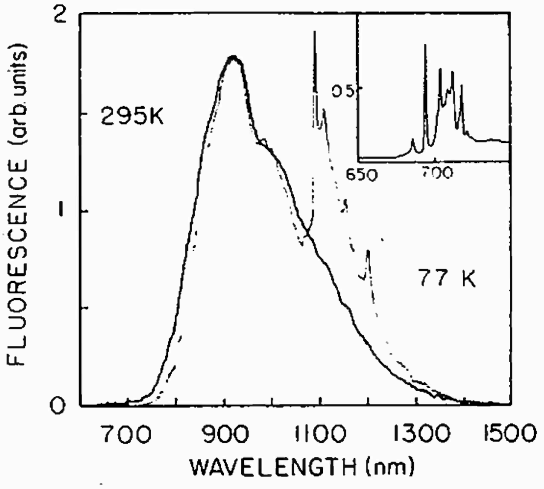

Fig. 5 Room temperature (thicker line) and liquid nitrogen temperature (thin line) fluorescence spectrum of Cr:Mg_2SiO_4 grown under standard conditions for 488-nm excitation parallel to b axis. The spectra were taken with PbS detector which was not sensitive enough to detect the 692-nm zero-phonon line and its sideband shown in the inset. These features were resolved with a photomultiplier tube with S-20 response.

The room temperature spectrum taken with sample 1, excited by the 488-nm line of Ar^+ laser, is a broad band spanning 680 - 1400 nm range. At liquid nitrogen temperature the spectrum breaks up into three structured bands. The fluorescence covering the 1100 - 1400 nm range is the Stokes-shifted counterpart of the near infrared absorption, and is attributed to $^3T_2 \rightarrow {}^3A_2$ transitions in Cr^{4+} ion. The sharp zero-phonon line corresponds to purely electronic transition between the $^3T_2$ and $^3A_2$ states and appears as a prominent feature in both absorption and emission spectra. Near infrared room temperature and liquid nitrogen temperature absorption and fluorescence spectra (fluorescence excited by 1064-nm radiation) for E ⊥ b axis are shown in Fig. 6. Features displayed in Fig. 6 are completely absent from the near infrared spectra of sample 2.

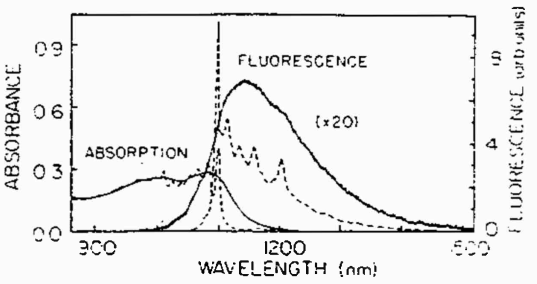

Fig. 6 Room temperature (solid line) and liquid nitrogen temperature (broken line) absorption and fluorescence spectra (fluorescence excited by 488-nm radiation) of Cr:Mg_2SiO_4 grown under standard conditions for E ⊥ b axis.

The sharp line at 692 nm observed at liquid nitrogen temperature is tentatively attributed to $^2E \rightarrow {}^4A_2$ transition (R-line) in Cr^{3+} ions. This line, followed by a structured sideband that extends to 750 nm is also present in the fluorescence spectrum of sample 2. These features are shown as insets in Figs. 5 and 7.

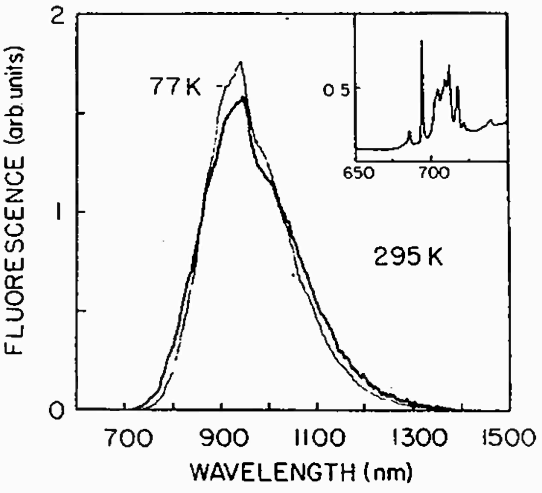

Fig. 7 Room temperature (thicker line) and liquid nitrogen temperature (thin line) fluorescence spectrum of Cr:Mg_2SiO_4 grown in a reducing atmosphere for 488-nm excitation and E ⊥ b axis. The spectra were taken with PbS detector which was not sensitive enough to detect the 692-nm zero-phonon line and its sideband shown in the inset. These features were resolved with a photomultiplier tube with S-20 response.

The room temperature spectrum of sample 2 extends only to 1200 nm, and shows contribution from Cr^{3+} ions predominantly.

The emission transitions for both Cr^{3+} and Cr^{4+} ions are indicated in the Tanabe-Sugano diagrams. Detailed analysis of the emission spectra will be presented in a forthcoming paper.

We have measured fluorescence lifetime as a function of wavelength both at room and liquid nitrogen temperatures using streak camera coupled to a spectrometer. The fluorescence lifetime for Cr^{4+} emission in 1100-1400 nm range is 2.7 μs at room temperature, and 25 μs at liquid nitrogen temperature. The 15 μs lifetime measured at shorter wavelengths, characteristics of Cr^{3+} fluorescence, did not change significantly at liquid nitrogen temperature. Temperature dependence of the fluorescence lifetime indicates presence of strong nonradiative relaxation for Cr^{4+} ions, which is not so prominent for Cr^{3+} ions in this temperature range.

Laser Operation

I. Pulsed Laser Action

Laser experiments were conducted with samples rich in Cr^{4+} in a stable cavity. Details of the cavity arrangement have been described elsewhere.[1,5] The fundamental and the second harmonic emissions from a Q-switched Nd:YAG laser operating at 10-Hz repetition rate were used for excitation of the near infrared and the visible bands, respectively. Pulsed laser action was observed for both the 1064-nm and 532-nm pumping.[1] The amplitude and duration of the Cr:Mg_2SiO_4 laser pulse, as well as its delay with respect to the pump pulse, varied with the pump pulse energy fluctuation. For similar level of excitation and within the time resolution of the experiment, no difference in the delay between the pump pulse and the output laser pulse for the two pump wavelengths was observed.The spectra of the free-running laser radiation for both the 1064-nm and 532-nm pumping peaked at 1235 nm and had linewidth of 30 nm and 27 nm, respectively. These facts clearly indicate that the same center is responsible for laser action for both the 1064-nm and 532-nm excitations. For 532-nm pumping there is a fast transfer of excitation from the states directly pumped to the upper lasing level. In case of 1064-nm pumping the lasing level is directly populated. Similar results were obtained for pumping with the 629-nm radiation obtained by stimulated Raman scattering of the 532-nm radiation in ethanol.

To improve the laser performance sample 1 was anti-reflection coated such that reflectivity over the 1050-1250 nm range was less than 0.5 %. Attempts were made to overlap the pump beam and the cavity mode more accurately. The sample was longitudinally pumped by 1064-nm, 10-ns pulses from a Q-Switched Nd:YAG laser in a cavity similar to that used earlier. Different sets of laser mirrors were used. Summary of laser performance for three different laser cavities is presented in Table 3. Center wavelengths shown in Table 3 differ for three different output couplers since those have slightly different wavelength-dependent transmission characteristics.

TABLE 3: Summary of Laser Parameters for Pulsed Laser Operation (1064-nm pumping)

Parameter	Output Coupling 13%	2%	6%
Lasing Wavelength	1200 nm	1235 nm	1250 nm
Free-running Bandwidth	-	30 nm	-
Threshold Abs. Energy	0.38 mJ	0.20 mJ	0.27 mJ
Slope Efficiency	22.8%	5.1%	12.1%
Gain Cross Section (10^{-19} cm^2)	1.40	1.44	1.40

Output energy of the forsterite laser as a function of absorbed pump energy for three different output couplers is shown in Fig. 8.

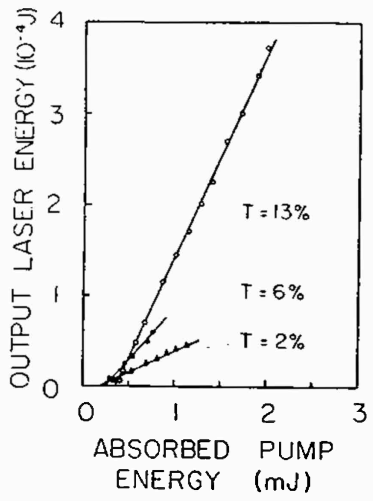

Fig. 8 Output energy of Cr:Mg_2SiO_4 laser as a function of absorbed pump energy for 1064-nm pumping and E ⊥ b axis for three different output couplers.

Using data from Table 4 we have estimated the passive loss L of the forsterite laser and calculated the laser gain cross section. Passive (internal) loss L can be estimated by taking the ratio of the threshold pump energies for two different output mirrors or taking the ratio of slope efficiencies,[12] assuming that

$$E_{thi} \sim L + T_i \qquad (1)$$

and

$$\eta_i \sim T_i/(L+T_i),\ i = 1,2 \qquad (2)$$

where T_i is the output mirror transmission. Loss L is then given by

$$L = (T_2 - R_{th}T_1)/(R_{th} - 1) \qquad (3)$$

where

$$R_{th} = E_{th2}/E_{th1}, \qquad (4)$$

or

$$L = (R_\Delta - 1)T_1T_2/(T_2 - R_\Delta T_1) \qquad (5)$$

where

$$R_\Delta = \eta_2/\eta_1. \qquad (6)$$

For various combinations of output mirrors a value of 11% for L was obtained by using both techniques.

Laser gain cross section shown in Table 4 for three different output mirrors was calculated using the expression[13]

$$\sigma = \frac{\pi\tau_P h\nu_P \omega_L^2 (L+T)(a^2+1)}{4\tau\left[1-\exp(-\alpha l)\right]\left[1-\exp(-\tau_P/\tau)\right]E_{Pth}} \qquad (7)$$

where τ_P is the pump pulsewidth, $h\nu_P$ is the pump photon energy, ω_L is the cavity mode spot size, L is laser internal loss, T is the output mirror transmission, $a=\omega_P/\omega_L$, where ω_P is the pump beam spot size, τ is the upper lasing level radiative lifetime taken to be ~25 μs, α is the absorption coefficient for the pump radiation, l is the length of the crystal, and E_{Pth} is the threshold pump energy incident on the crystal.

II. Continuous-Wave Laser Operation

To obtain cw laser action a sample of chromium-doped forsterite (sample 1) was placed at the center of a nearly concentric cavity formed by two 5-cm radius-of-curvature mirrors such that a cavity mode waist was 75 μm. The output mirror was dielectric coated to have ~1% transmission for the 1175 - 1250 nm range, and to transmit most of the 1064-nm pump beam. The pump radiation from a cw Nd:YAG laser was focused by a 75-mm focal length lens to pump the sample longitudinally along the 30 mm path length. The pump beam was linearly polarized along the b axis and propagated along the a axis of the crystal . The beam was chopped at a duty factor of 9:1 to reduce heating effects. The waist of the pump beam at the center of the sample was measured to be 70 μm.

Quasi-cw laser operation was obtained for pumping above the lasing threshold of 1.25 W of absorbed power. The measured slope efficiency was 6.8%. The cw output power of the Cr:forsterite laser as a function of absorbed pump power is displayed in Fig. 9. Laser operation was possible even when the pump beam was not chopped, but at 40% reduced output indicating losses induced by local heating.

The spectrum of the free-running laser output peaks at 1244 nm and has a bandwidth of 12 nm.

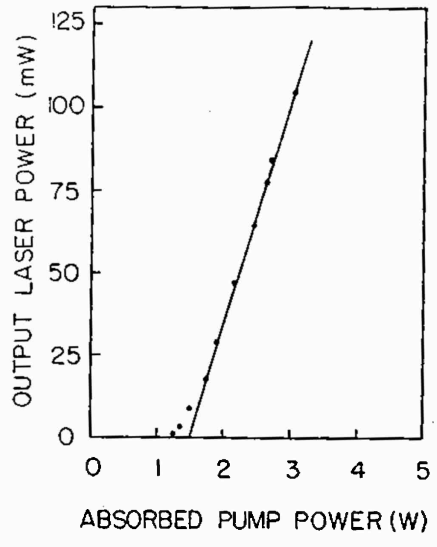

Fig. 9 Output power of the cw $Cr:Mg_2SiO_4$ laser as a function of absorbed pump power.

Using results obtained from CW lasing experiment several important parameters can be estimated. From an expression for the slope efficiency[13]

$$\eta = \lambda_P T/\lambda_L(L+T) \qquad (8)$$

where T is the total transmission of the cavity mirrors, L is the internal loss, and λ_P and λ_L are pump and lasing wavelengths, respectively, a value of 12.7% for L has been estimated. This value is in reasonable agreement with the value of 11% obtained from pulsed measurements.

An expression similar to Eq. (7)

$$P_{th} = \frac{\pi h\nu_P \omega_L^2 (L+T)(a^2+1)}{4\sigma\eta\left[1-\exp(-\alpha l)\right]} \qquad (9)$$

where P_{th} is the incident threshold pump power, was used to calculate the gain cross section from the CW measurements. A value of 1.47×10^{-19} cm^2 was obtained, in excellent agreement with the one obtained from pulsed laser experiments. Both values should be compared to the value of 1.98×10^{-19} cm^2 obtained from radiative lifetime and lineshape measurements. The discrepancy can arise from another loss mechanism such as excited state absorption.

From the gain cross section and threshold pump power, the threshold population inversion density was estimated using the threshold condition:[14]

$$2\sigma N_{th} l = L+T \qquad (10)$$

A value of 1.6×10^{17} cm^{-3} for the population inversion was calculated.

The key continuous-wave laser parameters are summarized in Table 5.

TABLE 5: Properties of cw Laser Operation of $Cr:Mg_2SiO_4$ Laser

Property	Value
Lasing Wavelength	1244 nm
Spectral Bandwidth (FWHM)	12 nm
Lasing Threshold (Absorbed Power)	1.25 W
Slope Efficiency	6.8%
Threshold Inversion Density	1.6×10^{17} cm^{-3}
Gain Cross Section	1.47×10^{-19} cm^2

III. Tunable Operation of Forsterite Laser

Tunable operation of Cr:forsterite laser has been obtained over the 1167 - 1345 nm spectral range,[5] extending the tuning range of chromium-doped laser crystals further into near infrared.

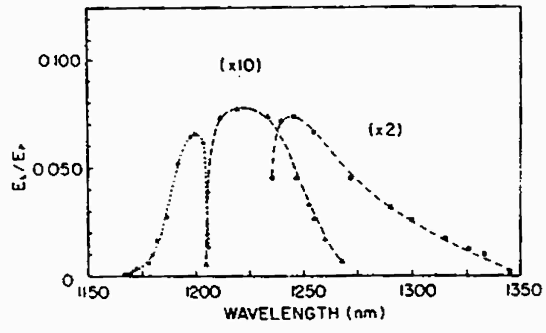

Fig. 10 The ratio of $Cr:Mg_2SiO_4$ laser output (E_L) to the absorbed pump energy (Ep) as a function of wavelength. The three curves correspond to the three output couplers used in tuning measurements.

Three different cavities, with a birefringent, single crystal quartz plate at

Brewster's angle as the intracavity dispersive element were used to obtain smooth continuous tuning. The ratio of the Cr:forsterite laser output to the absorbed pump energy as a function of wavelength is shown in Fig.10. The laser output peaks at 1200 nm with an energy per pulse of 125 μJ for an input absorbed energy of 1.9 mJ. The scale changes for the three curves arise from the differences in transmissions of the output coupling mirrors used in the three cavities.

Conclusion

Measurements of absorption and emission spectra , as well as the wavelength dependence of fluorescence lifetime provides convincing evidence that chromium ion may enter forsterite (Mg_2SiO_4) host in more than one valence states. Trivalent chromium (Cr^{3+}) enters substitutionally for divalent magnesium (Mg^{2+}) in two inequivalent octahedrally-coordinated sites, while tetravalent chromium (Cr^{4+}) substitutes presumably for Si^{4+} at tetrahedrally coordinated sites. Of the two Cr^{3+} centers, the one with mirror symmetry (C_s) is optically active and accounts for a number of features in absorption and emission spectra. The absorption and emission due to transitions within the states of Cr^{4+} ion overlap with those within the states of Cr^{3+} ion. The absorption and emission in the near infrared spectral region between 850 and 1150 nm is primarily due to transitions between the $^3A_2$ ground state and the first excited state $^3T_2$, of the Cr^{4+} ion. The four-level, vibronic mode of laser operation in Cr-doped forsterite feeds on $^3T_2 \rightarrow {}^3A_2$ transition.

Chromium-doped forsterite is an important laser in the near-infrared spectral region. It can be operated both in the pulsed and cw mode of operation and is tunable over 1167 - 1345 nm range. The large fluorescence bandwidth promises ultrashort pulse generation through mode-locked operation. Since large single crystals can be easily grown, the crystal has potential for being used as an amplifier medium in the near infrared spectral region.

Acknowledgments

We thank K. Yamagishi of Mitsui Mining and Smelting Co. of Japan for growing the Cr:Mg_2SiO_4 crystals used in this study, and A. Seas, Y. Takiguchi, and Y. Budansky for technical help. The research is supported by the Army Research Office, National Aeronautics and Space Administration, and City College of New York Organized Research.

References

1. V. Petričević, S. K. Gayen, R. R. Alfano, K. Yamagishi, H. Anzai, and Y. Yamaguchi, Appl. Phys. Lett. **52**, 1040 (1988); V. Petričević, S. K. Gayen, and R. R. Alfano, Appl. Phys. Lett. **53**, 2590 (1988).

2. For a list of Cr-based tunable solid state lasers see J. A. Caird, S. A. Payne, P. R. Staver, A. J. Ramponi, L. L. Chase, and W. F. Krupke, IEEE J. Quantum Electron. **24**, 1077 (1988), and references therein.

3. A. A. Kaminskii et. al., Inorg. Mater., **24**, 579 (1988).

4. V. Petričević, S. K. Gayen, and R. R. Alfano, Opt. Lett. **14**, 612 (1989).

5. V. Petričević, S. K. Gayen, and R. R. Alfano, Appl. Opt. **28**, 1609 (1989).

6. N. Nishide, Y. Segawa, P. H. Kim, S. Namba, and A. Masuyama, Reza Kagaku Kenkyu **7**, 89 (1985).

7. H. R. Verdun, L. M. Thomas, D. M. Andrauskas, T. McCollum, and A. Pinto, Appl. Phys. Lett. **53**, 2593 (1988).

8. H. Rager and G. Weiser, Bull. Mineral. **104**, 603 (1981).

9. H. Rager, Phys. Chem. Minerals **1**, 371 (1977).

10. L. V. Bershov, J. M. Gaite, S. S. Hafner, and H. Rager, Phys. Chem. Minerals **9**, 95 (1983).

11. S. Sugano, Y. Tanabe, and H. Kamimura, *Multiplets of Transition-Metal Ions in Crystals*, Academic, New York, 1970.

12. P. F. Moulton, J. Opt. Soc. Am. B, **3**, 125 (1986).

13. P. F. Moulton, IEEE J. Quantum Electron. **QE-21**, 1582 (1985).

14. H. G. Danielmeyer, in *Lasers*, A. K. Levine and A. De Maria, eds. (Dekker, New York, 1975), Vol. IV.

12. R. R. Alfano, V. Petričević, and A. Seas, "Chromium-Doped Forsterite Laser", in *Proceedings of the International Conference on Lasers '89,* December, 1989, New Orleans, Louisiana.

REPRINTED FROM PROCEEDINGS OF THE INTERNATIONAL CONFERENCE ON LASERS '89, DECEMBER 5-8, 1989

CHROMIUM DOPED FORSTERITE LASER

R. R. Alfano*, V. Petričević, and A. Seas
Institute for Ultrafast Spectroscopy and Lasers
The City College of New York
138th Street & Convent Avenue
New York, NY10031

Abstract

Spectroscopic, quantum electronic, and laser properties of chromium-doped forsterite ($Cr:Mg_2SiO_4$) are reviewed. Spectroscopic data suggest that the lasing center in chromium-doped forsterite is tetravalent chromium ion (Cr^{4+}), not the common trivalent chromium (Cr^{3+}). Pulsed, continuous-wave, and tunable operation in the 1167-1345nm region are presented.

Introduction

During the last 10 years tunable solid state lasers have emerged as an alternative to dye lasers. Dye lasers have the advantage of high gain, low cost, and there are many dyes spanning the visible and near infrared region. Many disadvantages of dye lasers such as toxicity, poor long term reliability, narrow wavelength range, make dye lasers unsuitable for hospital, airborn, mobile, or spaceborn use. Tunable solid state lasers are expensive to build and have lower gain coefficient. On the other hand, tunable solid state lasers offer broad tunability range, higher reliability, compactness and long term stability.

Chromium-doped forsterite ($Cr:Mg_2SiO_4$) laser is an important member of the ever growing family of tunable solid state lasers based on chromium ion as the lasing center.[1-3] Pulsed[1] and continuous-wave[4] laser operation have been achieved for 532-nm and 1064-nm. The tuning range now covers the 1167 - 1345 nm range.[5] The most interesting and distinguishing feature of laser action in $Cr:Mg_2SiO_4$ is that the lasing ion is not trivalent chromium (Cr^{3+}), as is the case with the rest of the chromium-based lasers, the active ion is tetravalent chromium (Cr^{4+}).

In this presentation, we review the spectroscopic and laser properties of chromium doped forsterite

Spectroscopic Properties

The spectroscopic properties of forsterite distinctly depend on the growth atmosphere since the relative concentration of Cr^{3+} and Cr^{4+} ions in Mg_2SiO_4 depends on the growth atmosphere. Growing the crystal in a reducing atmosphere the relative concentration of Cr^{4+} ions can be reduced and that of Cr^{3+} increased. We will compare measurements on crystals grown by Czochralski[6] method under standard conditions with those grown in reducing atmosphere, and attempt to identify the contributions from different centers.

Earlier spectroscopic work[8] on chromium-doped forsterite was based on the assumption that only trivalent chromium (Cr^{3+}) substitutes for the octahedrally coordinated Mg^{2+} ions in Mg_2SiO_4 host. There are two inequivalent Mg^{2+} sites in forsterite, one with mirror symmetry (C_s) and the other with inversion symmetry (C_i). Trivalent chromium ion enters the inversion and the mirror site in a ratio of 3:2. The existence of Cr^{3+} ions in the two sites in the ratio given above has been verified by EPR and ENDOR measurements.[9,10] Our recent spectroscopic measurements indicate that, in addition to Cr^{3+} ions in those sites, tetrahedrally coordinated Cr^{4+} ions are also present in the Czochralski-grown forsterite. Similar conclusions have been reached for crystals grown by LHPG method as well.[7]

The absorption spectrum of $Cr:Mg_2SiO_4$ grown under standard conditions (referred to as sample 1, henceforth), for different orientation of the crystal are shown in Fig. 1. The spectra are characterized by three broad absorption bands spanning the near ultraviolet to near infrared spectral regions. The absorption spectra depend strongly on the polarization of the incident radiation with respect to the crystallographic axes of the host. In particular, the peak position of the strongest band in the red-green spectral region shifts considerably with the polarization. Smaller shift has been observed in the near infrared region as well. The polarization dependence of the absorption spectra may be explained in terms of lower site symmetry of chromium ions invoking the polarization selection rules.

To distinguish between the contributions from Cr^{3+} and Cr^{4+} ions to the absorption spectra, we have complemented the absorption spectrum in Fig. 1 by the spectrum of sample 2 which was grown in a reducing atmosphere, shown in Fig. 2. Sample 2 contains mostly Cr^{3+} ions as compared to sample 1 which has both the Cr^{3+} and Cr^{4+} centers. The near infrared absorption band is almost missing in the spectrum of sample 2, which implies that the band is due to transitions within the states of Cr^{4+} ion.

For the visible and the near ultraviolet absorption regions the contributions from the two valence states cannot be distinguished so easily since the absorptions due to Cr^{3+} and Cr^{4+} ions overlap in these spectral regions. To gain further insight, we have analyzed both the spectra in terms of Tanabe-Sugano formalism.[11]

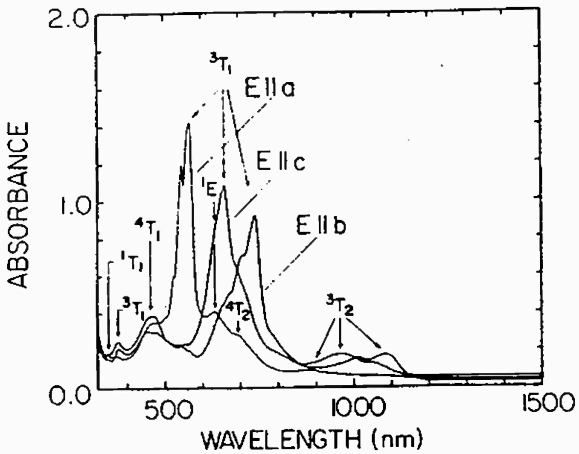

Fig. 1 Room temperature absorption spectrum of $Cr:Mg_2SiO_4$ grown under standard conditions for all three crystal orientations

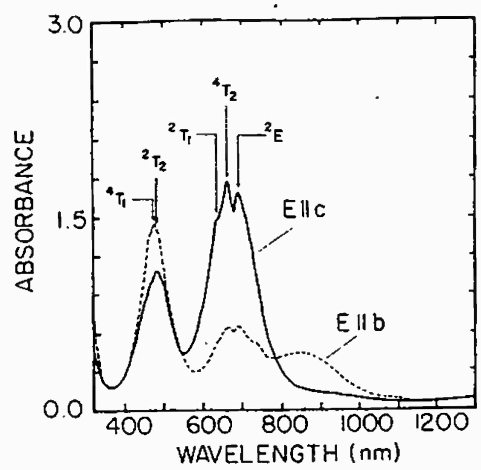

Fig. 2 Room temperature absorption spectrum of $Cr:Mg_2SiO_4$ grown in a reducing atmosphere for two different crystal orientations.

We have taken Cr^{3+} to be in octahedrally coordinated sites and Cr^{4+} to be in tetrahedrally coordinated sites. Comparison of the predicted values of tetrahedral Cr^{4+} and octahedral Cr^{3+} in forsterite with the measured values are presented in Tables 1 and 2, respectively. The transition assignments in Figs. 1 and 2 follow from this analysis.

TABLE 1: Energy Levels of $Cr^{4+}:Mg_2SiO_4$

Transition	Energy (cm^{-1}) Measured	Predicted
$^3A_2 \rightarrow {}^3T_2$	9,150	(9,150)
$^3A_2 \rightarrow {}^3T_1$	15,430	15,150
$^3A_2 \rightarrow {}^1E$	15,875	16,245
$^3A_2 \rightarrow {}^3T_1$	26,810	26,800
$^3A_2 \rightarrow {}^1T_1$	28,735	28,700
$^3T_2 \rightarrow {}^3A_2$	8,750	(8,750)

TABLE 2: Energy Levels of $Cr^{3+}:Mg_2SiO_4$

Transition	Energy (cm^{-1}) Measured	Predicted
$^4A_2 \rightarrow {}^4T_2$	15,100	(15,100)
$^4A_2 \rightarrow {}^2E$	14,450	14,600
$^4A_2 \rightarrow {}^2T_1$	15,380	15,300
$^4A_2 \rightarrow {}^2T_2$	21,050	21,300
$^4A_2 \rightarrow {}^4T_{1a}$	21,500	21,780
$^4A_2 \rightarrow {}^4T_{1b}$	33,780	33,940
$^4T_2 \rightarrow {}^4A_2$	11,100	(11,100)
$^2E \rightarrow {}^4A_2$	14,450	14,600

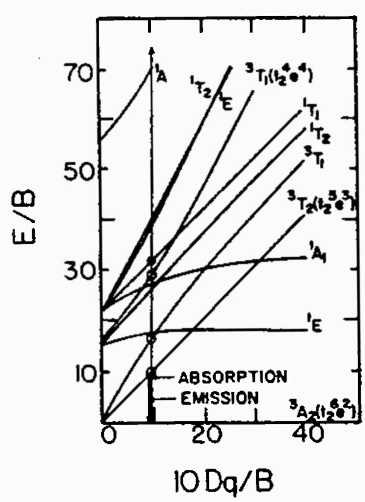

Fig. 3 Tanabe-Sugano diagram for Cr^{4+} in tetrahedral coordination.

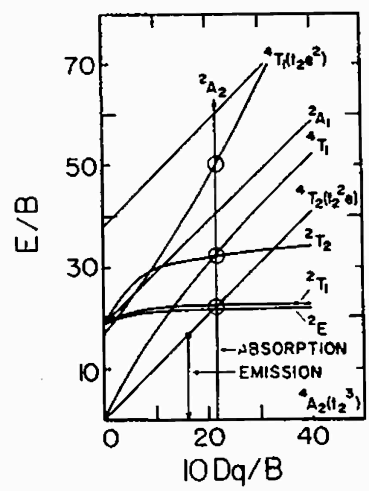

Fig. 4 Tanabe-Sugano diagram for Cr^{3+} in octahedral coordination.

Predicted values given in Table 1 are based on Tanabe-Sugano diagram for tetrahedral Cr^{4+} with parameters: B=970 cm^{-1}, C=3,980 cm^{-1}, and Dq=915 cm^{-1}. For bands whose position vary with the polarization of the incident light, average position (the centroid of three bands marked $^3T_1$ in Fig. 1, for example) is taken for this analysis. Predicted values shown in Table 2 are based on the Tanabe-Sugano diagram for octahedral Cr^{3+} with parameters: B=695 cm^{-1}, C=3,130 cm^{-1}, and Dq=1,510 cm^{-1}. The Tanabe-Sugano diagrams, with transitions indicated, are presented in Figs. 3 and 4.

The fluorescence spectra of Cr:forsterite taken for the Cr^{4+}-rich sample (sample 1) are shown in Figs. 5 and 6. The spectra for sample 2 (containing mostly Cr^{3+}) are shown in Fig. 7. The room temperature spectrum taken with sample 1, excited by the 488-nm line of Ar^+ laser, is a broad band spanning 680 - 1400 nm range. At liquid nitrogen temperature the spectrum breaks up into three structured bands. The fluorescence covering the 1100 - 1400 nm range is the Stokes-shifted counterpart of the near infrared absorption, and is attributed to $^3T_2 \rightarrow {}^3A_2$ transitions in Cr^{4+} ion. The sharp zero-phonon line corresponds to purely electronic transition between the $^3T_2$ and $^3A_2$ states and appears as a prominent feature in both absorption and emission spectra. Near infrared room temperature and liquid nitrogen temperature absorption and fluorescence spectra (fluorescence excited by 1064-nm radiation) for E||b axis are shown in Fig. 6. Features displayed in Fig. 6 are completely absent from the near infrared spectra of sample 2.

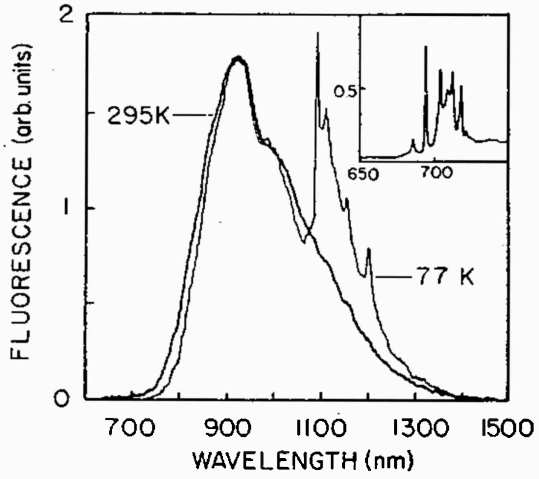

Fig. 5 Room temperature (thicker line) and liquid nitrogen temperature (thin line) fluorescence spectrum of $Cr:Mg_2SiO_4$ grown under standard conditions for 488-nm excitation parallel to b axis.

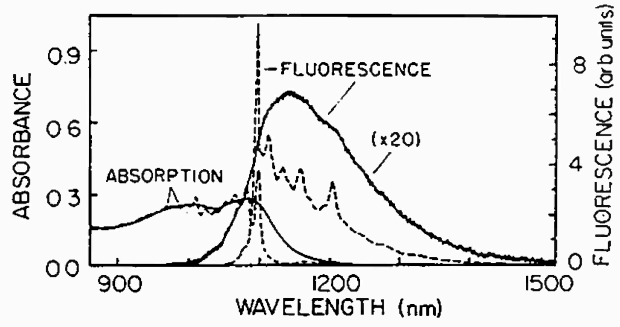

Fig. 6 Room temperature (solid line) and liquid nitrogen temperature (broken line) absorption and fluorescence spectra (fluorescence excited by 488 nm radiation) of $Cr:Mg_2SiO_4$ grown under standard conditions for E || b axis.

The sharp line at 692 nm observed at liquid nitrogen temperature is attributed to $^2E \rightarrow {}^4A_2$ transition (R-line) in Cr^{3+} ions. This line, followed by a structured sideband that extends to 750 nm is also present in the fluorescence spectrum of sample 2. These features are shown as insets in Figs. 5 and 7.

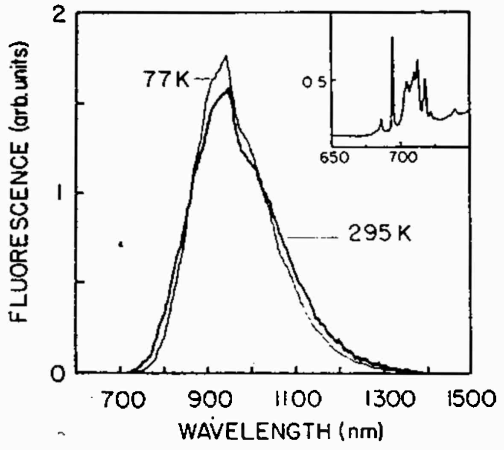

Fig. 7 Room temperature (thicker line) and liquid nitrogen temperature (thin line) fluorescence spectrum of $Cr:Mg_2SiO_4$ grown in a reducing atmosphere for 488-nm excitation and E || b axis. The spectra were taken with PbS detector which was not sensitive enough to detect the 692-nm zero-phonon line and its sideband shown in the inset. These features were resolved with a photomultiplier tube with S-20 response.

The room temperature spectrum of simple 2 extends only to 1200 nm, and shows contribution from Cr^{3+} ions predominantly. The emission transitions for both Cr^{3+} and Cr^{4+} ions are indicated in the Tanabe-Sugano diagrams.

We have measured fluorescence lifetime as a function of wavelength both at room and liquid nitrogen temperatures using streak camera coupled to a spectrometer. The fluorescence lifetime for Cr^{4+} emission in 1100-1400 nm range is 2.7 μs at room temperature, and 25 μs at liquid nitrogen temperature. The 15 μs lifetime measured at shorter wavelengths, characteristics of Cr^{3+} fluorescence, did not change significantly at liquid nitrogen temperature. Temperature dependence of the fluorescence lifetime indicates presence of strong nonradiative relaxation for Cr^{4+} ions, which is not so prominent for Cr^{3+} ions in this temperature range.

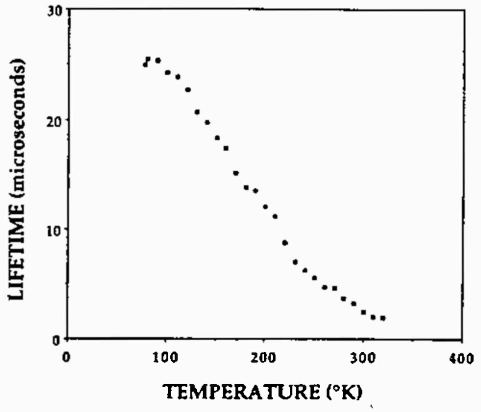

Fig. 8 Temperature dependence of the fluorescence lifetime of chromium-doped forsterite for 1064-nm excitation.

Laser Operation

I. Pulsed Laser Action

Laser experiments were conducted with samples rich in Cr^{4+} in a stable cavity. Details of the cavity arrangement is shown in figure 9 and have been described elsewhere.[1,5]

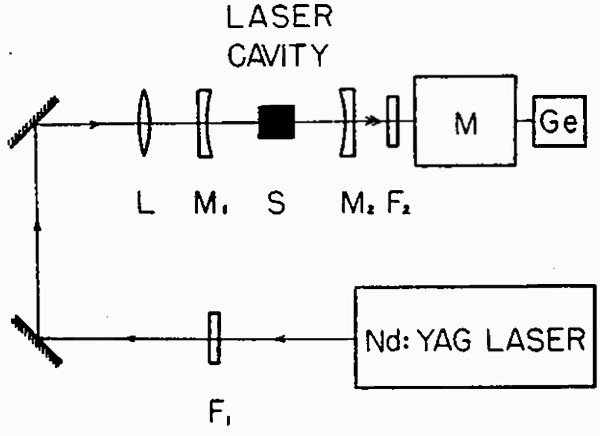

Fig. 9. Cavity arrangement for the forsterite laser

The fundamental and the second harmonic beams from a Q-switched Nd:YAG laser operating at 10-Hz repetition rate were used for excitation of the near infrared and the visible bands. Pulsed laser action was observed for both the 1064-nm and 532-nm pumping.[1] The amplitude and duration of the $Cr:Mg_2SiO_4$ laser pulse, as well as its delay with respect to the pump pulse, varied with the pump pulse energy fluctuation. For similar level of excitation and within the time resolution of the experiment, no difference in the delay between the pump pulse and the output laser pulse for the two pump wavelengths was observed. The spectra of the free-running laser radiation for both the 1064-nm and 532-nm pumping peaked at 1235 nm and had linewidth of 30 nm and 27 nm, respectively. These facts clearly indicate that the same center is responsible for laser action for both the 1064-nm and 532-nm excitations. In case of 1064-nm pumping the lasing level is directly populated. Similar results were obtained for pumping with the 629-nm radiation obtained by stimulated Raman scattering of the 532-nm radiation in ethanol.

To improve the laser performance, sample 1 was anti-reflection coated such that reflectivity over the 1050-1250 nm range was less than 0.5 %. Attempts were made to overlap the pump beam and the cavity mode more accurately. The sample was longitudinally pumped by 1064-nm, 10-ns pulses from a Q-Switched Nd:YAG laser in a cavity similar to that used earlier. Different sets of laser mirrors were used. Summary of the laser performance for three different laser cavities is presented in Table 3.

TABLE 3: Summary of Laser Parameters for Pulsed Laser Operation (1064-nm pumping)

Parameter	Output Coupling 13%	2%	6%
Lasing Wavelength	1200 nm	1235 nm	1250 nm
Free-running Bandwidth	-	30 nm	-
Threshold Abs. Energy	0.38 mJ	0.20 mJ	0.27 mJ
Slope Efficiency	22.8%	5.1%	12.1%
Gain Cross Section (10^{-19} cm^2)	1.40	1.44	1.40

Surface damage of the Cr:forsterite laser crystal was observed for pumping energies greater than 4mJ, for 5ns pulses, at 10Hz repetition rate, focused to 250μm radius spot.This corresponds to damage threshold energy density greater than 6J/cm^2, for 5ns pulses. Therefore, a 1cm diameter laser pumped forsterite rod can be used to generate high energy pulses in the joule range.

Output energy of the forsterite laser as a function of absorbed pump energy for three different output couplers is shown in Fig. 10.

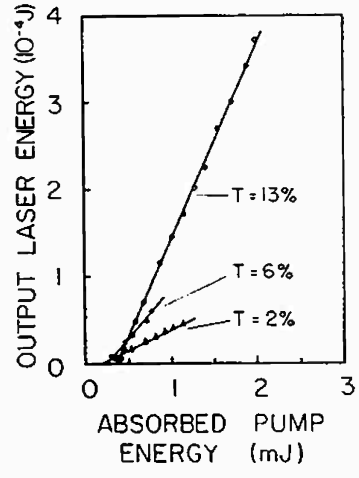

Fig. 10 Output energy of Cr:Mg_2SiO_4 laser as a function of absorbed pump energy for 1064-nm pumping and E ∥ b axis for three different output couplers.

Using data from Table 4 we have estimated the passive loss L of the forsterite laser to be 11%, and calculated the laser gain cross section.

Laser gain cross section shown in Table 4 for three different output mirrors was calculated using the expression[13]

$$\sigma = \frac{\pi \tau_P h\nu_P \omega_L^2 (L+T)(a^2+1)}{4\tau\left[1-\exp(-\alpha l)\right]\left[1-\exp(-\tau_P/\tau)\right]E_{Pth}}$$

where τ_P is the pump pulsewidth, $h\nu_P$ is the pump photon energy, ω_L is the cavity mode spot size, L is laser internal loss, T is the output mirror transmission, $a=\omega_P/\omega_L$, where ω_P is the pump beam spot size, τ is the upper lasing level radiative lifetime taken to be ~25 μs, α is the absorption coefficient for the pump radiation, l is the length of the crystal, and E_{Pth} is the threshold pump energy incident on the crystal.

II. Continuous-Wave Laser Operation

To obtain cw laser action a sample of chromium-doped forsterite (sample 1) was placed at the center of a nearly concentric cavity formed by two 5-cm radius-of-curvature mirrors such that a cavity mode waist was 75 μm. The output mirror was dielectric coated to have ~1% transmission for the 1175 - 1250 nm range, and to transmit most of the 1064-nm pump beam. The pump radiation from a cw Nd:YAG laser was focused by a 75-mm focal length lens to pump the sample longitudinally along the 30 mm path length. The pump beam was linearly polarized along the b axis and propagated along the a axis of the crystal . The beam was chopped at a duty factor of 9:1 to reduce heating effects. The waist of the pump beam at the center of the sample was measured to be 70 μm.

Quasi-cw laser operation was obtained for pumping above the lasing threshold of 1.25 W of absorbed power. The measured slope efficiency was 6.8%. The cw output power of the Cr:forsterite laser as a function of absorbed pump power is displayed in Fig. 11. Laser operation was possible even when the pump beam was not chopped, but at 40% reduced output indicating losses induced by local heating.

The spectrum of the free-running laser output peaks at 1244 nm and has a bandwidth of 12 nm.

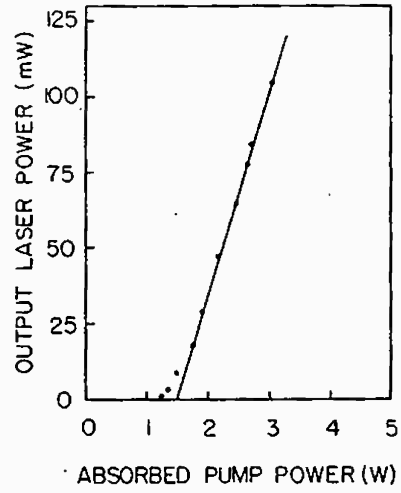

Fig. 11 Output power of the cw $Cr:Mg_2SiO_4$ laser as a function of absorbed pump power.

Using results obtained from CW lasing experiment, a value of 12.7% for L the internal loss has been estimated[12]. This value is in reasonable agreement with the value of 11% obtained from pulsed measurements. The gain cross section was estimated to be $1.47 \times 10^{-19} cm^2$, in excellent agreement with the value obtained from pulsed laser experiments. Threshold population inversion density was estimated to be $1.6 \times 10^{17} cm^{-3}$. The key continuous-wave laser parameters are summarized in Table 4.

TABLE 4: Properties of cw Laser Operation of $Cr:Mg_2SiO_4$ laser

Property	Value
Lasing Wavelength	1244 nm
Spectral Bandwidth (FWHM)	12 nm
Lasing Threshold (Absorbed Power)	1.25 W
Slope Efficiency	6.8%
Threshold Inversion Density	1.6×10^{17} cm^{-3}
Gain Cross Section	1.47×10^{-19} cm^2

III. Tunable Operation of Forsterite Laser

Tunable operation of Cr:forsterite laser has been obtained over the 1167 - 1345 nm spectral range,[5] using single crystal quartz birefringent plate, extending the tuning range of chromium-doped laser crystals further into near infrared. The ratio of the Cr:forsterite laser output to the absorbed pump energy as a function of wavelength is shown in Fig.12

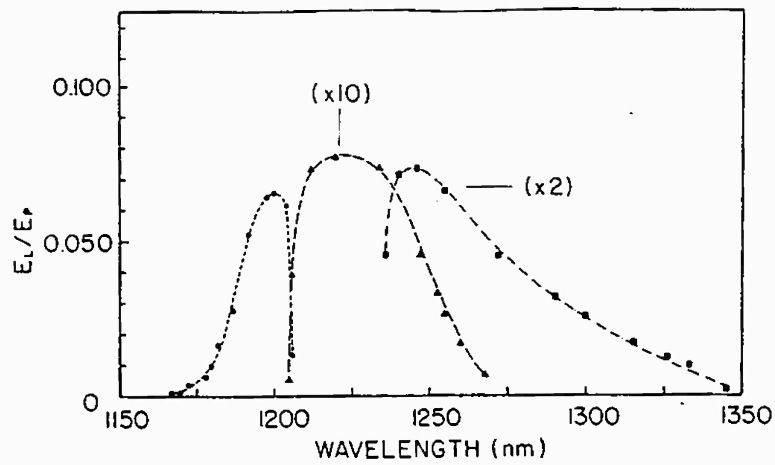

Fig. 12 The ratio of the Cr:forsterite laser output (E_L) to the absorbed pump energy (Ep) as a function of wavelength. The three curves correspond to the three output couplers used in tuning measurements.

Conclusion

Measurements of absorption and emission spectra , as well as the wavelength dependence of fluorescence lifetime indicate that chromium ion may enter forsterite (Mg_2SiO_4) host in more than one valence states. Trivalent chromium (Cr^{3+}) enters substitutionally for divalent magnesium (Mg^{2+}) in two inequivalent octahedrally-coordinated sites, while tetravalent chromium (Cr^{4+}) substitutes presumably for Si^{4+} at tetrahedrally coordinated sites. Of the two Cr^{3+} centers, the one with mirror symmetry (C_s) is optically active and accounts for a number of features in absorption and emission spectra. The absorption and emission due to transitions within the states of Cr^{4+} ion overlap with those within the states of Cr^{3+} ion. The absorption and emission in the near infrared spectral region between 850 and 1150 nm is primarily due to transitions between the $^3A_2$ ground state and the first excited state $^3T_2$, of the Cr^{4+} ion. The four-level, vibronic mode of laser operation in Cr-doped forsterite feeds on $^3T_2 \rightarrow {}^3A_2$ transition.

Chromium-doped forsterite is an important laser in the near-infrared spectral region. Table 5 lists the thermal and optical properties of forsterite and YAG crystals, which suggests that forsterite may be developed in a reliable tunable source of radiation for the near infrared region. Forsterite can be operated both in the pulsed and cw mode of operation and is tunable over 1167 - 1345 nm range. The large fluorescence bandwidth promises ultrashort pulse generation through mode-locked operation. Since large single crystals can be easily grown, the crystal has potential for being used as an amplifier medium in the near infrared spectral region and to produce joule energy pulses .

Table 5: Physical, Thermal and Optical Properties of Forsterite and YAG Crystals

	Forsterite	YAG
Chemical Formula	$Cr:Mg_2SiO_4$	$Nd:Y_3Al_5O_{12}$
Concentration (cm^{-3})	~3-6 x 10^{18}	1.38 x 10^{20}
Melting Point (°C)	1890	1970
Density (g/cm^3)	3.22	4.56
Moh's Hardness	7	8.5
Thermal Expansion Coeff.	9.5 x 10^{-6}	8.0 x 10^{-6}
Thermal Conductivity (W/cm°K)	0.08 (@ 300°K)	0.13 (@ 300°K)
$\partial n/\partial T$ ($°K^{-1}$)	Not Measured	7.3 x 10^{-6}
Emission Bandwidth	1350 cm^{-1}	6 cm^{-1}
Stimulated emission Cross Section (cm^{-2})	1.44 x 10^{-19}	6.5 x 10^{-19}
Relaxation time of Terminal Lasing Level	<10ps (Estimated)	30ns
Radiative Lifetime	25µs	550µs
Spontaneous Fluorescence	2.7µs	~230µs
Loss Coefficient	0.02 cm^{-1}	0.002 cm^{-1}
Index of Refraction	1.635	1.82 (@1.0µm)

* Presented the plenary talk

References

1. V. Petričević, S. K. Gayen, R. R. Alfano, K. Yamagishi, H. Anzai, and Y. Yamaguchi, Appl. Phys. Lett. 52, 1040 (1988); V. Petričević, S. K. Gayen, and R. R. Alfano, Appl. Phys. Lett. 53, 2590 (1988).
2. For a list of Cr-based tunable solid state lasers see J. A. Caird, S. A. Payne, P. R. Staver, A. J. Ramponi, L. L. Chase, and W. F. Krupke, IEEE J. Quantum Electron. 24, 1077 (1988), and references therein.
3. A. A. Kaminskii et. al., Inorg. Mater., 24, 579 (1988).
4. V. Petričević, S. K. Gayen, and R. R. Alfano, Opt. Lett. 14, 612 (1989).
5. V. Petričević, S. K. Gayen, and R. R. Alfano, Appl. Opt. 28, 1609 (1989).
6. N. Nishide, Y. Segawa, P. H. Kim, S. Namba, and A. Masuyama, Reza Kagaku Kenkyu 7, 89 (1985).
7. H. R. Verdun, L. M. Thomas, D. M. Andrauskas, T. McCollum, and A. Pinto, Appl. Phys. Lett. 53, 2593 (1988).
8. H. Rager and G. Weiser, Bull. Mineral. 104, 603 (1981).
9. H. Rager, Phys. Chem. Minerals 1, 371 (1977).
10. L. V. Bershov, J. M. Gaite, S. S. Hafner, and H. Rager, Phys. Chem. Minerals 9, 95 (1983).
11. S. Sugano, Y. Tanabe, and H. Kamimura, *Multiplets of Transition-Metal Ions in Crystals*, Academic, New York, 1970.
12. V. Petričević, S.K. Gayen, and R.R. Alfano, in *Tunable Solid-State Lasers*, Vol.5 of the OSA Proceeding Series, M.L. Shand and H.P. Jenssen, eds. (Optical Society of America, Washington, D.C., 1989), pp. 77-84.
13. P. F. Moulton, IEEE J. Quantum Electron. QE-21, 1582 (1985).

13. V. Petričević, A. Seas, and R. R. Alfano, "Forsterite Laser Tunes in Near-IR", Laser Focus World **26** (11),109 (1990).

Forsterite laser tunes in near-IR

New laser crystal uses Cr^{4+} as active medium, operates pulsed or CW, and tunes over the 1167- to 1345-nm range.

By V. Petricevic, A. Seas, and R. R. Alfano

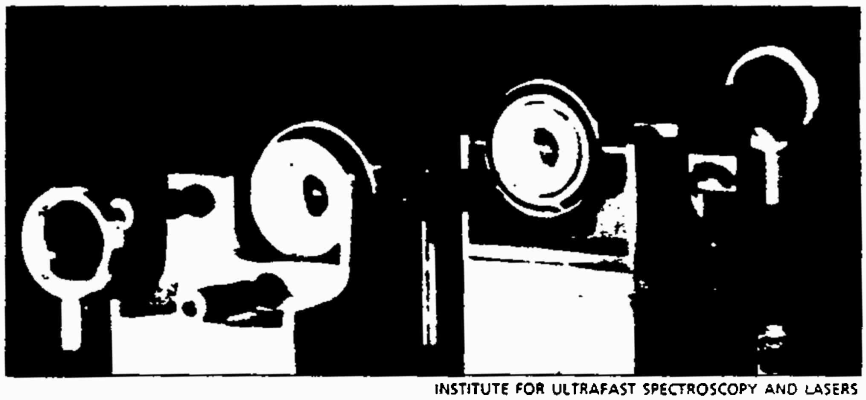

INSTITUTE FOR ULTRAFAST SPECTROSCOPY AND LASERS

Forsterite laser holds promise of supplying tunable joule-level pulses.

Research in tunable solid-state lasers has been extensive in the 1980s, prompted by the successful laser operation of alexandrite (Cr^{3+}-doped $BeAl_2O_4$) in 1979.[1,2] The thrust of these endeavors has been twofold: first to look for new host materials for the trivalent chromium ion (Cr^{3+}), and second to search for new ions that will exhibit laser action in common host crystals. [*See* LF World, *June 1990, p. 69, for a review of commercial tunable solid-state lasers.* —Ed.]

These efforts have been rewarded by the successful wavelength-tunable laser operation of Cr^{3+} in a number of hosts,[3-4,5] by the discovery of a new lasing ion, trivalent titanium (Ti^{3+}),[6,7] as well as by "rediscovery" of tunable phonon-terminated lasers based on the divalent ions Ni^{2+}, Co^{2+}, and V^{2+}.[8-12]

As a consequence of these research efforts of the past ten years, tunable solid-state lasers have emerged as an alternative to dye lasers. Dye lasers have advantages, such as high gain and low cost. But compared to solid-state lasers, dye lasers are often unsuitable for hospital, airborne, mobile, or spaceborne use because of their toxicity, long-term unreliability, and narrow tuning range.

The relative importance of tunable solid-state lasers—despite their being more expensive to build and characterized by lower gain coefficients—stems from their advantages compared to dye lasers. Among these advantages are broad tuning range, high reliability, compactness (particularly if they could be pumped by semiconductor diode lasers), and longer operational lifetimes. These properties make them suitable for spaceborne remote sensing, ranging, lidar, and optical communications. Tunable solid-state lasers also have potential for various medical, industrial, and basic scientific-research applications.

Several tunable solid-state laser materials and their corresponding tuning ranges are shown in Fig. 1. This article describes the laser and optical properties of Cr-doped forsterite ($Cr:Mg_2SiO_4$)—a new tunable laser material that fills the spectral void in the near-IR (see photo).

Properties of $Cr:Mg_2SiO_4$

Cr-doped forsterite has become an important member of the ever-growing family of tunable solid-state lasers based on the chromium ion as the lasing center.[13-20]

Both pulsed and continuous-wave (CW) laser operation have been obtained for Cr-doped forsterite with 532-, 578-, 629-, and 1064-nm pumping. The tuning range covers the spectral range from 1167 to 1345 nm, thus filling the void in the near-IR spectral region. This wavelength range is of technological importance because it covers the region of minimal dispersion in optical fibers. Lasers based on the chromium ion as the active center—these include the chromium-based lasers tabulated by Payne and others,[3] the more recently developed lasers based on Cr-doped crystals of

V. PETRICEVIC is a research scientist, A. SEAS is a research assistant, and R. R. ALFANO is director of the Institute for Ultrafast Spectroscopy and Lasers, Departments of Physics and Electrical Engineering, City College of New York, New York, NY 10031.

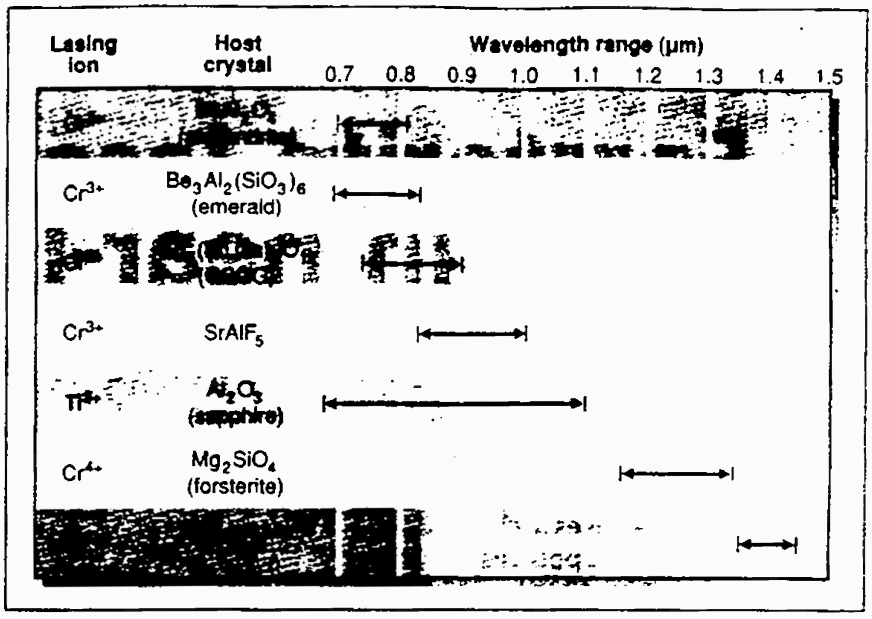

FIGURE 1. Tuning ranges for common tunable solid-state laser materials cover a broad spectrum.

others,[3] the more recently developed lasers based on Cr-doped crystals of calcium gallogermanate structure,[4] as well as those based on the Cr-doped YAG crystal,[5]—now span the broad spectral range of 695 to 1450 nm.

The most interesting and distinguishing feature of laser action in $Cr:Mg_2SiO_4$ is that the lasing ion is not trivalent chromium (Cr^{3+}), as is the case with other chromium-based lasers. Available experimental data suggest that the active ion in this crystal is tetravalent chromium (Cr^{4+}). Therefore, $Cr:Mg_2SiO_4$ is the first laser crystal in which the laser-active center is identified as Cr^{4+}.[14,15] As of this writing, Cr:YAG is the only other laser medium in which tetravalent chromium is the ion responsible for laser action.

Single crystals of Cr-doped forsterite used in our spectroscopic and laser experiments have been grown by the Czochralski method. The trivalent chromium ion enters as a substitute for Mg^{2+} in two inequivalent sites: one with inversion (C_i) and the other

optical properties

	Forsterite	Nd:YAG
Chemical formula	$Cr:Mg_2SiO_4$	$Nd:Y_3Al_5O_{12}$
Concentration (cm^{-3})	≈3–6 × 10^{18}	1.38 × 10^{20}
Melting point (°C)	1890	1970
Density (g/cm^3)	3.22	4.56
Moh's hardness	7	8.5
Thermal expansion coefficient	9.5 × 10^{-6}	8.0 × 10^{-6}
Thermal conductivity (W/cmK)	0.08 (300 K)	0.13 (300 K)
δ_n/δ_T (K^{-1})	not measured	7.3 × 10^{-6}
Stimulated emission cross section (cm^{-2})	1.44 × 10^{-19}	6.5 × 10^{-19}
Relaxation time of terminal lasing level	<10 ps (estimated)	30 ns
Radiative lifetime	25 μs	550 μs
Spontaneous fluorescence	2.7 μs	230 μs
Loss coefficient	0.02 cm^{-1}	0.002 cm^{-1}
Index of refraction	1.635	1.82 (@1.0 μm)

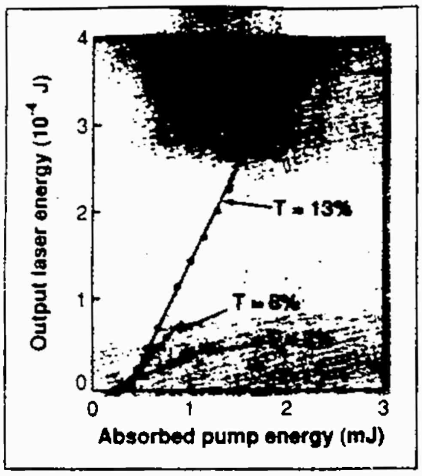

FIGURE 2. The output energy of the Cr:forsterite laser as a function of absorbed pump energy varies for three different output couplers.

with mirror (C_s) symmetry. In addition to Cr^{3+} ions in those sites, tetrahedrally coordinated Cr^{4+} ions are also present in Czochralski-grown forsterite. The relative concentration of Cr^{3+} and Cr^{4+} ions in Mg_2SiO_4 depends on the growing atmosphere. Growing the crystal in a reducing atmosphere allows the relative concentration of Cr^{4+} ions to be reduced and that of Cr^{3+} to be increased.

Spectroscopic measurements performed on $Cr:Mg_2SiO_4$ crystals grown under standard conditions (in an oxidizing atmosphere) and those grown in a reducing atmosphere include measurements of absorption spectra, fluorescence and excitation spectra, and lifetime measurements as a function of temperature.[16]

The results of these measurements provide convincing evidence that there are at least three inequivalent optically active centers in Cr-doped forsterite: trivalent chromium (Cr^{3+}) occupies two octahedrally coordinated sites, while tetravalent chromium (Cr^{4+}) substitutes for silicon (Si^{4+}) in a tetrahedral site. It is the tetrahedral Cr^{4+} that gives Cr-doped forsterite many unique and important properties. Lack of inversion symmetry at the tetrahedral site makes transition strengths of Cr^{4+} stronger than those of Cr^{3+}, and spectral features of Cr^{4+} are dominant in the spectra.

The emission is shifted considerably into the near-IR spectral region, which is important for eye-safe ranging, optical communications, and medical and scientific research applications. Tetra-

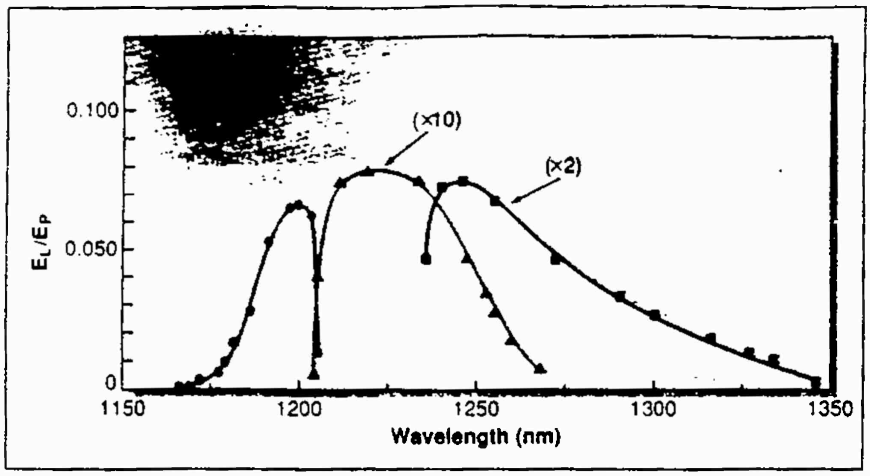

FIGURE 3. The ratio of the Cr:forsterite laser output (E_L) to the absorbed pump energy (E_P) is plotted as a function of wavelength.

hedral Cr^{4+} has three broad spin-allowed absorption bands that can be pumped efficiently for laser operation. This property is particularly important for flashlamp-pumped operation. The Cr^{4+} ion in a tetrahedral position is chemically stable because of high covalency with the surrounding oxygen ions.

The physical properties of Cr-doped forsterite also appear to be promising. Table 1 compares physical, thermal, and optical properties of forsterite and Nd:YAG crystals. The broad emission bandwidth suggests that Cr-doped forsterite may be developed as a reliable tunable source for the near-IR spectral region.

Modes of laser operation

Pulsed laser operation was obtained with samples rich in Cr^{4+} in a stable cavity. Details of the cavity arrangement have been described elsewhere.[13] Pulsed laser action was observed for both 1064- and 532-nm pumping. The spectra of the free-running laser radiation for both the 1064- and 532-nm pumping peaked at 1235 nm and had linewidths of 30 and

Table 2. Spectroscopic and laser properties of Cr:Mg_2SiO_4

Property	Value
Major pump bands	850–1200 nm 600–850 nm 350–550 nm
Fluorescence band	680–1400 nm
Room-temperature fluorescence lifetime	≈3 μs
Lasing wavelength (center)	1235 nm (pulsed) 1244 nm (CW)
Spectral bandwidth	30 nm (pulsed) 12 nm (CW)
Slope efficiency	23% (pulsed) 38% (CW)
Tuning range	1167–1345 nm
Gain cross section	≈1.45 × 10^{-19} cm^2

27 nm, respectively. Highest slope efficiency obtained to date is 23% for 1064-nm pumping, with an output mirror having 13% transmission at 1200 nm. Output energy of the forsterite laser as a function of absorbed pump energy for three different output couplers is shown in Fig. 2.

Surface damage of the $Cr:Mg_2SiO_4$ crystal was observed for pumping energies greater than 4 mJ of energy incident on the crystal, for 5-ns pulses, at 10-Hz repetition rate, focused to a 250-mm radius spot. This corresponds to damage-threshold energy density greater than 6 J·cm^{-2} for 5-ns pulses, which means that a 1-cm-diameter laser-pumped forsterite rod can be used to generate pulses of energy in the joule range.

CW laser operation was obtained using 1064-nm radiation from a CW Nd:YAG laser as the pumping source.[17] The lasing threshold was 1.25 W of absorbed power. The measured slope efficiency was 6.8%. The spectrum of the free-running laser output peaks at 1244 nm and has a bandwidth of 12 nm. Recently, we have measured slope efficiency as high as 38% for CW operation, and limiting slope efficiency that may be obtained if all passive losses are eliminated is estimated to be greater than 65%.[21]

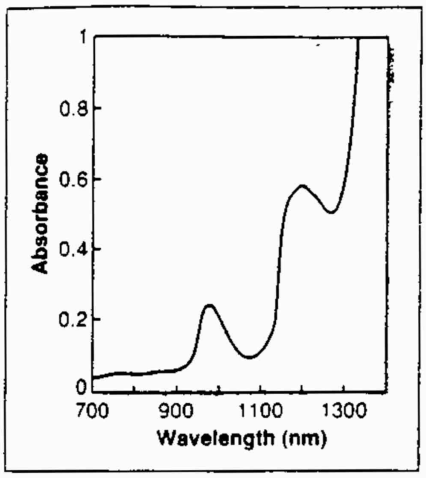

FIGURE 4. Absorption spectrum of water (1-cm pathlength) changes significantly over the tunable region of the Cr:forsterite laser.

Tunable operation of the Cr:forsterite laser has been demonstrated over the 1167- to 1345-nm spectral range.[18] A birefringent single-crystal quartz plate at Brewster's angle was used as the intracavity dispersive element. Three different output mirrors with transmission in adjacent wavelength ranges were used to cover the tuning range. The ratio of the laser output energy to the absorbed pump energy as a function of wavelength is shown in Fig. 3. Some of the important spectroscopic and laser parameters of $Cr:Mg_2SiO_4$ are listed in Table 2.

Cr-doped forsterite is the basis of a new solid-state laser tunable in the near-IR spectral range,[17] and other Cr^{4+}-doped crystals are under development.[20] The tuning range of Cr-doped forsterite covers the void spectral region, which is not by any other tunable solid-state laser (excluding color-center lasers).

Potential medical applications are interesting because the absorption

spectrum of water changes significantly within the tuning range of the Cr:forsterite laser (see Fig. 4). By changing the wavelength of the laser radiation, the penetration depth of radiation into an absorbing sample can be controlled. Because water is one of the major components of body tissue, the tunable output of the Cr:forsterite laser may find use in medical applications.

When used in conjunction with a titanium-doped sapphire laser, the Cr-doped laser may cover nearly the whole visible range (using second-harmonic generation) and the near-IR region up to 1350 nm. The large fluorescence bandwidth of Cr:forsterite has the potential for generating ultrashort pulses through mode-locked operation. Because large crystals can be easily grown, Cr-doped forsterite crystal has the potential to be used as an amplifier medium to produce joule-energy pulses.

ACKNOWLEDGMENTS

We thank Bob Guenther of the Army Research Office (ARO) for his support and Y. Terashima and K. Yamagishi of Mitsui Mining and Smelting Company and Mediscience Technology for providing us with forsterite crystals.

REFERENCES

1. J. C. Walling et al., *Opt. Lett. 4,* 182 (1979).
2. J. C. Walling et al., *IEEE J. Quantum Electron. QE-16,* 1302 (1980).
3. S. A. Payne et al., *J. Appl. Phys. 66,* 1051 (1989).
4. A. A. Kaminskii et al., *Phys. Stat. Sol (a) 112,* 197 (1989).
5. N. B. Angert et al., *Sov. J. Quantum Electron. 18,* 73 (1988).
6. P. F. Moulton, *J. Opt. Soc. Am. B3,* 125 (1986).
7. A. I. Alimpiev et al., *Sov. J. Quantum Electron. 16,* 579 (1986).
8. P. F. Moulton and A. Mooradian, *Appl. Phys. Lett. 35,* 838 (1979).
9. P. F. Moulton, *IEEE J. Quantum Electron. QE-18,* 1185 (1982).
10. P. F. Moulton, *IEEE J. Quantum Electron. QE-21,* 1582 (1985).
11. V. Brauch and U. Durr, *Opt. Commun. 55,* 35 (1985).
12. W. E. Knierim et al., *J. Opt. Soc. Am B3,* 119 (1986) and references therein.
13. V. Petricevic et al., *Appl. Phys. Lett. 52,* 1040 (1988).
14. V. Petricevic, S. K. Gayen, and R. R. Alfano, *Appl. Phys. Lett. 53,* 2590 (1988).
15. H. R. Verdun et al., *Appl. Phys. Lett. 53,* 2593 (1988).
16. V. Petricevic, S. K. Gayen, A. Seas, and R. R. Alfano, unpublished data.
17. V. Petricevic, S. K. Gayen, and R. R. Alfano, *Opt. Lett. 14,* 612 (1989).
18. V. Petricevic, S. K. Gayen, and R. R. Alfano, *Appl. Opt. 28,* 1609 (1989).
19. R. R. Alfano, V. Petricevic, and S. K. Gayen, "Chromium-doped Forsterite Laser System", US Patent #4,932,031, June 5, 1990.
20. R. R. Alfano and V. Petricevic, "Tetravalent Chromium as Laser-active Ion for Tunable Solid-State Lasers," US patent (allowed 1990).
21. V. Petricevic, A. Seas, and R. R. Alfano, to be submitted for publication.

14. S. K. Gayen, W. B. Wang, V. Petričević, S. G. Demos, and R. R. Alfano, "Picosecond Excite-and-probe Absorption Measurements of Nonradiative Transition Dynamics in Emerald", J. Lumin. **47**, 181 (1991).

Journal of Luminescence 47 (1991) 181–188
North-Holland

Picosecond excite-and-probe absorption measurement of nonradiative transition dynamics in emerald

S.K. Gayen [a], W.B. Wang, V. Petričević, S.G. Demos and R.R. Alfano

Institute for Ultrafast Spectroscopy and Lasers, Physics Department and Electrical Engineering Department, The City College of New York, New York, NY 10031, USA

[a] *Department of Physics and Engineering Physics, Stevens Institute of Technology, Hoboken, NJ 07030, USA*

Received 20 April 1990
Revised 22 June 1990
Accepted 23 June 1990

The nonradiative transition dynamics between the excited $^4T_2$ state and the metastable ^2E storage state of the trivalent chromium ion in emerald is investigated using the picosecond excite-and-probe absorption technique. An intra-$^4T_2$ state vibrational relaxation time of 23 ps, and a $^4T_2 \rightarrow {}^2E$ electronic relaxation time of 20 ps are obtained. The thermal repopulation rate of the $^4T_2$ state from the metastable ^2E level is $\sim 9.0 \times 10^9$ s^{-1}.

1. Introduction

Emerald [Cr^{3+}: $Be_3Al_2(SiO_3)_6$], a trivalent chromium-activated beryl, is one of the first room-temperature, frequency tunable laser crystals [1–4] which stimulated the recent surge in vibronic solid state laser research. Emerald, like alexandrite [1] operates in a four level, phonon terminated mode and exhibits gain over a 695–835 nm wavelength range. Its broad fluorescence bandwidth, together with a high gain cross section [2] and a 65 μs room temperature fluorescence lifetime [5] make emerald an excellent candidate for high power, Q-switched or mode-locked operation. Recently, highly efficient quasi-cw laser operation has been achieved in emerald over the 720–842 nm tuning range, with a maximum output of 1.6 W at a pump power of 3.6 W at 647.1 nm [6]. Although the spectroscopic [5–8] and laser properties [2,3] of the chromium ion in emerald are well documented, there is a lack of time-resolved experimental investigations of the nonradiative relaxation processes among the states involved in laser action in this system. Theoretical effort has involved analysis of emerald absorption, emission and thermal quenching of lifetime data using a single configuration coordinate model to investigate the temperature dependences of nonradiative transitions [9]. Knowledge about various loss mechanisms is crucial for better understanding the vibronic laser action, as well as for the fabrication of future generations of tunable laser crystals. Recently, we have investigated [10–13] by picosecond time-resolved spectroscopy the kinetics of nonradiative transitions among the excited pump states and metastable storage levels in a number of transition-metal ion-doped crystals: alexandrite, ruby and Ti^{3+} : Al_2O_3. In this paper, a picosecond excite-and-probe absorption study of nonradiative transition dynamics in emerald is presented.

Emerald is an intermediate field Cr^{3+}-based crystal characterized by broad band $^4T_2 \rightarrow {}^4A_2$ fluorescence. Its absorption spectrum consists of two broad bands at 640 and 420 nm attributed to the $^4A_2 \rightarrow {}^4T_2$ and $^4A_2 \rightarrow {}^4T_1$ transitions of the Cr^{3+} ion, respectively. These broad bands serve as pump bands for optical excitation. Optically excited $^4T_1$ and $^4T_2$ states relax predominantly via nonradiative transitions to the ^2E state. Since the $^2E \rightarrow {}^4A_2$ transitions are both first-order spin- and

parity forbidden, the ^2E level has a longer lifetime and is metastable. The $^2E \rightarrow {}^4T_2$ energy gap in emerald [5] is only 400 cm^{-1} compared to 2300 cm^{-1} in ruby and 800 cm^{-1} in alexandrite. This smaller energy gap allows significant thermal repopulation of the $^4T_2$ state from the ^2E at room temperature. The metastable ^2E state thus acts as a storage level for vibronic transitions from the $^4T_2$ state to the vibrational levels of the $^4A_2$ ground state.

The kinetics of intra-$^4T_2$ vibrational transitions, the $^4T_2 \rightarrow {}^2E$ electronic transition, and the $^2E \rightarrow {}^4T_2$ thermal repopulation have been investigated in our study. Higher-lying vibrational levels of the $^4T_2$-state are excited by a picosecond pump pulse, and the subsequent nonradiative transition dynamics is investigated by monitoring the time evolution of the optical absorption of an infrared picosecond probe pulse from the excited states. In section 2, we present a brief description of the experimental scheme, followed by an overview of the experimental results. A model for induced absorption in emerald and similar crystals is outlined in section 3. The model uses a simplified energy-level diagram for Cr^{3+} ions in beryl, where the states directly involved in laser action are considered. The metastable storage level is assumed to be constituted of both the ^2E and the $^2T_1$ level, a justified assumption since the two states are strongly coupled [5]. Under this assumption, the model ascribes the induced absorption to transitions from both the pump and the storage levels, and estimates the instantaneous population in the excited states from rate equations governing the population kinetics. The key nonradiative relaxation parameters for emerald obtained from a fit of the experimental data to this model are presented. The relaxation rates and decay times for emerald are then compared to those for similar tunable laser crystals.

2. Experimental arrangement and result

The experimental arrangement uses a frequency doubled 5 ps 527 nm pump pulse derived from a passively mode-locked Nd : glass laser to excite the higher-lying vibrational (HLV) levels of the $^4T_2$ state. Nonradiative relaxation of HLV levels results in a growth of the population in the zero vibrational level (ZVL) and lower-lying vibrational (LLV) levels of the $^4T_2$ state, as well as in the metastable ^2E state. This time evolution of the population is monitored by an infrared picosecond probe pulse which may be wavelength tuned from 2 to 5 μm. The probe pulse is generated by parametric amplification in a pair of $LiNbO_3$ crystals using a fraction of the same 1054 nm pulse that generates the pump pulse. Infrared transmission measurements are used to select the probe wavelength in such a way that the host and ground-state probe absorption is a minimum.

The experimentally measured quantity is the change in the optical density (OD) of the probe pulse, which for a given pump–probe delay time t, is given by

$$\Delta OD(t) = \log[(I_s/I_r)u/(I_s/I_r)p], \qquad (1)$$

where I_s/I_r is the transmitted probe-pulse intensity normalized with respect to the intensity of the probe pulse, and u and p stand for the unpumped and pumped conditions of the sample, respectively. The normalization of the probe-pulse intensity (I_s) with respect to the probe-pulse intensity before the sample (I_r), measured by picking up a fraction of the probe pulse with a beam-splitter–detector combination, is necessary to account for the pulse-to-pulse energy fluctuation. To improve the signal-to-noise ratio, the normalized probe intensity is averaged over ten laser pulses for each value of the delay time. The kinetics of excited state transitions is studied by measuring $\Delta OD(t)$ as a function of pump–probe delay time. Details of the experimental arrangement, detection scheme, signal averaging and processing technique have been reported elsewhere [10].

The hydrothermally grown emerald crystal used in this experiment was obtained from Vacuum Ventures, Inc. It contains 0.29 wt% Cr^{3+} which is equivalent [7] to a chromium-ion concentration of 8.9×10^{19} cm^{-3}. The value for the Cr^{3+} ion concentration is comparable to the value of 9.2×10^{19} cm^{-3} in emerald samples used in flashlamp-pumped laser experiments [2]. The sample is a rectangular parallelepiped, 9mm × 8mm × 5.5mm in dimension. Induced absorption measurements

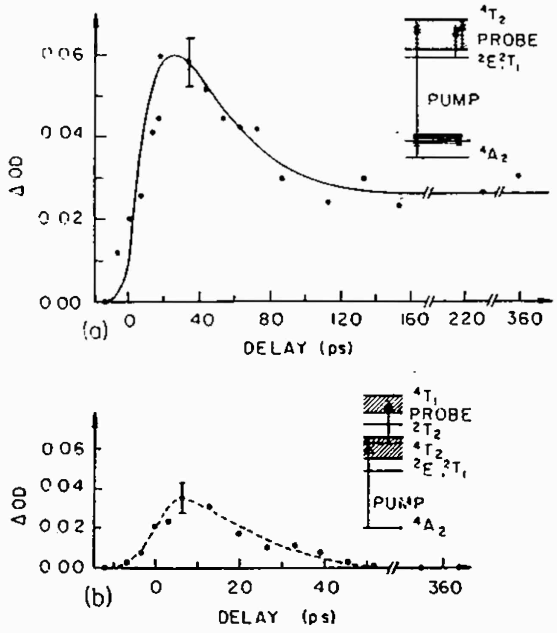

Fig. 1. Time evolution of the optical density (a) at 3.9 μm, and (b) at 2.16 μm in the metastable ($^2E+^2T_1$) state and the ZVL and LLV levels of the $^4T_2$ state of emerald at room temperature. The radii of the pump and the probe pulses at the sample position are both 0.35 mm. Both the pump and the probe pulses are linearly polarized parallel to the c_3 axis of the crystal. Insets show the relevant energy-level diagrams of emerald, and the pump, probe and relaxation transitions. The zero time is accurate within 5 ps. Size of a typical error bar is shown. The solid curve in (a) is a computer fit to the experimental data using the rate equations and relaxation rates described in the text.

were taken along the 5.5 mm path length of the sample.

The result of the present picosecond excite-and-probe absorption measurements in emerald at room temperature showing the time evolution of induced absorption at a probe wavelength of 3.9 μm is displayed in fig. 1(a). The probe wavelength of 3.9 μm was chosen carefully so that transitions from the ^2E state to the vibrational levels of the $^4T_2$ state are energetically possible, but the probability of transition from any HLV level of the $^4T_2$ state to the $^4T_1$ state or any other higher-lying state is vanishingly small. There is considerable ground state and host absorption at this probe wavelength which is accounted for using the scheme detailed in section 3. The positions and widths of the excited energy levels involved in the probe-pulse absorption are determined from the detailed excited-state absorption (ESA) spectra of emerald investigated by Fairbank, Klauminzer and Schawlow [8]. This accounts for the fact that the ion may relax in the excited state, and so the positions and widths determined from the ground state absorption spectrum may be different from those determined from the excited state absorption spectrum.

The terminal levels for probe transition which originates in the $^4T_2$-state zero or lower-lying vibrational levels have been taken to be the higher-lying $^4T_2$-vibrational levels. The probability for such multiphonon transitions within the vibrational levels of the same electronic state is expected to be low. However, the $^4T_2$-state (in general, the excited states of Cr^{3+} ion) contains perturbative admixtures of other states due to crystal-field, spin-orbit and vibronic interactions. Because of this mixing of wave functions the strict selection rules are relaxed making transitions more probable. In emerald, the static odd-parity crystal field $T_{2u}\chi_0$ and T_{1u} odd vibrations are effective in the mixing of states. The role of these two interactions has been elucidated in the analysis of emerald excited state absorption spectra by Fairbank et al. [8]. These authors also calculated the contribution of the spin-orbit interaction to the $^2E \rightarrow {}^2A_2$-transition oscillator strength in ruby, found it to be substantial, and predicted similar contributions in emerald as well. The admixtures between participating excited states in our study due to the interaction is mentioned above, are expected to be substantially higher, since, the energy denominators which appear in perturbation calculations are smaller than those in the ESA study of Fairbank et al. [8]. This is due to the fact that in our study, the participating excited states are within energy separations of a few hundred to a few thousand wave numbers (cm^{-1}), whereas ESA transitions studied by Fairbank et al. are in the visible, hence, the energy separations are more than ten thousand wave numbers. Odd-parity crystal field and odd vibrations relaxed the parity selection rule, and the spin-orbit interaction relaxed the spin selection rule enabling transitions between excited states involved in this case. In any reference to an

excited state, this small admixture of other states will be implicit.

The ΔOD versus pump–probe time delay curve is characterized by a 25 ± 5 ps rise time (time for the OD to grow from 10% to 90%) followed by a multicomponent decay. The faster component has a decay time (time for the OD to fall from 90% to 10% of the peak value above the flat region) of 65 ± 10 ps, whereas the longer lifetime component exhibits no appreciable change within the time scale of this measurement.

The longer lifetime component of the decay curve indicates that a "quasithermal equilibrium" has been reached between the ^2E and $^4T_2$ states. Further depopulation of the excited state is expected to be predominantly due to radiative transition. Since, the room temperature fluorescence lifetime of emerald is ~ 65 μs, no appreciable change in the population is expected within a few hundred picoseconds, consistent with the experimental observation. The rise time and the decay time for the faster component are dictated by the intra-$^4T_2$-state vibrational relaxation time, the $^4T_2 \rightarrow {}^2E$ electronic relaxation time, and the $^2E \rightarrow {}^4T_2$ thermal repopulation rate.

Supporting evidence for our assignment of the risetime primarily to the intra-$^4T_2$-state vibrational relaxation has been obtained by extending the measurement to a probe wavelength of 2.16 μm. The use of a second probe wavelength was guided by the following considerations. First, a 2.16 μm photon is energetic enough to initiate a transition from the pumped HLV levels of the $^4T_2$ state to the $^4T_1$ state, which was not energetically possible for a 3.9 μm photon. Second, the Franck–Condon factor (FCF) for transition between the ZVL of the ^2E-state and HLV levels of the $^4T_2$-state attainable by this probe photon is expected to be vanishingly small. This follows from the fact that the Franck–Condon factor, $|\langle 0|n\rangle|^2$, between the ZVL of one state and the nth vibrational level of the other state has its maximum value near $n = \Delta^2/2$, where Δ is the horizontal separation (in units of $(\hbar/M\omega)^{1/2}$) between the potential energy curves of the two states, and falls off rapidly as n changes from that value [14]. An examination of the energy level structure and spectra of emerald reveals that the maxima of the excited state probe absorption will be expected at around 3.9 μm, and that the absorption will be negligible at a probe wavelength of 2.16 μm. Similar considerations apply for transitions from the ZVL and LLV levels of the $^4T_2$ state. Also, there is no significant ground state or host absorption at 2.16 μm. All these factors lead to the expectation that any change in optical density at this probe wavelength will be attributable primarily to transitions from the populated HLV levels of the $^4T_2$ state to the levels of the $^4T_1$ state.

The room temperature time evolution of induced absorption at 2.16 μm is shown in fig. 1(b). The salient features of the curve are a resolution limited sharp rise time followed by a 35 ± 10 ps decay. The resolution limited rise time indicates the increase of population in the pumped HLV levels as long as the pump pulse is on. The 35 ± 10 ps decay time reflects the vibrational relaxation time of the pumped HLV levels. This relaxation leads to the growth of the population in the ZVL and LLV levels of the $^4T_2$ state, and subsequently to the ^2E state. The decay time of 35 ± 10 ps agrees with the 25 ± 6 ps rise time of OD at 3.9 μm, and lends qualitative support to the assignment of rise time to the vibrational relaxation of pumped HLV levels.

3. Induced absorption model

In order to obtain a more detailed understanding of experimental results, as well as to extract key nonradiative relaxation rates we introduce a rate-equation model for excited state transition dynamics. A simplified energy level structure for the chromium ion in emerald is used. The state that is optically excited is the $^4T_2$ state with possible perturbative admixtures of other states as mentioned earlier. The metastable storage level, referred to as the ^2E state, consists in fact of the coupled ^2E and $^2T_1$ states [5]. The time evolution of the optical absorption from the excited metastable and $^4T_2$ states following the excitation of some HLV levels of the $^4T_2$ state is described by the excited state absorption coefficient:

$$\alpha_e(t) = N_1(t)\sigma_1 + N_2(t)\sigma_2, \qquad (2)$$

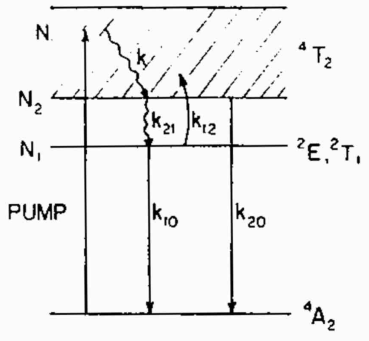

Fig. 2. Schematic diagram showing relevant transitions and transition rates, for 3.9 μm probe absorption. The metastable level is the coupled ^2E and $^2T_1$ state. The rates and populations are explained in the text.

where N_1 and N_2 are instantaneous population densities (ions/cm^3) and σ_1 and σ_2 are cross sections for probe absorption in the metastable state and the $^4T_2$ state, respectively. The transitions and transition rates are shown schematically in fig. 2. The population kinetics of the $^4T_2$ and the ^2E states are governed by the following rate equations

$$\frac{dN}{dt} = -kN + \beta P(t), \tag{3}$$

$$\frac{dN_1}{dt} = k_{21}N_2 - k_{12}N_1 - k_{10}N_1, \tag{4}$$

and

$$\frac{dN_2}{dt} = kN + k_{12}N_1 - k_{21}N_2 - k_{20}N_2, \tag{5}$$

where $N(t)$ is the instantaneous population density in the $^4T_2$-state HLV levels which are directly excited by the pump pulse, $P(t)$ is the pump photon flux density (photons/cm^{3}s), k is the intra-$^4T_2$ vibrational relaxation rate, k_{21} is the $^4T_2 \rightarrow {}^2E$ electronic relaxation rate, k_{12} is the thermal refilling rate of $^4T_2$ from ^2E, k_{10} and k_{20} are radiative transition rates from the ^2E and $^4T_2$ states, respectively, $\beta = 1 - \exp(-\alpha L)$ is the fraction of the pump photons absorbed by the pump volume of the sample, α is the ground-state absorption coefficient for pump pulse, and L is the length of the sample.

Because the radiative lifetimes are of the order of milliseconds to microseconds, the radiative transition rates k_{10} and k_{20} are extremely small compared to nonradiative rates, and may be neglected in the kinetics study of the first few hundred picoseconds. The rate equations were solved numerically using the fourth-order Runge–Kutta method [15]. The temporal profile of the pump pulse was taken as a Gaussian [16] of 5 ps FWHM. The arbitrary constants in the solution of the differential equations were determined from the condition that initially populations in the excited states are zero, and the final condition that at sufficiently large times the populations in the ^2E and $^4T_2$ states obey the Boltzmann distribution law:

$$\frac{N_2}{g_2} = \frac{N_1}{g_1}\exp(-\Delta E/k_B T), \tag{6}$$

where g_1 and g_2 are the degeneracies of the metastable and $^4T_2$ states, respectively, ΔE is the metastable level $\rightarrow {}^4T_2$-state energy gap and k_B is the Boltzmann constant. As pointed out earlier in this work, we have assumed after ref. [5] that the ^2E and $^2T_1$ states are strongly coupled and that they form the metastable storage level. Accordingly, the degeneracy of the pump state, g_2 is taken to be 12 and that of the metastable level, g_1 to be $(4 + 6) = 10$. The energy gap between the pump band and the storage level is taken to be 400 cm^{-1} [5].

Experimentally, the change in the optical absorption of the probe pulse between the pumped and unpumped conditions of the sample is measured as a function of delay time. This change for delay time t_d is given by,

$$\Delta\mathrm{OD}(t_d) = \mathrm{OD}_p(t_d) - \mathrm{OD}_u(t_d),$$

where the subscripts p and u stand for pumped and unpumped conditions of the sample. In terms of a population in different states,

$$\Delta\mathrm{OD}(t_d) = \left[\sigma_1 N_1(t_d) + \sigma_2 N_2(t_d) + \sigma_g N_g(t_d)\right] L - N_0\sigma_g L, \tag{7}$$

where N_g is the instantaneous chromium ion density in the ground state, σ_g is the ground state absorption cross section at probe wavelength by a chromium ion, and N_0 is the total density of Cr^{3+} ions in the sample. Now,

$$N_g(t_d) = N_0 - \beta\int_{-\infty}^{t_d} P(t)\,dt. \tag{8}$$

Substituting (8) in (7) gives:

$$\Delta OD(t_d) = \sigma_1 N_1(t_d) L + \sigma_2 N_2(t_d) L - \sigma_g L \beta \int_{-\infty}^{t_d} P(t)\, dt. \quad (9)$$

Equation (9) would be the exact expression for ΔOD. if the probe pulse were a delta function. However, the duration of the probe pulse is comparable to that of the pump pulse and is of the same order of magnitude as the relaxation times under consideration. Hence, the expression in eq. (9) has to be replaced by a corresponding expression involving the convolution of the probe pulse with the system response, and will be of the form:

$$\Delta OD(t_d) = A_1(t_d) + A_2(t_d) + B(t_d), \quad (10)$$

where

$$A_i(t_d) = -\log\left[\frac{\int_{-\infty}^{\infty} I(t - t_d) \exp(-N_i \sigma_i L)\, dt}{\int_{-\infty}^{\infty} I(t)\, dt}\right], \quad i = 1, 2, \quad (11)$$

$$B(t_d) = -\log\left[\frac{\int_{-\infty}^{\infty} I(t - t_d) \exp\left[\beta \sigma_g L \int_{-\infty}^{t_d} P(t)\, dt\right] dt}{\int_{-\infty}^{\infty} I(t)\, dt}\right]. \quad (12)$$

and $I(t)$ is the intensity of the probe pulse. The background absorption due to the host alone, is the same for both the pumped and unpumped cases. Since, experimentally the change in optical absorption is obtained from the ratio of transmitted intensities for the pumped and unpumped conditions of the sample, this contribution cancels out. However, this will be true only if the probe absorption due to the host is not bleached by the pump pulse. Measurements of the probe transmission as a function of the pump pulse intensity indicate no bleaching at the intensity levels used in this experiment.

A fit to the experimental data to eqs. (10)–(12) assuming a Gaussian probe pulse [17] of estimated 3.5 ± 0.5 ps FWHM, and using the transition rates k, k_{21}, and k_{12} as well as the ratio σ_2/σ_1 as variable parameters is displayed by the solid line in fig. 1(a). The transition rates k_{12} and k_{21} are not independently variable, but are related by the Boltzmann condition:

$$k_{12} = \left(\frac{g_2}{g_1}\right) k_{21} \exp\left(-\frac{\Delta E}{k_B T}\right).$$

The values of the parameters obtained from the fit are: $k = 4.4 \times 10^{10}\ s^{-1}$, $k_{21} = 5.1 \times 10^{10}\ s^{-1}$, $k_{12} = 9.0 \times 10^{9}\ s^{-1}$, and $\sigma_2/\sigma_1 = 95$. It was observed that the fit is more sensitive to the sum $k_{12} + k_{21}$ than to k_{12} and k_{21} independently. The individual rates are estimated from the thermal equilibrium Boltzmann condition.

4. Discussion

The present picosecond excite-and-probe absorption measurement together with the model fit yields a number of key relaxation times. The vibrational relaxation rate k is estimated to be $4.4 \times 10^{10}\ s^{-1}$, which implies a vibrational relaxation time of ~ 23 ps for the transition from the pumped HLV levels to the bottom of the $^4T_2$ adiabatic potential energy parabola. The value of $5.1 \times 10^{10}\ s^{-1}$ for the nonradiative relaxation rate k_{21} for the electronic transition between the $^4T_2$ state and the metastable level leads to a relaxation time of ~ 20 ps. The metastable state → $^4T_2$-state thermal repopulation rate is found to be $9.0 \times 10^9\ s^{-1}$. The uncertainty in the values of these parameters may stem from group dispersion effects, fluctuations in the duration of the pump and the probe pulses, and the sensitivity of the fit to the experimental data with respect to variations in the values of parameters used. We estimate an overall uncertainty of 20% in the values of relaxation times quoted above from those factors. The intra-$^4T_2$ vibrational relaxation rate in emerald turns out to be comparable to the $^4T_2 \rightarrow {}^2E$ electronic nonradiative relaxation rate. This is unusual but not surprising, since a larger energy degradation (~ 4750 cm^{-1}, difference in energy between the HLV levels reached by the pump pulse and the ZVL) is involved in vibrational relaxation than in electronic relaxation (400 cm^{-1}) for the 527 nm excitation of the $^4T_2$ band.

The ratio of σ_2/σ_1 obtained from the fit was used with the experimentally measured value of the optical density, and experimental parameters such as pump pulse energy, spot sizes of the pump and probe pulses, and chromium ion density in the sample to estimate the absorption cross section at 3.9 μm from the excited states. The excited state absorption (ESA) cross section at 3.9 μm from the ^2E state is estimated to be 2×10^{-20} cm^2, and from the $^4T_2$ state to be 1.9×10^{-18} cm^2. In view of the size of the error bars in the induced absorption data and the uncertainties in determining the various experimental parameters that enter the estimation of these cross sections, we assign an uncertainty of a factor of five in the absolute values for ESA cross sections. The order of magnitude larger ESA cross section from the $^4T_2$ state at 3.9 μm compared to that from the ^2E state is consistent with the behavior observed in alexandrite at similar wavelengths. This smaller value of the ESA cross section from the ^2E state may be attributed to the fact that $^2E \rightarrow {}^4T_2$ transitions are both first-order spin- and parity forbidden. The absolute magnitude of the ESA cross section from the ^2E state in the infrared is, however, comparable to that in the visible region of the electromagnetic spectrum.

The nonradiative relaxation rates for intra-$^4T_2$ vibrational transitions, $^4T_2 \rightarrow$ metastable level electronic transitions, and the metastable level $\rightarrow {}^4T_2$ thermal repopulation rate of the chromium ion in emerald are comparable to the corresponding transition rates in alexandrite [12]. In ruby the relaxation times were shorter than the resolution limit of the experiment, which led to an upper limit of 5 ps for the $^4T_2$-state nonradiative lifetime [10]. The intra-$^4T_2$-state vibrational relaxation time of the chromium ion in ruby is expected to be considerably smaller than the 5 ps upper limit, which includes the $^4T_2 \rightarrow {}^2E$ electronic relaxation time as well. The vibrational relaxation time of 17 ps in alexandrite is smaller than the 23 ps obtained in emerald. These values suggest a relationship between the intra-$^4T_2$ vibrational relaxation rate and the strength of the crystal field surrounding the chromium ion. The crystal field parameters Dq for ruby, alexandrite and emerald are 1820 cm^{-1}, 1680 cm^{-1} and 1620 cm^{-1}, respectively. So, the intra-$^4T_2$ vibrational relaxation rate appears to decrease as the crystal field strength decreases. However, to establish the exact nature of this dependence a theoretical study with more experimental data for chromium ions in different crystal fields is necessary.

In summary, the picosecond excite-and-probe absorption measurement, together with the simple model for induced absorption, provide first time-resolved estimates of some key excited state nonradiative relaxation parameters. A detailed theoretical model, that takes into consideration the complex nature of lasing-ion excited states and all relevant interactions, is necessary for a more quantitative understanding of the nonradiative transition dynamics between excited states of vibronic laser crystals.

Acknowledgements

We would like to acknowledge Dr. Richard Mandle of Vacuum Ventures, Inc. for providing us with a piece of undoped beryl. The research is supported by Army Research Office, National Aeronautics and Space Administration, and City University Faculty Award program.

References

[1] J.C. Walling, O.G. Peterson, H.P. Jenssen, R.C. Morris and E.W. O'Dell, IEEE J. Quantum Electron. QE-16 (1980) 1302.
[2] M.L. Shand and J.C. Walling, IEEE J. Quantum Electron. QE-18 (1982) 1829.
[3] J. Buchert, A. Katz and R.R. Alfano, IEEE J. Quantum Electron. QE-19 (1983) 1478.
R.R. Alfano and J. Buchert, Emerald laser, chromium doped beryllium silicate laser systems, US Patent 44464761, 7 August 1981.
[4] P.F. Moulton, J. Opt. Soc. Am. B 3 (1986) 125.
[5] P. Kisliuk and C.A. Moore, Phys. Rev. 160 (1967) 307.
[6] S.T. Lai, J. Opt. Soc. Am. B 4 (1987) 1286.
[7] D.L. Wood, J. Chem. Phys. 42 (1965) 3404.
[8] W.M. Fairbank, Jr., G.K. Klauminzer and A.L. Schawlow, Phys. Rev. B 11 (1975) 60.
[9] W.H. Fonger and C.W. Struck, Phys. Rev. B. 11 (1975) 3251.
[10] S.K. Gayen, W.B. Wang, V. Petričević, R. Dorsinville and R.R. Alfano, Appl. Phys. Lett. 47 (1985) 455.

[11] S.K. Gayen, W.B. Wang, V. Petričević and R.R. Alfano, in: Proc. Int. Conf. on Lasers '85, ed. C.P. Wang, (STS Press, McLean, VA, 1986) p. 622.
[12] S.K. Gayen, W.B. Wang, V. Petričević and R.R. Alfano, Appl. Phys. Lett. 49 (1986) 437.
[13] S.K. Gayen, W.B. Wang, V. Petričević, K.M. Yoo and R.R. Alfano, Appl. Phys. Lett. 50 (1987) 1494.
[14] For a discussion of Franck–Condon factors and their model calculations for Cr^{3+} ions, see R. Englman, in: Nonradiative Decay of Ions and Molecules in Solids (North-Holland, Amsterdam, 1979) p. 116.
[15] M.J. Romanelli, in: Mathematical Methods for Digital Computers, eds. A. Ralston and H.S. Wilf (Wiley, New York, 1960) p. 110.
[16] N.H. Schiller, M. Foresti and R.R. Alfano, J. Opt. Soc. Am. B 2 (1985) 729.
[17] A. Seilmeier, K. Spanner, A. Laubereau and W. Kaiser, Opt. Commun. 24 (1978) 237.

15. V. Petričević, A. Seas, and R. R. Alfano, "Effective Gain Measurements in Chromium-Doped Forsterite", OSA Proceedings of the Advanced Solid-State Lasers Conference, March 5-7, 1990, Salt Lake City, Utah, to be published.

Effective Gain Measurements in Chromium-Doped Forsterite

V. Petričević, A. Seas, and R. R. Alfano

Institute for Ultrafast Spectroscopy and Lasers
Departments of Physics and Electrical Engineering
City College of New York, New York, NY10031

ABSTRACT

Effective gain cross-section in tetravalent chromium-doped forsterite laser crystal was measured over the 1180-1330 nm spectral range. The experiment was performed using two collinear laser beams in a pump-and-probe arrangement. The peak gain cross section from this measurement is estimated to be 1.9×10^{-19} cm^2 at 1215 nm which is comparable to the value of ~2 $\times 10^{-19}$ cm^2 predicted by fluorescence linewidth and lifetime measurements. These results indicate that excited-state absorption is not a major loss mechanism in tetravalent chromium-doped forsterite.

I. INTRODUCTION

Chromium-doped forsterite ($Cr:Mg_2SiO_4$) is an important tunable solid-state laser system for the near infrared spectral range. It operates in both pulsed [1]-[3] and continuous-wave [4] mode of operation. Its output can be tuned over the 1167-1345 nm range [5]. The most interesting feature that distinguishes this laser system from other chromium-based lasers is that the lasing ion is tetravalent chromium (Cr^{4+}) in a tetrahedrally coordinated site [2],[3],[6]-[8]. While the spectroscopic properties of chromium-doped forsterite have been studied in some detail [6]-[9], the evaluation of the potentials of this crystal for application as a practical laser system are far from being complete. In this work, we present pump-and-probe measurements of the effective gain cross-section in chromium-doped forsterite. Results of these measurements show the effect of the excited-state absorption (ESA) on the performance of chromium-doped forsterite as a laser crystal.

The most important parameter that characterizes a laser system is the gain cross-section. The gain cross section can be estimated using the Einstein relation which gives gain as a function of the radiative lifetime and fluorescence lineshape. However, very often there is a discrepancy between the values predicted by this relation and the values observed in laser experiments. Lower values of the gain cross section measured in laser experiments are in many cases explained by the existence of loss mechanisms such as excited-state absorption. The net or effective gain cross section is then given by

$$\sigma_{EFF} = \sigma_E - \sigma_{ESA} - \sigma_G \qquad (1)$$

where σ_E is the gain cross section, which can be calculated using the Einstein relation, σ_{ESA} is the excited-state absorption cross section, and σ_G is the ground-state absorption cross section which is negligible in most cases.

ESA is a loss mechanism which impedes or, in some cases, completely inhibits laser action in tunable solid-state laser materials. It has been shown that it severely affects laser performance of V^{2+}-doped crystals [10],[11], prevents laser action in Mn^{2+}-doped crystals [12], and limits the slope efficiency of $Cr^{3+}:Mg_3Ga_2Li_3F_{12}$ laser [13]. It is also present, although without such a detrimental effect, in well developed tunable solid-state lasers such as alexandrite [14]. Absence of ESA is one of the most important advantages of $Ti:Al_2O_3$ laser [15].

In this paper, we present measurements of the effective gain cross-section in $Cr:Mg_2SiO_4$ over

the part of its tuning range. These measurements were undertaken as an attempt to estimate the effect of ESA on laser performance of chromium-doped forsterite laser.

II. EXPERIMENTAL

The $Cr:Mg_2SiO_4$ sample used in this study is a 38 mm long and 4 mm in diameter single-crystal laser rod with end facets anti-reflection coated for the 1.1-1.4 μm spectral range. The crystal was grown by Czochralski technique at the Electronic Materials Research Laboratory of the Mitsui Mining and Smelting Co., Ltd., Japan. The total chromium ion concentration in the crystal is 3-4 x 10^{18} cm^{-3}. The crystal contains both Cr^{3+} and Cr^{4+} ions with the relative concentration of Cr^{3+} and Cr^{4+} ions unknown. The Cr^{4+} concentration was increased by growing the crystal in more oxidizing atmosphere (~1 % oxygen partial pressure). The ground-state absorption spectrum of $Cr:Mg_2SiO_4$ for E ∥ b axis is shown in Fig. 1. The spectrum shows contributions from both the active ions, Cr^{3+} and Cr^{4+}. The transition assignments in Fig. 1 were made [6],[9] using Tanabe-Sugano diagrams for Cr^{3+} ions in octahedral coordination and Cr^{4+} in tetrahedral coordination.

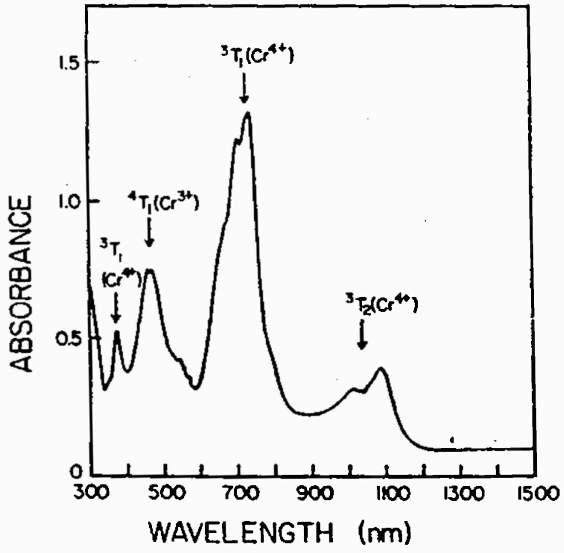

Figure 1. Room temperature absorption spectrum of $Cr:Mg_2SiO_4$ for E ∥ b axis.

The effective gain measurements were performed using standard pump-and-probe arrangement. As a pump source the fundamental 1064-nm radiation from a pulsed Nd:YAG laser was used to selectively populate only the $^3T_2$ state of the Cr^{4+} ion, the upper lasing level of the chromium-doped forsterite laser. The choice of a probe beam source depends on the wavelength range that is being investigated. In the wavelength region where the emission is too intense, i.e. in the tuning range of the laser crystal under investigation, tungsten or xenon lamps cannot be used, since the fluorescence from the sample overwhelms the probe beam [10],[11]. Therefore, we decided to use laser as a probe source. A tunable Cr:forsterite laser appeared to be an ideal probe beam source for this measurement.

The experimental setup used to measure the effective gain cross-section is shown schematically in Fig. 2. The $^3T_2$ state of the Cr^{4+} ion was populated by 1064-nm pump beam obtained from a Q-switched Nd:YAG laser operating at 10 Hz repetition rate. The pump beam was weakly focused to a 400-μm radius spot on the sample by a 1-m focal length lens. Typical pump beam energy incident on the sample was ~1 mJ per pulse, of which 79 % was absorbed in the sample. The excited state was probed by a collinearly propagating probe beam. The weak probe beam (typically ~25 μJ per puise) was obtained from a tunable Cr:forsterite laser pumped by the same Nd:YAG laser used to pump the sample. Wavelength tuning of the probe beam was accomplished by using a birefringent plate at Brewster's angle as an intracavity dispersive element and by changing the output mirror [5]. The delay between the pump pulse and the probe pulse was smaller than 100 ns. Since the room temperature lifetime of the $^3T_2$ state in chromium-doped forsterite is 2.7 μs, no appreciable depopulation of the excited state takes place before the arrival of the probe pulse. Probe beam was focused on the sample by 30-cm focal length lens to a 150-μm radius spot. The pump and probe beams were carefully overlapped in the sample using two 0.8-mm apertures so that the probe beam was fully concentric within the pump-beam. The overlap of the two beams was checked by scanning a razor blade mounted on a translation stage across the beam in both vertical and horizontal directions, before and behind the sample.

The effective gain cross section was estimated from the ratio of the transmitted probe intensity for the pumped and unpumped conditions of the sample, respectively. The transmitted probe

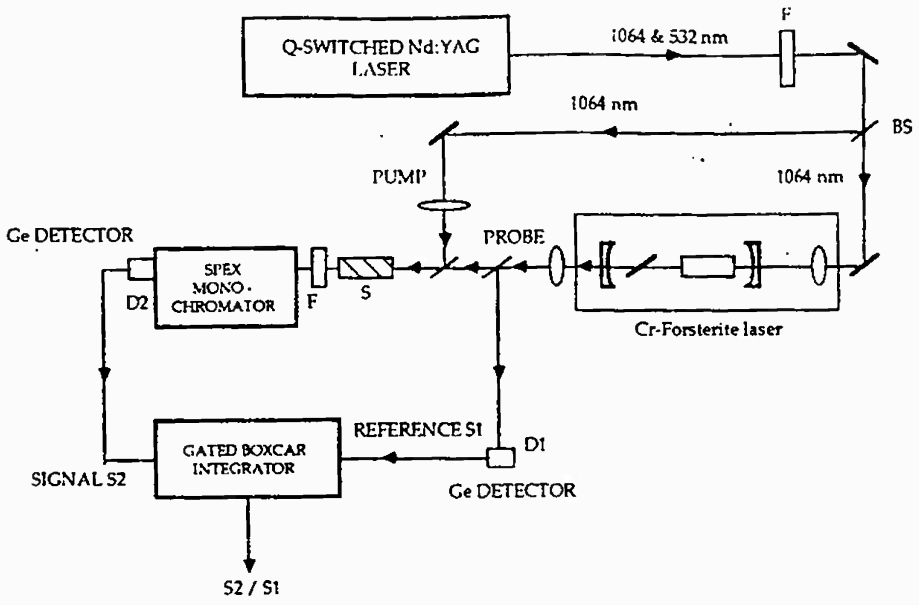

Figure 2. Experimental setup used to measure the effective gain cross-section in Chromium-doped forsterite.

intensity was normalized with respect to probe intensity before the sample to account for the pulse-to-pulse energy fluctuations. The probe beam intensity before the sample was monitored with a beam splitter and a fast germanium photodiode D_1. The transmitted probe beam was analyzed by a 1/4-meter spectrometer and its intensity was monitored by an identical germanium photodiode D_2. A gated boxcar integrator was used to obtain the average ratio S_2/S_1, where S_2 is the signal proportional to the intensity of the transmitted probe beam measured by a germanium detector D_2 at the end of the spectrometer, and S_1 is proportional to the intensity of the probe beam before the sample measured by a germanium detector D_1. The average was taken over 100 laser shots to enhance the signal-to-noise ratio.

Excited-state population density (N_E) was estimated by measuring the pumped volume of the sample and the energy of the pump pulse absorbed in the crystal, assuming that each absorbed pump photon creates one excited ion. The pumped volume of the crystal was estimated by measuring the size of the pump beam at the position of the sample. Since the pump beam was weakly focused with a long focal-length lens and a 0.8 mm aperture was used in front of the sample, the transverse beam intensity distribution was measured to be approximately uniform, with the beam radius of 0.4 mm throughout the crystal.

III. RESULTS

The normalized probe transmission S_2/S_1 was used to determine the value of the effective gain cross-section in chromium-doped forsterite. It has been shown [18],[19] that the effective gain cross section σ_{EFF} can be calculated using the expression

$$\sigma_{EFF} = \sigma_E - \sigma_{ESA} - \sigma_G = -(1/N_E\ell)\ln R, \qquad (2)$$

where σ_E is the gain cross section, σ_{ESA} is the excited-state absorption cross section, σ_G is the ground state absorption cross section at probe wavelength, N_E is the excited-state population density of , ℓ is the length of the crystal and R is defined by

$$R = (S_2/S_1)_u/(S_2/S_1)_p. \qquad (3)$$

The subscripts u and p refer to unpumped and pumped cases, respectively.

The measured effective (net) gain cross section as a function of wavelength in the 1180-1330 nm wavelength region is presented in Fig. 3 by triangles superimposed on the fluorescence spectrum. The near-infrared portion the absorption spectrum is also displayed for comparison.

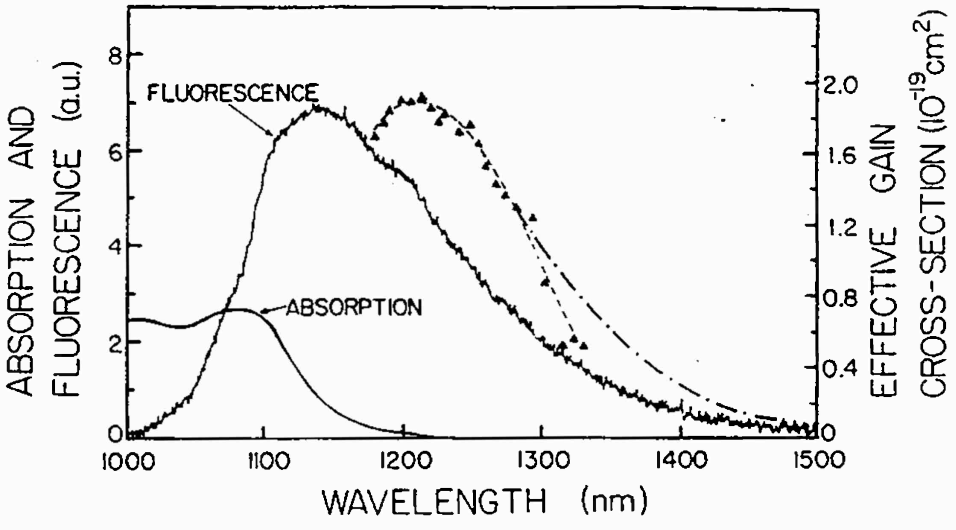

Figure 3 The Fluorescence spectrum for 1064-nm excitation ant the infrared absorption spectrum of chromium-doped forsterite (solid line) and the effective gain cross-section (triangles and broken line). Dot-dash curve shows the expected gain in case there is no ESA.

IV. DISCUSSION

In Cr-doped forsterite the laser-active ion is tetrahedrally coordinated tetravalent chromium, Cr^{4+} and therefore the possible transitions that may affect laser operation occur between different states of the Cr^{4+} ion.

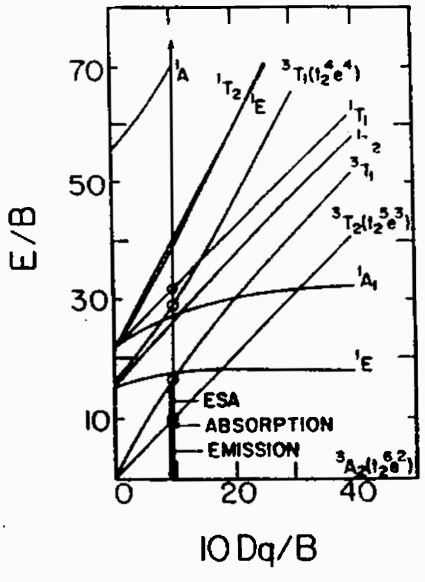

Figure 4 Tanabe-Sugano diagram for Cr^{4+} in tetrahedral coordination. Crystal field parameter Dq=915 cm^{-1} and Raccah parametr B=970 cm^{-1}. The possible $^3T_2 \rightarrow {}^3T_1$ excited-state absorption is indicated by an arrow.

For near-infrared pumping (e.g. 1064-nm radiation from Nd:YAG laser) only the $^3A_2 \rightarrow {}^3T_2$ transition between the ground state and the first excited state of the Cr^{4+} ion takes place, that is only Cr^{4+} ions are being excited. The ESA transitions are then expected to originate from the relaxed $^3T_2$ state of the Cr^{4+} ion.

From the Tanabe-Sugano diagram for tetravalent chromium in Cr:Mg_2SiO_4, shown in Fig. 4, it is possible to predict the wavelength of the peak of the ESA. Using Dq=915 cm^{-1} and B=970 cm^{-1} a maximum of ESA due to $^3T_2 \rightarrow {}^3T_1$ transition may be expected at ~1500 nm.

It has been suggested [16], [17] that the same $^3T_2 \rightarrow {}^3T_1$ transition may be responsible for limited tuning range of the Cr:YAG laser, besides Cr:forsterite the only other successful Cr^{4+}-based laser system, to date. The same process may be the reason that laser experiments in Cr^{4+}-doped garnets such as GSGG, GSAG and YSGG were unsuccessful so far.

The salient features of the gain curve obtained from the pump-and-probe measurements shown in Fig. 3 are the peak value of 1.9 x 10^{-19} cm^2 at 1215 nm and the shape of the curve. The shift of the peak of the gain curve with respect to the peak of the fluorescence curve in Fig. 3 is a consequence of the overlap of the fluorescence band with the low energy tail of the absorption band. The shape of

the gain curve, which is expected to follow the fluorescence curve, deviates slightly from it in the wavelength range beyond 1300 nm as shown by dot-dash curve. The higher than expected decrease of the gain in this range most likely arises from the onset of the ESA. This is in agreement with the predicted wavelength of ESA approaching 1500 nm. This is also in accordance with the suggested ESA in Cr:YAG and Cr: GSGG.

The results of the pump-and-probe experiment show that in the case of chromium-doped forsterite the role of ESA is not so prominent in the bigger portion of the tuning range. The measured values of the net gain cross section are in good agreement with the value of $\sim 2 \times 10^{-19}$ cm^2 for the peak gain cross section obtained from radiative lifetime and fluorescence lineshape measurements. These values are also in excellent agreement with the gain cross-sections obtained from both pulsed and continuous-wave laser experiments. The gain cross sections estimated from different measurements are summarized in Table 1.

V. CONCLUSIONS

The effective gain cross-section in chromium-doped forsterite laser crystal has been measured over the 1180-1330 nm spectral range. The close agreement between the measured effective gain cross section and the peak gain cross-section predicted using radiative lifetime and fluorescence linewidth indicates that ESA cross section is considerably smaller than the gain cross section. This agreement implies that ESA is not a major loss mechanism in chromium-doped forsterite for wavelengths shorter than 1300 nm. There is a possibility of the onset of a weak ESA occuring beyond 1300 nm.

ACKNOWLEDGMENTS

We thank Mr. K. Yamagishi of the Mitsui Mining and Smelting Co., Ltd., Japan for growing the Cr:Mg_2SiO_4 crystal used in this study and Professor S. K. Gayen for helpful discussion. The research is supported by the Army Research Office and National Aeronautics and Space Administration.

Table 1: ESTIMATES OF GAIN CROSS SECTION FROM DIFFERENT MEASUREMENTS

Experiment	λ (nm)	σ (cm^2)
Linewidth and Lifetime Measurements	1140	2×10^{-19} (calculated)
CW Laser Operation	1244	1.47×10^{-19}
Pulsed Laser Operation	1235	1.44×10^{-19}
Pump-and-probe Experiment	1200	1.8×10^{-19}

REFERENCES

1. V. Petričević, S. K. Gayen, R. R. Alfano, K. Yamagishi, H. Anzai, and Y. Yamaguchi, Appl. Phys. Lett. **52**, 1040 (1988).
2. V. Petričević, S. K. Gayen, and R. R. Alfano, Appl. Phys. Lett. **53**, 2590 (1988).
3. H. R. Verdun, L. M. Thomas, D. M. Andrauskas, T. M. Collum, and A. Pinto, Appl. Phys. Lett. **53**, 2593 (1988).
4. V. Petričević, S. K. Gayen, and R. R. Alfano, Opt. Lett. **14**, 612 (1989).
5. V. Petričević, S. K. Gayen, and R. R. Alfano, Appl. Opt. **28**, 1609 (1989).
6. V. Petričević, S. K. Gayen, and R. R. Alfano, in *Tunable Solid-State Lasers*, Vol. 5 of the OSA Proceeding Series, M. L. Shand and H. P. Jenssen, eds. (Optical Society of America, Washington, D.C., 1989), pp. 77-84.
7. H. R. Verdun, L. M. Thomas, and D. M. Andrauskas, in *Tunable Solid-State Lasers*, Vol. 5 of the OSA Proceeding Series, M. L. Shand and H. P. Jenssen, eds. (Optical Society of America, Washington, D.C., 1989), pp. 85-92.
8. R. Moncorge, D. J. Simkin, G. Cormier, and J. A. Capobianco, in *Tunable Solid-State Lasers*, Vol. 5 of the OSA Proceeding Series, M. L. Shand and H. P. Jenssen, eds. (Optical Society of America, Washington, D.C., 1989), pp. 93-97.
9. V. Petričević, S. K. Gayen, A. Seas, and R. R. Alfano, J. Lumin., submitted for publication.
10. R. Moncorge and T. Benyattou, Phys. Rev. B **37**, 9177 (1988).
11. S. A. Payne, L. L. Chase, and G. D. Wilke, Phys. Rev. B **37**, 998 (1988).
12. R. Clausen and K. Petermann, IEEE J. Quantum Electron. **24**, 1114 (1988).
13. J. Caird, S. A. Payne, P. R. Staver, A. J. Ramponi, L. L. Chase, and W. E. Krupke, IEEE J. Quantum Electron. **24**, 1077 (1988).
14. M. L. Shand and J. C. Walling, IEEE J. Quantum Electron. QE-18, 1152 (1982).
15. P. F. Moulton, J. Opt. Soc. Am. B **3**, 125 (1986).
16. A. P. Shkadarevich, in *Tunable Solid-State Lasers*, Vol. 5 of the OSA Proceeding Series, M. L. Shand and H. P. Jenssen, eds. (Optical Society of America, Washington, D.C., 1989), pp. 60-65.
17. G. M. Zverev and A. V. Shestakov, in *Tunable Solid-State Lasers*, Vol. 5 of the OSA Proceeding Series, M. L. Shand and H. P. Jenssen, eds. (Optical Society of America, Washington, D.C., 1989), pp. 66-70.
18. V. Petričević, A. Seas, and R. R. Alfano, to be published.
19. D. S. Hamilton, S. K. Gayen, G. J. Pogatshnik, R. D. Ghen, and W. J. Miniscalco, Phys. Rev. B **39**, 8807 (1989).

16. V. Petričević, A. Seas, and R. R. Alfano, "Slope Efficiency Measurements of Chromium-Doped Forsterite Laser", Opt. Lett., accepted for publication.

Slope Efficiency Measurements of Chromium-Doped Forsterite Laser

V. Petričević, A. Seas and R. R. Alfano
Institute for Ultrafast Spectroscopy and Lasers
and
Center for Analysis of Structures and Interfaces
Departments of Physics and Electrical Engineering
City College of New York, New York, NY 10031

Abstract

The slope efficiency of the continuous-wave chromium-doped forsterite ($Cr:Mg_2SiO_4$) laser has been measured using four different output mirrors. The maximum slope efficiency of 38% was achieved using 11% output coupler. The extrapolated limiting slope efficiency in the absence of passive losses is estimated to be 65%. This value corresponds to an intrinsic quantum efficiency of 77%, which is similar to the efficiencies determined for mature tunable solid state laser systems.

MS # 90 - 33
Optics Letters

Chromium-doped forsterite ($Cr:Mg_2SiO_4$) is an important tunable solid state laser which fills the void in the spectral region between 1100 - 1350 nm. Pulsed[1-4] and continuous-wave[5] laser action was obtained and tunability over the 1130 - 1367 nm was demonstrated.[6,7] The unique property of chromium-doped forsterite is that the lasing center was identified as tetravalent chromium (Cr^{4+}) substituting for tetrahedrally coordinated Si^{4+}.[8,9] Tetrahedral Si^{4+} site occupied by Cr^{4+} ions lacks inversion symmetry and provides odd-parity field necessary to relax the parity selection rule, making electric dipole transitions possible. This results in high transition strengths observed in the absorption spectra where Cr^{4+} features are dominant, and in relatively short radiative lifetime τ_R of 25 μs, as well as in high stimulated emission cross section of the order of 2×10^{-19} cm^2.[8,10] Room-temperature quantum yield η was estimated from the ratio between the room-temperature fluorescence lifetime τ and the radiative lifetime ($\eta = \tau/\tau_R$) to be ~10%. The highest slope efficiency of the Cr:forsterite laser previously reported[8] was 23%. When the inverse slope efficiency is plotted as a function of the inverse output coupling factor, (when different output mirrors are used), the limiting slope efficiency η_o, which can be achieved in the absence of passive losses, can be determined. In this paper, we follow the approach of Caird et al.[11] to determine the limiting slope efficiency and estimate the role of various loss mechanisms on laser performance of the Cr: forsterite laser.

The equation for the output power slope efficiency

$$\eta_s = (\lambda_P/\lambda_L)(T/L+T) \qquad (1)$$

which gives the slope efficiency as a function of the output coupling parameter T and loss L, was originally derived by Danielmeyer,[12] and later modified by Caird et

al.[11] to make allowance for a possibility of nonunity pumping efficiency and to include a loss factor due to excited-state absorption (ESA).

The inverse output power slope efficiency $1/\eta_s$ and the inverse of the limiting slope efficiency $1/\eta_o$ are connected by a linear relationship:[11]

$$\eta_s^{-1} = \eta_o^{-1}(1+LT^{-1}), \qquad (2)$$

where

$$\eta_o = \eta_P(\lambda_P/\lambda_L)(\sigma_{EFF}/\sigma_E). \qquad (3)$$

In equations (2) and (3) η_P is the pumping efficiency, λ_P is the pump wavelength, λ_L is the lasing wavelength, σ_E is the gain cross section, and σ_{EFF} is given by

$$\sigma_{EFF} = \sigma_E - \sigma_{ESA} \qquad (4)$$

where σ_{ESA} is the excited state absorption cross section.

It is obvious from the equation (3) that in order to achieve the quantum defect limited value of the slope efficiency λ_P/λ_L the excited state absorption cross section σ_{ESA} must be negligible and the pumping efficiency must be close to unity.

The value of the limiting slope efficiency η_o can be obtained by extrapolating the inverse slope efficiency η_s^{-1} as a function of the inverse output coupling T^{-1} to $T^{-1} = 0$. η_o can be used to estimate the excited state absorption cross section, i.e. the deviation of the effective gain cross section from the stimulated emission cross section predicted by the lineshape and the lifetime measurements.

The sample used in these laser experiments is a 4.5 mm x 9 mm x 9 mm rectangular parallelepiped with the three mutually orthogonal axes oriented along the *b*, *c*, and *a* crystallographic axes of the crystal. The *a* axis is parallel to the 4.5 mm

side of the crystal and perpendicular to the 9 mm x 9 mm face. The crystal contains 0.04 at. % of Cr ions, which is equivalent to a total chromium ion concentration of 1.1×10^{19} ions/cm^3. The relative concentrations of Cr^{3+} and Cr^{4+} ions is not known.

The limiting slope efficiency of the Cr:Mg_2SiO_4 laser was measured using a standard 3-mirror astigmatically compensated cavity.[13] The three-mirror cavity was chosen not because the Brewster-cut crystal was used, but rather because of its flexibility and usefulness for other applications, such as mode locked operation, when a possibility of changing the length has to be combined with small mode size and when tighter focusing is needed. The experimental setup is shown in Fig. 1. The 5-cm-radius back mirror and the 10-cm-radius folding mirror have 99.99% reflectivity over the 1200 - 1300 nm range and high transmission (>80%) for the pump 1064-nm radiation. Output coupling factor T was varied by changing the flat output mirror. Four different output couplers with transmission of 0.65%, 3.4%, 7.8 %, and 11 % over the 1200 - 1300 nm spectral range and transmission >85% for 1064-nm radiation were used. Since transmission is high for pump radiation wavelength of 1064 nm for all three mirrors of the cavity, no corrections were made to account for the second pass absorption of the portion of the pump beam that is reflected back from the output coupler.

The chromium-doped forsterite crystal was placed at the center of the short arm of the three-mirror cavity and was pumped longitudinally with 1064-nm radiation from a cw Nd:YAG laser. The pump beam was linearly polarized along the *b* axis and propagated along the *a* axis of the crystal. The position of the 7.5-cm-focal-length lens was adjusted for the best overlap of the pump beam and the cavity mode by monitoring the output power. The pump beam was chopped at a duty cycle of 15:1 to reduce thermal effects.

The experimental results are summarized in Table 1. The inverse slope efficiency as a function of output coupling is shown in Fig. 2. The inverse slope efficiency extrapolates to a limiting power slope efficiency of η_o = ~65 %. If this value is multiplied by the ratio of the laser and pump wavelengths (λ_L/λ_P), an exstrapolated quantum slope efficiency or intrinsic quantum efficiency η_q, as defined by Chase et al.[14], of 77% is obtained. Although considerably smaller than unity, this is still one of the highest values ever measured for a tunable solid-state laser.[1]

The slope of the line in Fig. 2 represents the passive loss of ~10% which is due to a combination of effects such as reflection loss, less than perfectly parallel faces of the crystal, incomplete overlap of the pumped volume and cavity mode volume, as well as residual absorption and scattering loss. Parallelism of the sample is not known. The absorption and scattering loss is estimated from the transmission spectrum of the crystal corrected for Fresnel loss to be <0.5% for the 4.5-cm path length and therefore does not play a major role.

The deviation of the measured intrinsic quantum efficiency from unity can be explained either by the presence of the ESA or by pumping efficiency $\eta_P < 1$.

To estimate the role of ESA, the effective gain (σ_{EFF}) was measured using standard pump-and-probe arrangement. The details of the experiment will be published elsewhere.[10] The measured effective (net) gain cross section as a function of wavelength in the 1180-1330 nm wavelength region is presented in Fig. 3 by triangles superimposed on the fluorescence spectrum. The near-infrared portion of the absorption spectrum is also displayed for comparison.

The salient features of the gain curve obtained from the pump-and-probe measurements shown in Fig. 3 are the peak value of 1.9×10^{-19} cm^2 at 1215 nm and

the shape of the curve. The shift of the peak of the gain curve with respect to the peak of the fluorescence curve in Fig. 3 is a consequence of the overlap of the fluorescence band with the low energy tail of the absorption band. The shape of the gain curve, which is expected to follow the fluorescence curve deviates slightly from it in the wavelength range beyond 1300 nm as shown by a dot-dash curve. The higher than expected decrease of the gain in this range most likely arises from the onset of the ESA. This is in agreement with the predicted wavelength of ESA approaching 1700 nm.[10]

The results of the pump-and-probe experiment show that in the case of chromium-doped forsterite the role of ESA is not so prominent in the larger portion of the tuning range. The measured values of the net gain cross section are in good agreement with the value of ~2.11 x 10^{-19} cm^2 for the peak gain cross section calculated using results of the lineshape and radiative lifetime measurements.[10] These values are also in excellent agreement with the gain cross-sections obtained from both pulsed and continuous-wave laser experiments.[5,8] The gain cross sections estimated from different measurements are summarized in Table 2.

Since the measurements of the effective gain did not show presence of significant excited state absorption, the only remaining possibility is $\eta_P < 1$. One possible loss mechanism that may give rise to smaller-than-unity pumping efficiency is excited state absorption of the pump radiation, as suggested by Verdun et al.[15] The possibility of a process involving absorption or inelastic scattering from the excited state is also confirmed by the presence of a faint visible radiation which was observed when the forsterite is pumped by a continuous-wave 1064-nm radiation.

In conclusion, the limiting slope efficiency and the intrinsic quantum efficiency of the chromium-doped forsterite laser has been measured. The measured intrinsic quantum efficiency is one of the highest ever reported for a tunable solid-state laser. To account for the discrepancy between the quantum defect limited efficiency and the measured limited slope efficiency (i. e. the deviation of the measured intrinsic quantum efficiency from unity), effect of ESA was investigated by measuring the effective gain cross section using pump-and-probe technique. The effective gain cross-section in chromium-doped forsterite laser crystal has been measured over the 1180-1330 nm spectral range. The close agreement between the measured effective gain cross section and the peak gain cross-section predicted using radiative lifetime and fluorescence linewidth indicates that ESA cross section is considerably smaller than the gain cross section. This agreement implies that ESA is not a major loss mechanism in chromium-doped forsterite for wavelengths shorter than 1300 nm. There is a possibility of the onset of a weak ESA occuring beyond 1300 nm. As a possible loss mechanism that may be responsible for the observed discrepancy an excited state absorption in the pump wavelength region is suggested.

This work is supported in part by Army Research Office and National Science Foundation.

References:

1. V. Petričević, S. K. Gayen, R. R. Alfano, K. Yamagishi, H. Anzai, and Y. Yamaguchi, Appl. Phys. Lett. **52**, 1040 (1988).

2. V. Petričević, S. K. Gayen, and R. R. Alfano, Appl. Opt. **27**, 4162 (1988).

3. V. Petričević, S. K. Gayen, and R. R. Alfano, Appl. Phys. Lett. **53**, 2590 (1988).

4. H. R. Verdun, L. M. Thomas, D. M. Andrauskas, T. McCollum, and A. Pinto, Appl. Phys. Lett. **53**, 2593 (1988).

5. V. Petričević, S. K. Gayen, and R. R. Alfano, Opt. Lett. **14**, 612 (1989).

6. V. Petričević, S. K. Gayen, and R. R. Alfano, Appl. Opt. **28**, 1609 (1989).

7. V. G. Barishevskii, M. V. Korzhik, A. E. Kimaev, M. G. Livshitz, V. B. Pavlenko, M. L. Meilman, and B. I. Minkov, Zh. Prikl. Spectrosk. **53**, 7 (1990).

8. V. Petričević, S. K. Gayen, and R. R. Alfano, in *Tunable Solid-State Lasers*, Vol. 5 of the OSA Proceeding Series, M. L. Shand and H. P. Jenssen, eds. (Optical Society of America, Washington, D.C., 1989), pp. 77-84.

9. H. R. Verdun, L. M. Thomas, D. M. Andrauskas, and A. Pinto, in *Tunable Solid-State Lasers*, Vol. 5 of the OSA Proceeding Series, M. L. Shand and H. P. Jenssen, eds. (Optical Society of America, Washington, D.C., 1989), pp. 85-92.

10. V. Petričević, A. Seas, and R. R. Alfano, OSA Proceedings of the Advanced Solid-State Lasers Conference, March 5-7, 1990, Salt Lake City, Utah, to be published.

11. J. A. Caird, S. A. Payne, P. R. Staver, A. J. Ramponi, L. L. Chase, and W. F. Krupke, IEEE J. Quantum Electron. **24**, 1077 (1988).

12. H. G. Danielmeyer, in *Lasers*, A. K. Levine and A. De Maria, eds. (Dekker, New York, 1975), Vol. IV.

13. H. W. Kogelnik, E. P. Ippen, A. Dienes, and C. V. Shank, IEEE J. Quantum Electron. **QE-8**, 373 (1972).

14. L. L. Chase and S. A. Payne, Optics and Photonics News, Vol. 1, No. 8, 16 (Aug. 1990).

15. H. R. Verdun and A. Pinto, Bull. Am. Phys. Soc. **35**, 1499 (1990). Presented at the Sixth Interdisciplinary Laser Science Conference (ILS-VI), September 16-19, 1990, Minneapolis, Minnesota.

Figure Captions:

Figure 1 Schematic diagram of the experimental arrangement for measuring the limiting slope efficiency of Cr:forsterite laser: C, light chopper; F_1, variable neutral density filter; L, focusing lens; M_1, 5-cm radius back mirror; M_2, 10-cm radius folding mirror; M_O, output mirror; S, sample; T, birefingent tuning plate; F_2, 1064-nm cutoff filter, Cr:forsterite laser emission-transmitting filter; PM, power meter.

Figure 2 Inverse slope efficiency $1/\eta_s$ as a function of inverse output coupling $1/T$ for cw Nd:YAG-pumped continuous-wave Cr:Mg_2SiO_4laser. 10% uncertainty in the measured slope efficiencies was assumed. Extrapolating the data limiting slope efficiency of η_o >65 % is obtained.

Figure 3 The Fluorescence spectrum for 1064-nm excitation and the infrared absorption spectrum of chromium-doped forsterite (solid line) and the effective gain cross-section (triangles and broken line). Dot-dash curve shows the expected gain in case there is no ESA.

TABLE 1: Slope Efficiency and Threshold of cw Cr:Mg_2SiO_4 Laser for Various Output Couplers

Output Mirror Transmission [%]	Slope Efficiency [%]	Threshold Absorbed Power [mW]	Output Wavelength [nm]
0.65	5.69	500	1260
3.4	24.65	1200	1258
7.8	31.76	1600	1265
11	37.85	1800	1242

TABLE 2: Estimates of Gain Cross Section From Different Measurements

Experiment	λ (nm)	σ (cm^2)	Reference
Linewidth and Lifetime Measurements	1140	2.11×10^{-19} (calculated)	10
CW Laser Operation	1244	1.47×10^{-19}	8
Pulsed Laser Operation	1235	1.44×10^{-19}	8
Pump-and-probe Experiment	1200	1.8×10^{-19}	10

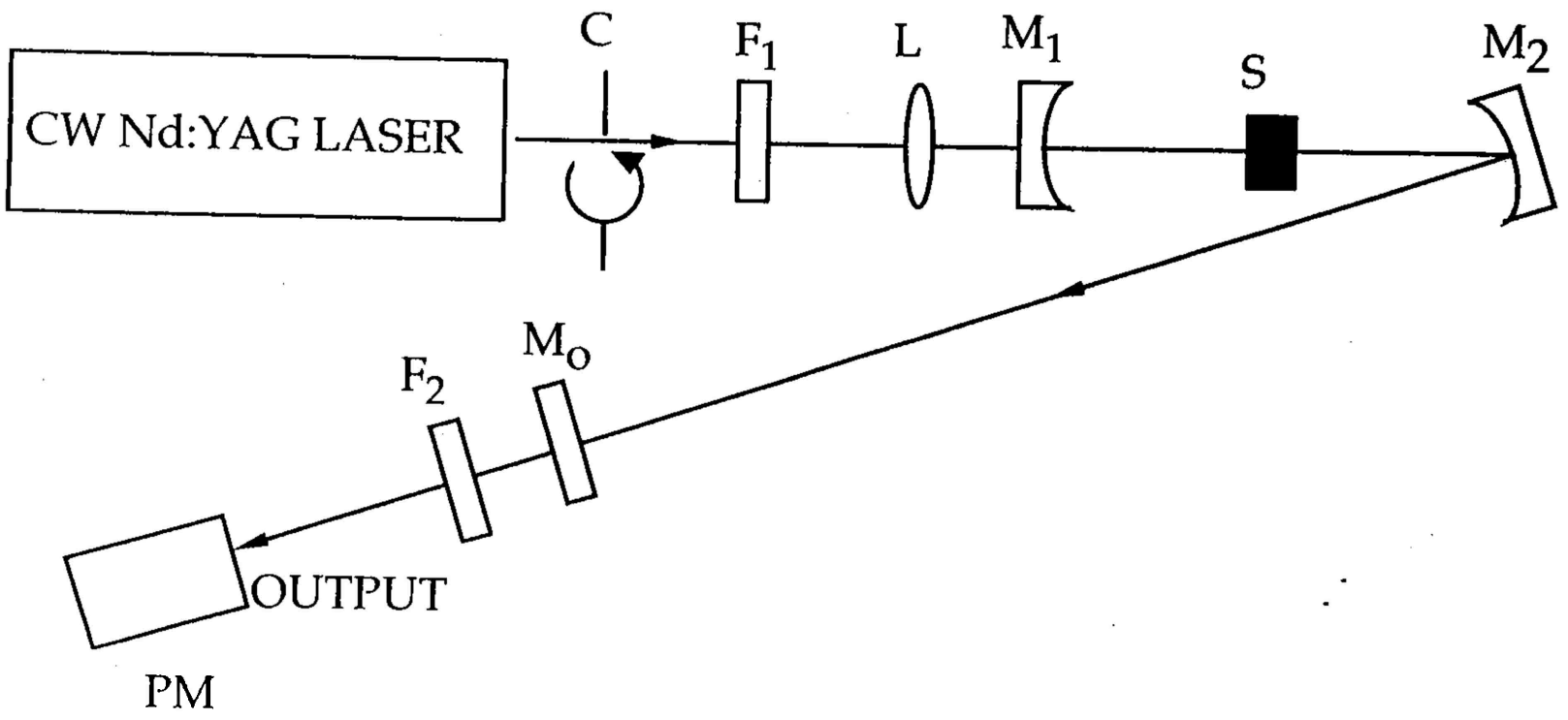

Figure 1

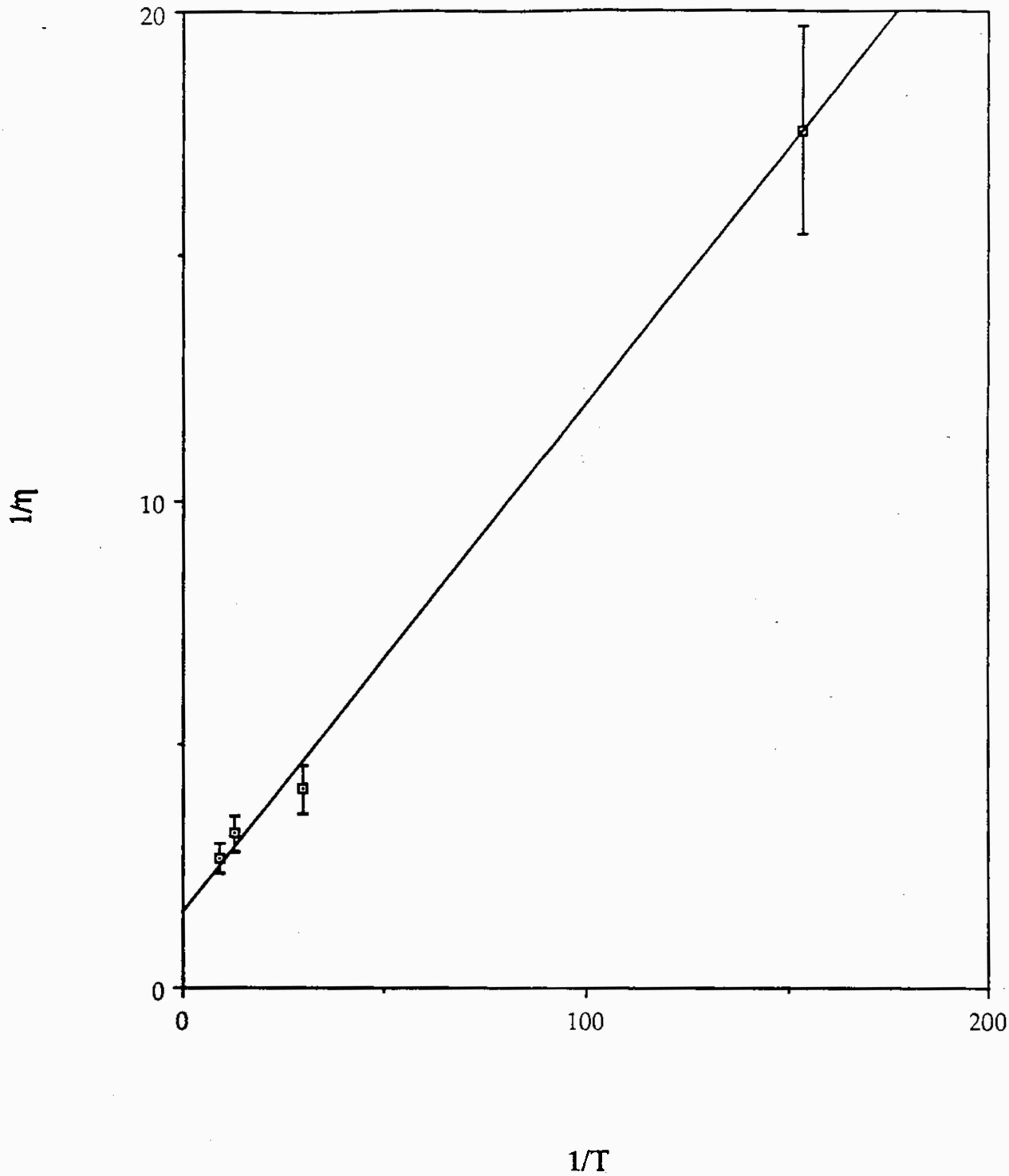

Figure 2

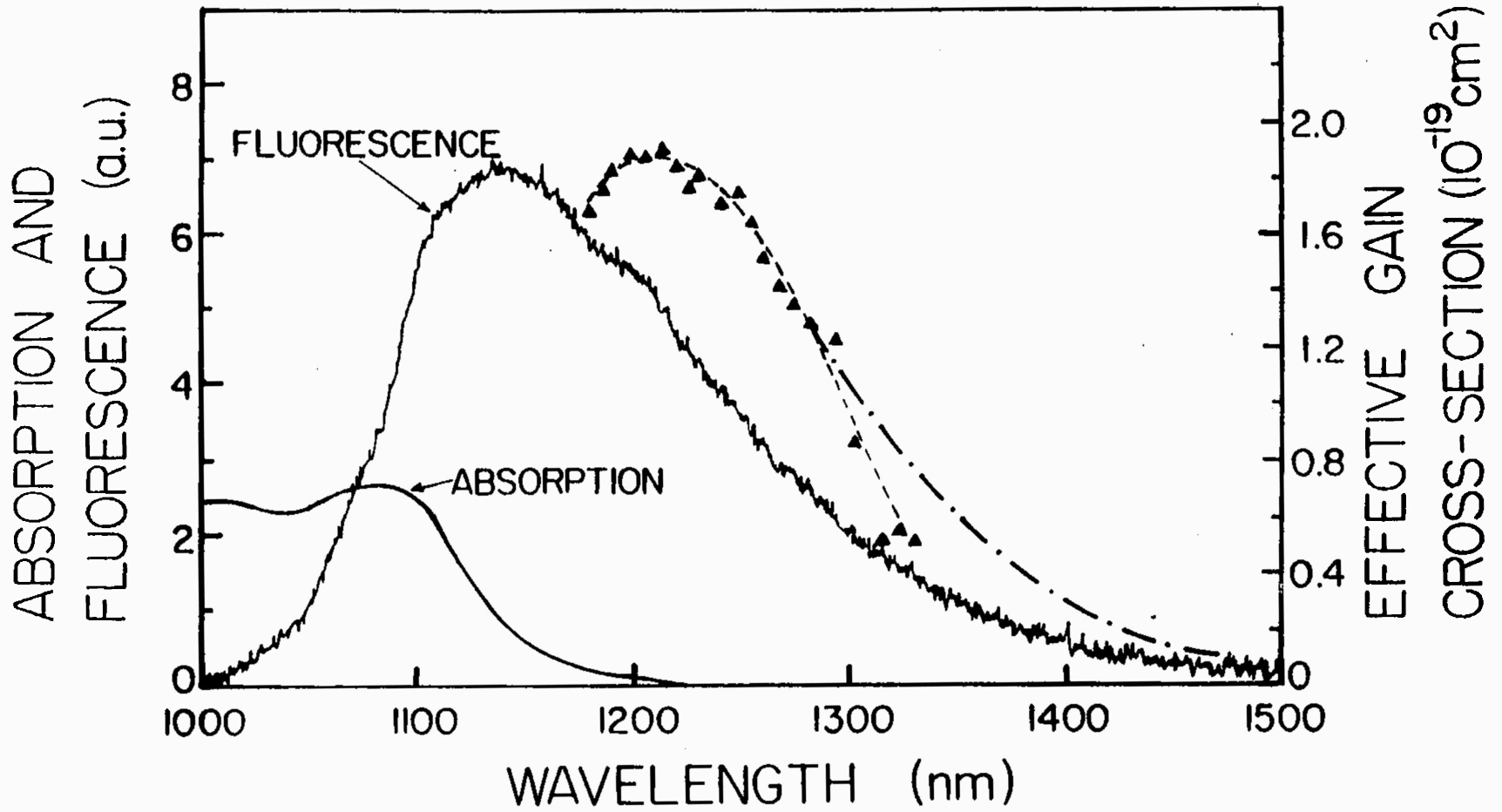
ABSORPTION AND
FLUORESCENCE (a.u.)
FLUORESCENCE
ABSORPTION
0
2
4
6
8
1000
1100
1200
1300
1400
1500
WAVELENGTH (nm)
EFFECTIVE GAIN
CROSS-SECTION (10^{-19}cm^2)
0
0.4
0.8
1.2
1.6
2.0

Figure 3

Abstracts & Presentations

1. S. K. Gayen, V. Petričević, R. R. Alfano, K. Yamagishi, and K. Moriya, "Spectroscopic Properties of Cr^{3+}:Mg_2SiO_4: A New Tunable Solid State Laser Crystal", Bull. Am. Phys. Soc. 33, 810 (1988). Presented at the March Meeting of the American Physical Society, 21-25 March, 1988, New Orleans, Louisiana.

2. V. Petričević, S. K. Gayen, R. R. Alfano, K. Yamagishi, and K. Moriya, "Room-Temperature Pulsed Laser Action in Cr^{3+}:Mg_2SiO_4", Bull. Am. Phys. Soc. 33, 811 (1988). Presented at the March Meeting of the American Physical Society, 21-25 March, 1988, New Orleans, Louisiana.

From the Program of the 1988 March Meeting of the APS, 21-25 March 1988, New Orleans, Louisiana.

SESSION S10: OPTICAL PROPERTIES: IONS IN SOLIDS II
Friday afternoon, 25 March 1988
La Galerie 5 at 14:30
Y. Chen, presiding

14:30
S10 1 A New Third Order Contribution to Spin-Forbidden Rare Earth Optical Transition Intensities. M. C. DOWNER* and G. W. BURDICK, University of Texas at Austin; * D. K. SARDAR, University of Texas at San Antonio.-- We show by quantitative calculation that numerous spin-forbidden linear optical transitions in trivalent rare earth ions acquire a major fraction of their intensity from hitherto neglected contributions involving spin-orbit linkages in excited configurations. The strong effect of analogous linkages has been demonstrated in two-photon absorption[1,2]. We present a revised analysis of observed linear absorption intensities for Eu^{3+} and Gd^{3+}, which shows that the new contribution is often comparable to, and sometimes larger than, standard contributions. We thereby demonstrate an improved fit to observed intensities. In addition previously fitted phenomenological parameters[3] must be modified substantially, suggesting that re-analysis of linear intensity data for all trivalent rare earths is warranted.
* Partially supported by an IBM Faculty Development Award
* Supported by the Robert A. Welch Foundation
1. B. R. Judd and D. R. Pooler, J. Phys. C 15, 591 (1982).
2. M. C. Downer and A. Bivas, Phys. Rev. B 28, 3677 (1983).
3. W. T. Carnall, P. R. Fields, and K. Rajnak, J. Chem. Phys. 49, 4412 (1968).

14:42
S10 2 Laser-Induced Gratings in Eu^{3+}-Doped Glasses. E.G. BEHRENS and R.C. POWELL, Oklahoma State Univ.*--Holographic gratings were produced in Eu^{3+}-doped phosphate and silicate glasses using crossed laser beams tuned to resonance with the absorption transition to the $^5D_2$ level of the Eu^{3+} ion. These are stable at room temperature and are associated with local structural changes in the glass due to radiationless relaxation of the Eu^{3+} ions. The use of these gratings in demultiplexing multifrequency laser beams is demonstrated. The scattering efficiencies for different glass compositions and Eu concentrations are reported. The scattering efficiency of the grating is shown to decrease as the size of the network modifier ions is increased. Measurements of the Bragg scattering angle for different wavelengths show that the wavelength of the induced refractive index gratings is twice the wavelength of the light intensity pattern used to write the gratings.
*Supported by the U.S. Army Research Office

14:54
S10 3 Spectroscopic Properties of Cr^{3+}: Mg_2SiO_4: A New Tunable Solid-State Laser Crystal. S. K. GAYEN, V. PETRICEVIC, R. R. ALFANO, City College of New York;* KIYOSHI YAMAGISHI, KAZUO MORIYA, Mitsui Mining and Smelting Co. Ltd. -- Recently, we have observed near infrared room-temperature vibronic laser action in Cr^{3+}:Mg_2SiO_4. Characteristics of the absorption and fluorescence spectra, fluorescence lifetime, energy-level structure, and other spectroscopic properties relevant to laser action in this system are reported. The absorption spectrum is characterized by broadband transitions from the $^4A_2$ state to the $^4T_2$ and $^4T_1$ states of the Cr^{3+} ion. The low-temperature fluorescence spectrum exhibits broadband $^4T_2$ to $^4A_2$ emission, as well as $^2E \rightarrow {}^4A_2$ zero-phonon line accompanied by its vibrational sideba-

[illegible] depend strictly [illegible] of the exciting light. The room-temperature fluorescence lifetime is 15 μs. An energy-level diagram of the system is constructed.

*Supported by NASA, APO & Hamamatsu Photonics KK.

15:06

S10 4 Room-Temperature Pulsed Laser Action in $Cr^{3+}:Mg_2SiO_4$. V. PETRIČEVIĆ, S. K. GAYEN, R. R. ALFANO, City College of New York;* KIYOSHI YAMAGISHI, KAZUO MORIYA, Mitsui Mining and Smelting Co. Ltd.-- Room-temperature near infrared vibronic pulsed laser action in trivalent chromium activated forsterite ($Cr^{3+}:Mg_2SiO_4$) is reported. The stable laser resonator is formed by two 30-cm-radius mirrors placed 20 cm apart. The mirrors have high transmission at the pump wavelength of 532 nm, and high reflectivity over the lasing spectral region. The single crystal of $Cr^{3+}:Mg_2SiO_4$ placed at the center of the cavity is longitudinally pumped by the second harmonic of a Q-switched Nd:YAG laser operating at a 10-Hz repetition rate. Emission cross section, spectral range, slope efficiency, and other relevant laser parameters will be presented.

* Supported by NASA, ARO and Hamamatsu Photonics KK.

15:18

S10 5 Photoluminescence Studies of the Alkalide Na+C222Na- Probed with a Picosecond Laser.* R.S. BANNWART, M. DeBACKER, F.N. TIENTEGA, J.L. DYE, and S.A. SOLIN., Michigan State U.--Alkalides are novel compounds containing alkali metal anions. The counterion in these compounds is an alkali metal cation complexed by an organic cage molecule, such as cryptand C222. Time-correlated single photon counting measurements have been made in the temperature range 2K to 80K in order to study the photoluminescence and photoluminescence lifetimes of the electronic states. The light source used was a Nd:YAG-R6G mode-locked cavity-dumped synchronously pumped dye laser with a pulse width of 6 psec. An emission at 670 nm, presumably due to the band gap, was found which has a lifetime of 4.5 ± 0.2 ns. A near edge state with a lifetime of 1.5 ± 0.2 ns was also found. The dependence of the photoluminescence on excitation intensity has been studied, and evidence for intensity dependent irreversible decomposition at 4.2 K has been found. This work has been extended to additional alkalides.

* Supported by the NSF under grant DMR 84-03494 and by the MSU Center for Fundamental Materials Research.

15:30

S10 6 Energy Level Diagram for Mn^{2+} Ions in Villemite. K.C. MISHRA, J.K. BERKOWITZ, B.G. DEBOER, E.A. DALE, GTE Electrical Products; and K.H. JOHNSON, MIT.-- The electronic energy levels associated with manganese impurity in villemite have been obtained using the SCF-MS-Xα cluster procedure. The calculations have been performed assuming substitutional sites for Mn in zinc orthosilicate crystals. Different oxidation states have been considered. Using the molecular orbital energies, an energy level diagram is presented for Mn^{2+} and is compared with experiment. Optical absorption peaks obtained on the basis of the calculated molecular orbital energies compare very well with experiment for divalent manganese ions.

15:42

S10 7 Transmutation Induced Tritium in $LiNbO_3$ Single Crystals.* R. GONZALEZ, University of Madrid, Y. CHEN and M. M. ABRAHAM, Oak Ridge National Laboratory.--Irradiation of $LiNbO_3$ single crystals with thermal neutrons has produced tritium ions by transmutation of ^6Li atoms via the nuclear reaction [illegible] barns. The natural abundance of the [illegible] isotope is 7.4%. Following subsequent heat treatments, infrared absorption measurements have been used to identify the stretching frequencies associated with OH^- and OT^- ions. OD^- ions were added to the crystals by a further heat treatment in D_2O vapor.

*Research sponsored by DARPA under Interagency Agreement 40-1611-85 with Martin Marietta Energy Systems, Inc., contract DE-AC05-84OR21400 with USDOE.

15:54

S10 8 Diffusion of Deuterons in $LiTaO_3$ Crystals.* R. HANTEHZADEH, L.E. HALLIBURTON, Oklahoma State University, C.Y. CHEN, North Carolina State University, R. GONZALEZ and Y. CHEN, Oak Ridge National Laboratory. -- Diffusion coefficients of deuterons in $LiTaO_3$ single crystals have been measured by monitoring the growth of OD^- infrared absorption bands in samples heated in D_2O vapor. Electric-field enhanced diffusion of deuterons was also demonstrated. Electron-nuclear-double-resonance experiments on the deuterated crystals have shown that the structure previously reported in the electron paramagnetic resonance spectrum of a radiation-induced trapped-hope center in $LiTaO_3$ is not due to a hyperfine interaction with protons.

*Supported by contract AFOSR-85-0270, and by DARPA under Interagency agreement 40-1611-85 with Martin Marietta Energy Systems, Inc., contract DE-AC05-84OR21400 with USDOE.

Supplementary Program

S10 9 First Principles Determination of the Electronic Structure of Aluminum Impurities in Villemite. K.C. MISHRA, B.G. DEBOER, J.K. BERKOVITZ, E.A. DALE, GTE Electrical Products; K. H. JOHNSON, MIT.-- Electronic wavefunctions and energies associated with Al ions in villemite have been obtained using the SCF-MS-Xα molecular orbital procedure. A novel procedure is proposed to obtain the excited state configuration of the impurity ions from the variation of the intersphere charges associated with the states of the transition. The physical significance of the procedure will be discussed. Using this approach, the absorption and emission peaks are predicted to be 235 nm and 415 nm, respectively, in very good agreement with the experimental values of 235 nm and 412 nm[1].

1 H. Hess, A. Heim and M. Scala, J. Electrochem. Soc., 130, 2443 (1983).

SESSION S11: RARE EARTH: TRANSITION METAL MAGNETIC ALLOYS

Friday afternoon, 25 March 1988
Mardi Gras F at 14:30
N. C. Koon, presiding

14:30

S11 1 Are There Any Trends in the Magnetic Behavior of Permanent Magnets? G.C. HADJIPANAYIS and W. GONG, Kansas State University—The hard magnetic properties of several permanent magnet materials have been investigated to determine any trends in their magnetic characteristics. The materials studied were $Nd_{15}Fe_{77}B_8$, $SmCo_5$, $Sm_2(Co,Fe,Cu,Zr)_{17}$, ferrites and Au-Co magnets. The magnetic properties measured include initial magnetization curves, hysteresis loops, field and temperature dependence of coercivity, remanence curves and magnetic

3. V. Petričević, S. K. Gayen, and R. R. Alfano, "Lasing and Spectroscopic properties of Chromium-Activated Forsterite", Bull. Am. Phys. Soc. **33**, 1626 (1988). **Invited** paper presented at the Fourth International Laser Science Conference (ILS-IV), October 2-6, 1988, Atlanta, Georgia.

in the gas phase. [illegible] a polarized ArF excimer laser. Alignment of HS photofragments relative to the excimer laser polarization was detected using a polarized dye laser by rotation of the dye laser polarization relative to the excimer laser polarization. Observing rotationally resolved fluorescence excitation spectra allowed determination of the alignment of HS in the $^2\Pi_{3/2}$ electronic ground state for rotational states J = 1.5 - 6.5 using both the $^rQ_{21}$ and the R_1 absorption branches. The results from each branch were compared

11:30

MD 7 Laser Double-Resonance Measurements of HF (J=13) Rotational Relaxation with Rare Gases, H_2, and D_2, CRAIG A. TAATJES and STEPHEN R. LEONE, University of Colorado and Joint Institute for Laboratory Astrophysics -- The relaxation rates of HF (J=13) with rare gases (He, Ne, Ar, Kr, Xe), H_2, and D_2 have been measured by use of a two-laser double-resonance technique. The rates of relaxation by rare gas collision partners fall sharply through the series He-Ne-Ar, then rise again through Ar-Kr-Xe. This shows the effectiveness of both highly impulsive and highly attractive collisions in rotational relaxation of HF. The rates with H_2 and D_2 are ten times higher than those with rare gases, pointing out the importance of rotation-to-rotation transfer in rotational relaxation. Because these measurements give new information about the intermolecular potentials at close range, they are likely to be important in theoretical modeling of the rotation-to-translation transfer in such systems as the HF chemical laser.

SESSION ME: NEW DEVELOPMENTS IN SOLID STATE LASERS

Monday morning, 3 October 1988
Trinidad/Madrid Rooms at 9:30
Clifford R. Pollock, organizer
W. F. Krupke, presiding

Invited paper

9:30

ME 1 Advances in Diode Lasers for Solid State Laser Pumps, DAVID F. WELCH, Spectra Diode Labs--The advances in high power diode laser arrays has greatly impacted the application base of solid state lasers. Highly efficient, compact, stable and highly reliable solid state lasers are a result in part to the advances in diode laser research. Diode laser arrays have been shown to emit greater than 6 W cw from a 100 um aperture and over 38 W cw from a 1 cm aperture with only 20% of the aperture active. Total efficiencies of 57% percent have been achieved. These devices have also shown to be highly reliable with lifetimes >30,000 hrs at 1 W cw from a 200 um aperture source, and >5,000 hrs for a 5 W cw 1 cm aperture array.

Contributed papers

10:00

ME 2 Laser diode pumped 1μ Nd:YAG and Nd:BEL lasers, RICHARD SCHEPS, PETER POIRIER and JOSEPH MYERS, NAVAL OCEAN SYSTEMS CENTER, and DON HELLER, ALLIED SIGNAL CORP.--Performance data for laser diode-pumped cw Nd:YAG and Nd:BEL lasers are presented. Two single stripe emitters are used as the pump source, each emitting up to 1 watt in the pump band. The heat sinks for the laser diodes are temperature controlled to allow for wavelength tunability. The resonator is a hemispherical design. Output and pump threshold [illegible] both hosts were realized. [illegible] the Nd:YAG rod was in excess of [illegible] slope pump to laser cavity photon efficiency of approximately 50 percent. In addition, a rod of Nd:BEL was pumped in the same resonator with comparable performance. Results for both hosts at the fundamental and also the doubled wavelength will be presented. To our knowledge these are the highest cw end-pumped power and efficiencies reported for Nd:YAG and Nd:BEL to date.

10:15

ME 3 A Diode End-pumped Nd:$YAlO_3$ Laser,* PADETHA TIN and L. D. SCHEARER, University of Missouri-Rolla--Following our earlier work on lamp-pumped Nd doped $YAlO_3$ crystals[1], we have successfully end-pumped a small "a-axis" crystal of this material with a 500mW, cw diode laser. The Spectra-Diodes 500mW pump laser emitting at 800nm yielded more than 55mW of laser emission at 1079nm. The cavity consisted of the 0.7mm long crystal, one end coated for high reflectivity at 1080nm and high transmission (>80%) at 800nm, a spherical, coated lens (f=30mm), and a plane 95% reflecting output mirror. Thresholds were below 50mW and as low as 8mW with a high reflectivity mirror. Laser emission was obtained at 1064.5, 1072.9, 1079.5, 1091, and 1084nm with the addition of a Lyot filter to the cavity. Each of these bands could be tuned through several nm with an uncoated, 0.25mm thick etalon in the cavity. Gain and tuning curves for the system will be presented.

* Research supported by Polatomic, Inc.

1. L. D. Schearer and M. Leduc, J. Quant. Electr. QE-22, 756 (1986).

Invited papers

10:30

ME 4 Progress in the Development of New Laser Materials, R.C. Morris, Allied-Signal, Inc.--The development of solid-state laser gain media has proceeded in fits and starts since the discovery of the ruby laser in 1960. While lasing action has since been observed in numerous substances, surprisingly few have completed the rigorous and costly transition from interesting substance to engineering material. During the past several years, there has been an acceleration in the rate of development of solid-state lasers, driven in part by new laser device applications, and several single crystal laser hosts have emerged which offer promise as true engineering materials. The number of "interesting substances" has also expanded. These developments will be reviewed in the context of the interplay between materials science, laser engineering, and crystal growth process development.

11:00

ME 5 Lasing and Spectroscopic Properties of Chromium-Activated Forsterite,* V. PETRICEVIC, S. K. GAYEN, and R. R. ALFANO Institute for Ultrafast Spectroscopy and Lasers, City College of New York--Near-infrared vibronic laser action in chromium-doped forsterite ($Cr:Mg_2SiO_4$) for both visible and near-infrared pumping and different crystal orientations will be presented. The free-running laser output peaks at 1235 nm and has a bandwidth of 25 nm. Using a quartz birefrigent filter at Brewster's angle in the cavity the laser output has been tuned over the 1175-1270 nm spectral range. The room-temperature absorption and emission spectra are characterized by broadband transitions between the states of the chromium ion. At low temperatures, the fluorescence spectrum exhibits sharp zero-phonon lines accompanied by structured vibrational sidebands. Characteristics of the absorption and emission spectra fluorescence lifetime, energy-level structure, and laser parameters such as slope

efficiency, spectral and temporal profiles, emission cross sections will be reported.

*Supported by NASA ARO, Mitsui Mining and Smelting Co., Hamamatsu Photonics KK, and CCNY Organized Research.

I. V. Petricevic, S. K. Gayen, R. R. Alfano, K. Yamagishi, H. Anzai, and Y. Yamaguchi, Appl. Phys. Lett. 52, 1040 (1988).

Contributed papers

11:30

ME 6 Birefringence of Solid-State Laser Media: Broadband Tuning Discontinuities and Application to Laser Line Narrowing, J.S. Krasinski, Y.B. Band*, D.F.Heller, and P.A. Papanestor, Allied-Signal Inc. -- The natural birefringence of optically anisotropic broadly tunable solid-state laser media can be exploited to provide substantial spectral narrowing of the laser output. Lasers employing such media frequently tune discontinuously, due to birefringence effects. Once these effects are understood and controlled, continuously tunable, spectrally narrow laser output results. When the the polarization axis of the medium is slightly misaligned with respect to intracavity polarizing elements, or when the laser operates well above threshold, the laser tunes continuously but exhibits a periodic modulation of the output power as a function of frequency. For large misalignment, or near threshold operation, the laser generates narrow bandwidth output and the laser frequency hops during tuning. Narrow bandwidth operation with continuous tunability is obtained using an intracavity birefringent compensator. Experimental results using alexandrite as the birefringent gain medium are presented.
* Permanent Address, Ben-Gurion University, Beer-Sheva, Israel

11:45

ME 7 Tunable cw laser action of Er^{3+} in double sensitized fluoroaluminate glass at room temperature, E. HEUMANN, M. LEDIG, D. EHRT, and W. SEEBER, Friedrich-Schiller University Jena, E.W. DUCZYNSKI, H.J.v.d.HEIDE, and G. HUBER, University Hamburg--Spectroscopic measurements indicate an efficient energy transfer from Cr via Yb to Er in fluoroaluminate glass. As a result cw lasing was obtained for the first time in this glass at room temperature. Double step pumping via Cr and Yb with a krypton laser yields a threshold pump power of less than 100 mW for the glass laser at 1.56 µm. Using mirrors of different spectral reflection characteristic the tunability of the Er-fluoroaluminate glass laser is demonstrated.
Efficient flashlamp pumping of this glass via Cr and Yb or pumping with LED-arrays via Yb can be expected.

SESSION MF: PLENARY II
Monday afternoon, 3 October 1988
Imperial Ballroom, Salon B at 13:30
A. C. Tam, presiding

13:30

MF 1 Spin Polarization of Atoms and Nuclei by Laser Pumping.* W. Happer, Princeton University -The nuclear spins of noble gases can have relaxation times as long as several hours. By spin-exchange laser pumping, nuclear spin polarisations approaching 100% can be generated in mixtures of alkali vapors with noble gases at densitites of several amagats. Such gases are interesting targets for nuclear scattering experiments. In the heavier noble gases the polarization transfer rates are greatly enhanced by the formation of alkali-noble gas van der Waals molecules. The long relaxation times lead to magnetic resonance linewidths on the order of 10^{-4} Hertz, so that it is possible to measure extremely small spin interactions, including coherent quadrupole interactions with the container walls. The nuclei of radioactive noble gases can be polarized by the same methods.
* Supported by AFOSR grant 81-0104-C.

SESSION MG: APPLICATIONS OF LASER/SURFACE INTERACTIONS
Monday afternoon, 3 October 1988
Imperial Ballroom, Salon B at 14:30
A. C. Tam, organizer
A. C. Tam and S. D. Allen, presiding

Invited papers

14:30

MG 1 Progress in Laser Applications to Surface Science: Trieste Conference, E. Ward Plummer, University of Pennsylvania--abstract not available.

15:00

MG 2 Bridging Concepts Between Single Atom Ejection and Gross Surface Explosions Upon Laser Ablation, R. W. DREYFUS, IBM Res. Thomas J. Watson Research Center, Yorktown Heights, NY 10598.- Single atoms, radicals and polyatomic clusters are ejected from various solids following irradiation with pulsed excimer laser light. Our experiments utilize laser-induced fluorescence measurements and plasma probes to study the ejection process. At low excimer fluences (i.e. removing <<monolayers/pulse) ejection is similar to molecular photodissociation in that photochemical and/or thermal pathways appear to produce the dissociation. At the other fluence extreme, gross surface ablation (removing ~3nm to 1µm) introduces many complicated interactions, e.g. free electron plasmas, gas phase collisions, surface morphological, optical and chemical changes. The present discussion centers on evaluating these higher order effects by looking at the transition region (~monolayer removed) and comparing these results with both higher and lower fluence regions. While no one concept covers all wavelengths, fluences or materials, two generally valid concepts are: at $\leq 1 J/cm^2$ the luminous plasma effects the plume but not the surface, and the chemical and physical perfection of the surface controls the near threshold etching behavior. At fluences significantly above threshold, the comparison between photochemical ablation and (thermal) vaporization requires an evaluation in terms of many parameters and interactions.

15:30

MG 3 Data Storage using Laser-Induced Phase Transformation in Thin Films, Martin Chen, IBM Almaden Research Center--abstract not available.

Contributed papers

16:00

MG 4 Laser Induced Refractive Index Change in Polymers, D. S. DUNN and A. J. OUDERKIRK, 3M Corporate Research--Pulsed UV laser irradiation of polymers has been shown to produce a thin, approximately 50 nm thick, layer with reduced refractive index on the polymer surface. This refractive index change decreases the polymer reflectivity. The reflectivity decrease is broadband, covering the spectral range 400-800 nm, suggesting the existence of a graded refractive index profile from the polymer surface to the bulk. This laser-based process does not texture the polymer so the antireflective structures produced are very durable and resistant to fingerprints. Possible reaction mechanisms and applications of this technology will be discussed.

4. V. Petričević, S. K. Gayen, and R. R. Alfano, "Continuous-Wave and Tunable Laser Operation of Chromium-Activated Forsterite Laser", Bull. Am. Phys. Soc. 34, 965 (1989). Presented at the March Meeting of the American Physical Society, 20-24 March, 1989, St. Louis, Missouri.

results of optical studies which have allowed us to study behavior of Cr^{3+} at disordered sites within a mullite ceramic host. The results indicate that the existence of these low field ions, which are likely connected with sites on the microcrystalline surfaces, accounts for most of the spectroscopic anomalies previously noted in these materials. Furthermore, energy transfer from ordered high field to disordered low field ions is observed. The resulting complex spectra are deconvoluted by means of the recently developed technique of Saturation Resolved Fluorescence (SRF) spectroscopy.
*Supported by US DOE under contract DE–FG–09–87ER45291

Supplementary Papers

Q16 10 FTIR in-situ Annealing Study of Hydrogen-Bonded OH Groups in an Amorphous Silicon Dioxide Film*, Z. YIN [a], D. V. TSU [b], G. LUCOVSKY [b], and F. W. SMITH [a]. [a] City College of New York and [b] North Carolina State Univ. — The annealing behavior of the IR absorption in an amorphous silicon dioxide film deposited by Remote PECVD has been studied via in-situ FTIR spectroscopy up to 350°C, with emphasis on the thermal response of the hydrogen-bonded OH groups. Both irreversible and reversible effects of annealing have been observed, with the former effects associated with the loss from the film of hydrogen contained in OH groups. Dramatic reversible changes in the O-H(s) absorption band (3100-3700 cm^{-1}) associated with thermally-induced weakening (and possibly breaking) of the O-H···O hydrogen-bonded groups have been observed for the first time in this film. These results and additional reversible changes observed for the main Si-O(s) band will be discussed in detail.

* Research supported at CCNY by US DOE grant DE-FG02-87ER45317 and at NCSU by ONR contract N000014-C-79-0133

Q16 11 Light Scattering Studies of Calcium–Aluminate Based Oxide Glasses and Halide Glasses. J. SCHROEDER, L.G. HWA, AND X.S. ZHAO, Department of Physics and Center for Glass Science and Technology, C.T. MOYNIHAN, Department of Materials Engineering and Center for Glass Science and Technology, Rensselaer Polytechnic Institute, Troy, NY 12180–3590 — Rayleigh–Brillouin scattering measurements on various Calcium–Aluminate based oxide glasses and halide glasses as a function of temperature and composition have been performed. The Landau–Placzek ratio and Brillouin shifts are calculated from the Rayleigh–Brillouin scattering spectrum of both glass systems. The total intrinsic loss, consisting of the Rayleigh Scattering, multiphonon edge contributions and impurity absorption are obtained for these potential low–loss optical waveguide materials. The technique of high temperature light scattering allows us to determine the temperature and time dependence of the Landau–Placzek ratio of the ZBLAN glass up to and through the glass transition temperature. Thereby, any extrinsic loss mechanisms are probed in this low loss halide glass.

The authors gratefully acknowledge the support of this work through NRL–N00014–88–K–2033 and NSF–DMR–88–01004.

SESSION Q17: IONS IN SOLIDS

Friday morning, 24 March 1989
Room 273 at 8:00
J. C. Thompson, presiding

8:00

Q17 1 Continuous-wave and Tunable Laser Operation of Chromium-activated Forsterite Laser. V. PETRICEVIC, R. R. ALFANO, The City College of New York;* S. K. GAYEN, The City College of New York, and Stevens Institute of Technology. -- The continuous wave laser action in chromium-activated forsterite ($Cr:Mg_2SiO_4$) at room-temperature is reported. The experimental arrangement uses longitudinal pumping by 1064-nm radiation from a cw Nd:YAG laser in a nearly-concentric cavity. The laser emission is centered at 1244 nm, and has a spectral bandwidth of 12 nm. Continuous tunability over the 1167-1345 nm spectral range has also been demonstrated for the pulsed mode of operation with a single-plate birefringent filter as the intracavity dispersive element. Relevant laser and quantum electronic properties of the Cr:forsterite system will be presented.
* Supported by ARO, NASA, and CCNY Organized Research.

8:12

Q17 2 Electron-Excited Optical Emission from H_2O Adsorbed on Potassium Halides at 78°K. E.T. ARAKAWA and M. KAMADA*, Oak Ridge National Laboratory†--Electron-excited optical emissions from H_2O adsorbed on KCl and KBr crystals at 78°K have been investigated. A vibronic structure with constant energy intervals of about 0.12 eV was observed in the wavelength region of 440-740 nm, indicating that it originates from O_2^- ions. Exposure of the crystal surfaces to water vapor increased the emission intensity, but exposure to oxygen suppressed it. The temperature dependence of the O_2^- emission intensity showed an anti-correlation with that of the OH emission intensity. These results indicate that the O_2^- ions may be produced through dissociation of adsorbed H_2O by electron excitation.

* Present address: U. Osaka Prefecture, Sakai 591, Osaka, Japan

† Operated by Martin Marietta Energy Systems, Inc., for the USDOE under contract DE-AC05-84OR21400.

8:24

Q17 3 $Bi^{3+} \rightarrow Eu^{2+}$ Energy Transfer in CaS. M.D. HILL*, K. CHAKRABARTI**, V.K. MATHUR, R.J. ABBUNDI -- Naval Surface Warfare Center, White Oak, Silver Spring, MD 20903-5000.-- $Bi^{3+} \rightarrow Eu^{2+}$ energy transfer is observed in both the photoluminescence and the optically stimulated luminescence spectrum of $CaS:Bi^{3+},Eu^{2+},Sm^{3+}$. The $^3T_{1u} \rightarrow {}^1A_{1g}$ emission of Bi^{3+} excites the $^8S_{11/2}(4f) \rightarrow {}^2T_{2g}(5d)$ transition of the Eu^{2+}, therefore, a broad $^2T_{2g} \rightarrow {}^8S_{11/2}$ emission band of Eu^{2+} is observed when a Bi^{3+} absorption band is excited. Optically stimulated luminescence (OSL), observed subsequent to exposure to 480nm light, shows the Eu^{2+} emission only.[1] OSL observed after exposure to ionizing radiation shows the Eu^{2+} emission predominantly due to $Bi^{3+} \rightarrow Eu^{2+}$ energy transfer.

[1] K. Chakrabarti, V.K. Mathur, and R.J. Abbundi, Phys. Rev B (in press)

* Virginia Polytechnic Institute and State University, Blacksburg, VA 24061
** On leave from Southwestern Oklahoma State University, Weatherford, OK 73096

8:36

Q17 4 A New Contribution to Spin-Forbidden Rare Earth Optical Transitions Intensities. G.W. BURDICK and M.C. DOWNER†, U. Texas at Austin*; D.K. SARDAR*, U. Texas at San Antonio. We expand upon recent quantitative calculations[1] which show that numerous parity- and spin-forbidden linear optical transitions observed in trivalent rare earth ions acquire a major fraction of their intensity from hitherto neglected contributions involving spin-orbit linkages within excited configurations. Extending our revised analysis of observed linear absorption intensities for Gd^{3+} and Eu^{3+} to

5. S. K. Gayen, V. Petričević, and R. R. Alfano, "Spectroscopic and Quantum Electronic Properties of Chromium-Activated Forsterite", in *Quantum Electronics and Laser Science Conference, 1989 Technical Digest Series, Vol 12,* (Optical Society of America, Washington D.C. 1989) pp. 172-173, presented at the Quantum Electronics and Laser Science (QELS) Conference, Baltimore, Maryland,April 24-28, 1989.

thicknesses. The contribution to loss from the interfaces is thus divided out, and the bulk loss value is obtained. An example of such a measurement for fused silica, from 10 to 125 GHz, is shown in Fig. 2. Our results are consistent with previous data. The resolution in the refractive index measurement is determined by the temporal resolution of the experiment, sample thickness, and its uniformity. With the samples used, and our present time resolution for delay (0.5 ps), this accuracy is ±1%. The experimental resolution in the determination of loss is given by the fluctuations in the laser power and is estimated to be 5%.

The quasioptical nature of this measurement technique can be exploited to characterize samples in other configurations, for example, in reflection. Another consequence is that by placing lenses in front of both antennas we increased the received signal strength permitting much wider (>15-cm) separation between the antennas. An added benefit is that the beam can be collimated, thus eliminating the need to correct for the refraction that occurs in the samples. This is easily checked by using fused silica which has a negligible loss at microwave frequencies. Results using this configuration are also presented. **(12 min)**

1. D. H. Auston, in *Picosecond Optoelectronic Devices*, C. H. Lee, Ed. (Academic, Orlando, 1984), pp. 73–117 and references therein.
2. See, for example, A. H. Harvey, Ed., *Microwave Engineering* (Academic, London, 1963).
3. K. S. Yngvesson, D. H. Schaubert, T. L. Korzeniowski, E. L. Kollberg, T. Thungren, and J. F. Johansson, IEEE Trans. Antennas Propag. **AP-33**, 1392 (1985).
4. A. P. DeFonzo, and C. Lutz, Appl. Phys. Lett. **51**, 212 (1987).
5. Y. Pastol, G. Arjavalingam, J.-M. Halbout, and G. V. Kopcsay, to be published in Electron. Lett.

The poor efficiency of most Cr lasers has previously been attributed to the overlap of the excited-state absorption (ESA) band with the emission band.[2] Arguments were presented which show that the peak positions of the ESA and emission bands are strongly influenced by the nature of the Jahn-Teller effect (JTE) in the $^4T_2$ excited state. Direct measurements of the ESA spectrum of Cr:LICAF indicate that this host material resists the JT distortion sufficiently so as to minimize the overlap between the ESA and emission features. The ESA is found, however, to provide a non-negligible detriment to the laser performance for Cr:LISAF.

The JTE of the $^4T_2$ state is due to dynamic nuclear displacements in the e_g mode. In this work, we provide two independent measures of the JT energy of Cr:LICAF. One method is based on the shift of the ESA peak from the position which is predicted on the basis of crystal field theory; the other involves the interpretation of the splittings of the zero-phonon lines of the $^4T_2$ state (known as the Ham effect[3]). We attempt to reconcile the two calculations.

The reduced influence of the ESA band at the lasing wavelengths is also in part due to the nature of the statistically induced transition moment. The substitutional Al site is predominantly octahedral in character, and, therefore, the Cr^{3+} ion is surrounded by six fluorines. There exists, however, a small static distortion of t_{2u} symmetry, which is responsible for inducing significant oscillator strength into the spectral features. We use group theory to relate the statistically induced transition strengths for all the relevant transitions, including the ground and excited-state absorptions, and the emission band. It is shown that the t_{2u} field increases the transition moment for the π-polarized emission but not for the ESA that occurs near the emission band, thus accounting for the reduced influence of the ESA at the lasing wavelengths.

(Invited paper, 25 min)

1. S. A. Payne, L. L. Chase, H. W. Newkirk, L. K. Smith, and W. F. Krupke, IEEE J. Quantum Electron., to be published.
2. J. A. Caird, S. A. Payne, P. R. Staver, A. J. Ramponi, L. L. Chase, and W. F. Krupke, IEEE J. Quantum Electron. **QE-24**, 1077 (1988).
3. F. S. Ham, Phys. Rev. A. **8**, 1727.

Thursday 27 April

Thursday **AFTERNOON**

27 April 1989 **THKK**

CONVENTION CENTER ROOM 307

2:30 PM Solid State Lasers: 2

David C. Hanna, University of Southampton, U.K., Presider

THKK1 Properties of Cr^{3+} in new fluoride host crystals

STEPHEN A. PAYNE, L. L. CHASE, L. K. SMITH, H. W. H. LEE, Lawrence Livermore National Laboratory, P. O. Box 5508, Livermore, CA 94550.

We recently discovered a new class of Cr^{3+} solid-state laser based on the fluoride host materials having the colquiriite structure $LiCaAlF_6$ (LiCAF)[1] and $LiSrAlF_6$ (LISAF). We found that these materials exhibit efficient laser performance, as determined with a Kr laser-pumped experimental configuration. By taking the passive losses of the laser crystals into account, we find that the extrapolated slope efficiencies of Cr:LICAF and Cr:LISAF are 67 and 53%, respectively, while the quantum defect-limited efficiency is 80%. On the other hand, most other Cr lasers typically have efficiencies that are <30%.[2] The question arises as to what favorable properties of these hosts are responsible for the efficient laser performance of Cr:LICAF and Cr:LISAF.

The polarized absorption spectra of Cr:forsterite both at room and liquid-nitrogen temperatures for different orientations of the crystallographic axes are shown in Fig. 1. The spectra are characterized by three bands centered at [illegible] and 480 nm, respectively, for E ⊥ c orientation. The position of the 750-nm band changes with polarization. At liquid nitrogen temperature sharp lines appear in the spectra. The room-temperature fluorescence spectrum is a broad band spanning the 700–1400-nm range. At liquid nitrogen temperature the fluorescence spectrum breaks up into three structured bands as displayed in Fig. 2.

A careful analysis of the emission and absorption spectra reveals that there are two optically active centers in chromium-activated forsterite, and both centers contribute to the observed emission and absorption spectra. The strong polarization dependence of the 750-nm absorption band is consistent with transitions between states of Cr^{3+} ion in a site of low symmetry. The fluorescence band spanning the 1100–1400-nm range is the Stokes-shifted counterpart of the 850–1100-nm absorption band. Laser action is observed over part of this fluorescence band. We attribute this IR absorption and emission to transitions between states of another center other than Cr^{3+}, presumably Cr^{4+} in a tetrahedral site. The wavelength dependence of fluorescence lifetime provides further indication that the emission in the 1100–1400-nm range and that in the 700–1100-nm range arise from two different centers. Complementary spectroscopic measurements and their analysis in terms of standard theory for optical transitions in impurity-ion-doped crystals are presented to gain insight into laser emission in chromium-activated forsterite. **(12 min)**

1. V. Petricevic, S. K. Gayen, R. R. Alfano, K. Yamagishi, H. Anzai, and Y. Yamaguchi, Appl. Phys. Lett. **52**, 1040 (1988).
2. V. Petricevic, S. K. Gayen, and R. R. Alfano, Appl. Opt. **27**, 4162 (1988).

THKK3 Energy transfer studies between Cr^{3+} and Tm^{3+} in scandium and aluminum garnets

G. J. QUARLES, LEON ESTEROWITZ, U.S. Naval Research Laboratory, Washington, DC 20375-5000; A. ROSENBAUM, G. ROSENBLATT, Sachs/Freeman Associates, Inc., Landover, MD 20785-5396.

Recent papers have reported on the properties of scandium and aluminum garnets doped with trivalent chromium, thulium, and holmium for 2-μm laser operation.[1-3] However, there have been no systematic investigations of the transfer efficiencies between Cr^{3+} and Tm^{3+} in various hosts and how these efficiencies change with activator and sensitizer concentration. The present work includes both experimental and theoretical studies of the transfer efficiencies in YAG, YSAG, and YSGG. Preliminary results indicate that the energy transfer mechanism is due to a dipole–dipole interaction. The results provide a basis for the optimization of the Cr^{3+} and Tm^{3+} concentrations in flash-pumped 2-μm laser material. This requires simultaneous maximization of the energy transfer and minimization of the thermal loading associated with high Cr^{3+} concentrations.

Several samples with widely varying Cr^{3+} and Tm^{3+} concentrations were studied experimentally. The transfer efficiencies were obtained by measuring the decay rate of the Cr^{3+} ions from the mixed $^4T_2/^2E$ states as a function of Tm^{3+} ion concentration. The $^4T_2$ band was excited with 10-ns pulses at 568 nm from a YAG-pumped dye laser using rhodamine 590 dye. The Cr^{3+} emission was selected by a monochromator, detected with a photomultiplier tube, signal averaged, and stored by a transient digitizer. Decay rates were monitored at several wavelengths across the $^4T_2/^2E$ emission band, and no differences were observed. The time resolution of the detection system was better than 1 μs. Quantum efficiencies of the $Cr \rightarrow Tm$

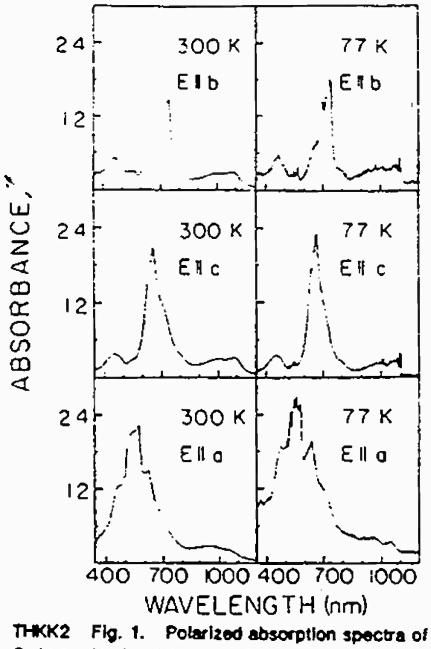

THKK2 Fig. 1. Polarized absorption spectra of Cr:forsterite for different orientations of the host crystal.

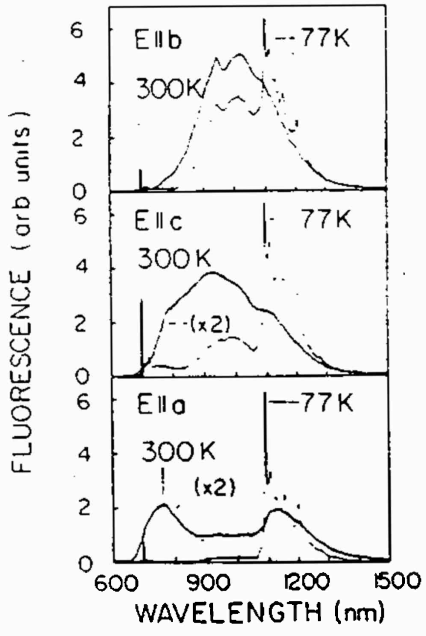

THKK2 Fig. 2. Fluorescence spectra of Cr:forsterite for three different crystallographic orientations.

6. V. Petričević, S. K. Gayen, and R. R. Alfano, "A Broadly-Tunable Room-Temperature Chromium-Activated Forsterite Laser", in *Conference on Lasers and Electro-Optics, 1989 Technical Digest Series, Vol 11,* (Optical Society of America, Washington D.C. 1989) pp. 22-24, presented at the Conference on Lasers and Electro-Optics (CLEO), Baltimore, Maryland, April 24-28, 1989.

Monday MORNING
24 April 1989 MH
CONVENTION CENTER ROOM 310

10:30 AM Tunable Lasers: 2

James Harrison, Schwartz Electro-Optics, Inc., Presider

MH1 Multistage Ti:Al_2O_3 amplifier system

K. F. WALL, P. LACOVARA, R. L. AGGARWAL, P. A. SCHULZ, A. SANCHEZ, MIT Lincoln Laboratory, Lexington, MA 02173.

We have designed and assembled a longitudinally pumped multistage Ti:Al_2O_3 amplifier system intended to produce pulsed tunable single frequency radiation from 750 to 850 nm with an output energy of 1 J/pulse at 10 Hz. This system is composed of three major subsystems: (1) a cw Ti:Al_2O_3 master oscillator; (2) a Ti:AL_2O_3 amplifier; and (3) a frequency doubled Nd:YAG pump laser.

The master oscillator is a cw Ti:Al_2O_3 single frequency ring laser[1] pumped by a cw Ar-ion laser and is tunable from ~750 to 850 nm. At the peak of the gain profile this oscillator provides a signal of ~0.5 W. A broadband isolator consisting of a Faraday rotator and a compensating polarization rotator provides 30 dB of isolation over the tuning range of the master oscillator. Pockels cells are used to gate the cw beam as well as to shape temporally the pulse intensity.

The Ti:Al_2O_3 amplifier consists of four stages: a four-pass preamplifier; a two-pass amplifier; and two single-pass amplifiers, as shown schematically in Fig. 1. Each stage consists of a Ti:Al_2O_3 crystal cut at the Brewster angle to minimize reflection losses. The signal and pump beams propagate almost collinearly (~1°) and are polarized along the c axis of the crystal (π polarization) to maximize the gain. The length of each crystal, ranging from 1.2 to 3.2 cm, is chosen so that essentially all the pump beam is absorbed (>95%).

The Nd:YAG pump laser consists of a Q-switched mode-locked oscillator, a common three-stage amplifier chain, and four parallel two-stage power amplifier chains resulting in four output beams at 1.06 μm, as shown in Fig. 2. This pump laser provides a macropulse 180 ns in duration consisting of 100-ps mode-locked pulses spaced 10 ns apart. The macropulse repetition rate is 10 Hz. The average power of each output beam at 1.06 μm is 20 W. Frequency doubling to 532 nm is accomplished using 5-cm long KD*P crystals with type II phase matching. Typically, we achieve 25% doubling efficiency resulting in 5 W of 532-nm radiation in each output beam.

We measured a gain of 2×10^4 for the four-pass preamplifier and a gain of 1×10^3 for the two-pass amplifier. Gain measurements for the two single-pass amplifier stages are in progress. Pump beam inhomogeneities (hot spots) give rise to amplified spontaneous emission noise in the signal. We are investigating the use of random phase plates[2] to eliminate the hot spots by smoothing out the spatial profile of the pump beams.

(12 min)

1. P. A. Schulz, IEEE J. Quantum Electron. QE-24, 1039 (1988).
2. Y. Kato, K. Mima, N. Miyanaga, S. Arinaga, Y. Kitagawa, M. Nakatsuka, and C. Yamanaka, Phys. Rev. Lett. 11, 1057 (1984).

MH2 Alexandrite laser with narrow spectral resolution and high power capabilities

E. ARMANDILLO, European Space Research & Technology Center, 1 Keplerlaan, Noordwijk, The Netherlands; E. NAVA, G. MOMBRINI, CISE Tecnologie Innovative S.p.A., P.O. Box 12081, 20134 Milan, Italy; C. MALVICINI, Quanta System, 18 Via Venezia Giulia, 20157 Milan, Italy

Alexandrite is the best developed NIR tunable solid state laser crystal. Its wide tunability range and good physical properties, including the possibility of efficient flashlamp optical pumping, make it the right source for lidar/DIAL measurements of important chemical-physical parameters of the atmosphere. We built and tested a Q-switched alexandrite laser designed to fulfill the requirements of single-longitudinal-mode near-diffraction-limited tunable emission in high energy pulses (0.5–1 J).

A ring regenerative slave amplifier similar to that described in Ref. 1 was injected with a low power master oscillator.

The alexandrite master oscillator consists of a 1/4- × 4-in. Alexandrite rod pumped in a double-elliptical chamber and a stable resonator (Fig. 1). For single-mode operation a multiplate birefringent filter and sapphire resonant output reflector acting as a temperature tunable frequency filter are used. An intracavity aperture controls the single-transverse-mode oscillation.

From this oscillator we obtained 600-MHz bandwidth, 5-mJ energy Q-switched pulses to inject the slave cavity.

The slave regenerative ring amplifier consists of a three-mirror cavity, 1/4- × 4-in. alexandrite rod in a double elliptical pump chamber, birefringent tuner, and Brewster angle KD*P Pockels cell. The Pockels cell is triggered by the master pulse via a photodiode. From the injected amplifier we obtained narrow bandwidth (600-MHz) emission in pulses of 1-J output energy.

Tests are in progress to define frequency jitter and stability, temporal width, and amplitude stability.

The system will be mounted in a ground-based lidar/DIAL facility for measurements of atmospheric water vapor concentration, pressure, and temperature. Preliminary results are presented.

(12 min)

1. V. Micheau, F. de Rougemont, and R. Frey, Appl. Phys. B 39, 219 (1986)

MH3 Applications of new solid state lasers to the production of tunable VUV and XUV coherent radiation

C. H. MULLER III, DEAN P. GUYER, C. E. HAMILTON, D. D. LOWENTHAL, Spectra Technology, Inc., 2755 Northup Way, Bellevue, WA 98004; T. D. RAYMOND, A. V. SMITH, Sandia National Laboratories, Albuquerque, NM 87185

We have recently demonstrated[1] a 7.5% efficient near-diffraction-limited coherent VUV source operating at ~130 nm. The VUV wavelengths are obtained by two-photon resonant four-wave mixing in Hg vapor. The high energy conversion efficiency results from mixing very high quality collimated single-mode laser beams over 1-m interaction lengths. The collimated geometry is very important because it allows tractable modeling, area scaling of the process to higher energies, and high optical quality of the output wave. Output VUV energies exceeding 1.25 mJ/pulse in 8-mm diam beams have been obtained. The VUV wavelength is tunable from 120 to 140 nm by adjusting the pump wavelengths for proper index matching conditions.

The pump wavelengths for 130.2-nm generation are 777, 405, and 255 nm. The 405-nm wavelength is doubled [illegible] nm wavelength is doubled 765-nm radiation. At the present time the 765-, 777-, and 810-nm wavelengths are generated by three ring dye laser master oscillators. These cw wavelengths are then amplified to the millijoule level in commercial pulsed dye amplifiers. A final stage amplification occurs in titanium:sapphire (Ti:S).

With the recent demonstration[2] of a stable high energy single-longitudinal-mode Ti:S oscillator, the ring dye lasers and all subsequent stages of dye amplifiers can now be replaced by a single Ti:S oscillator and amplifier for each fundamental wavelength. The simplification is enormous in that eighteen dye oscillators/amplifiers can be replaced with three compact Ti:S oscillators and three Ti:S amplifiers. The result of these simplifications would be an all solid state tabletop coherent VUV source.

The high energy and high optical quality of the VUV output wave suggest that this source could be used for subsequent nonlinear mixing to the XUV region of the spectrum. As shown in Fig. 1, a 43.6-nm XUV source can be constructed by frequency tripling 130.7-nm VUV radiation in neon. In addition, a tunable 60.4-nm XUV source[3] would result from frequency mixing 130.7 nm with 800 nm, also in neon, as illustrated in Fig. 1. Generating XUV from VUV with high efficiency and at sizable energy levels has not previously been possible; the only VUV sources available were of very low energy and inefficient. However, development of an efficient high energy and energy scalable source at STI now provides the driver for an efficient XUV source. Furthermore, this XUV source can be driven with an all solid state laser system.

We discuss the characteristics of our 130-nm source, recently developed single-mode Ti:S oscillators (Fig. 2), and their use with tabletop VUV and XUV sources. **(Invited paper, 25 min)**

1. C. H. Muller III, D. D. Lowenthal, M. A. DeFaccio, and A. V. Smith, "High-Efficiency, Energy-Scalable, Coherent 130-nm Source by Four-Wave Mixing in Hg Vapor," Opt. Lett. 13, 651 (1988).
2. K. W. Kangas, D. D. Lowenthal, and C. H. Muller III, "Single-Longitudinal-Mode, Tunable, Pulsed, Ti:Sapphire Laser Oscillator," Opt. Lett. 14, 21 (1989).
3. A. V. Smith, "A Proposed Light Source for Vacuum Ultraviolet Photolithography," Sandia Report SAND 88-1316•UC-13 (June 1988).

MH4 Broadly tunable room temperature chromium activated forsterite laser

V. PETRICEVIC, S. K. GAYEN, R. R. ALFANO, CUNY-City College, Institute for Ultrafast Spectroscopy & Lasers, New York, NY 10031.

There is a need for near IR coherent radiation in the technologically important areas of ranging, remote sensing, and optical communications. Chromium activated forsterite (Cr:Mg_2SiO_4) is emerging[1,2] as a practical tunable near IR laser suitable for such needs. We present the characteristics of laser emission in Cr:forsterite.

The room temperature absorption and emission spectra of chromium-doped forsterite are shown in Fig. 1. The absorption spectrum is characterized by three broad absorption bands centered at 1050, 750, and 480 nm, respectively. The emission spectrum spans the 700–1400-nm range with its peak at 1100 nm. Both the absorption and emission spectra exhibit sharp line structures at liquid nitrogen temperatures. Careful study of the absorption and emission spectra reveals that the lasing ion may not be the usual trivalent ionic state of chromium but presumably the tetravalent state.

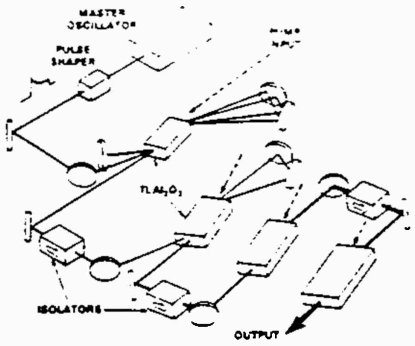

MH1 Fig. 1. Schematic of the Ti:Al_2O_3 amplifier system. The master oscillator is a cw Ti:Al_2O_3 single frequency ring laser. The Ti:Al_2O_3 amplifier consists of four stages: a four-pass preamplifier, a two-pass amplifier, and two single-pass amplifiers. The pump source is a frequency doubled Nd:YAG laser.

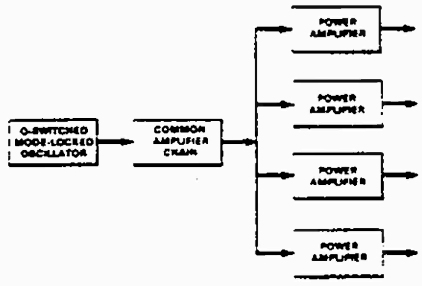

MH1 Fig. 2. Schematic of the Nd:YAG pump laser. The Nd:YAG pump laser consists of a Q-switched mode-locked oscillator, a common three-stage amplifier chain, and four parallel two-stage power amplifier chains resulting in four output beams at 1.06 μm. This pump laser provides a macropulse 180 ns in duration consisting of 100-ps mode-locked pulses spaced 10 ns apart. The macropulse repetition rate is 10 Hz.

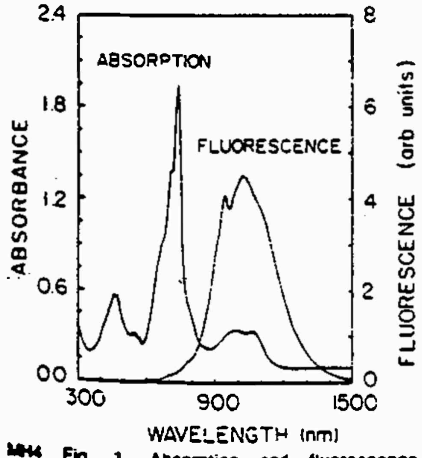

MH4 Fig. 1. Absorption and fluorescence spectra of Cr:forsterite at room temperature. Both the spectra were taken for the $E \| b$ axis and excitation along the a axis. The thickness of the sample along the a axis is 4.5 mm, and chromium ion concentration in the sample is 6.9×10^{18} ions/cm^3.

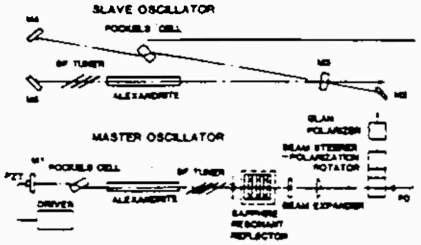

MH2 Fig. 1. Layout of the master–slave alexandrite oscillator.

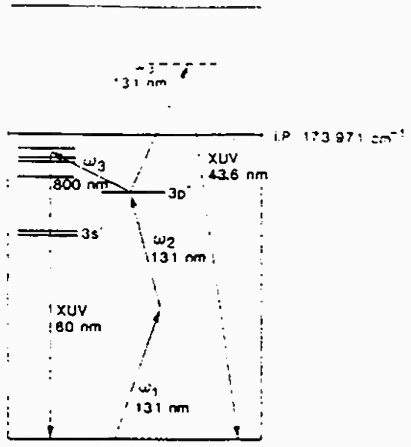

MH3 Fig. 1. Simplified energy level diagram for neon showing frequency tripling and mixing conversion schemes for the generation of XUV coherent radiation.

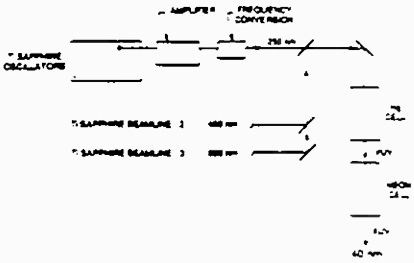

MH3 Fig. 2. Schematic of all solid state Ti:sapphire laser-pumped XUV coherent source.

MH4 Table I. Spectroscopic and Lasing Properties of Cr:Forsterite

Property	Values
Absorption bands	350–520 nm, 600–850 nm, and 870–1180 nm
Fluorescence band	700–1400 nm
Fluorescence lifetime	15 μs at 300 K
Pulsed laser action:	
Center wavelength and bandwidth	1235 nm, ~25 nm
Output power slope efficiency	21%
Tuning range	1167–1268 nm
Continuous wave laser action:	
Center wavelength and bandwidth	1244 nm, ~12 nm
Output power slope efficiency	~7%
Effective emission cross section	~1 × ~10^{-19} cm^2

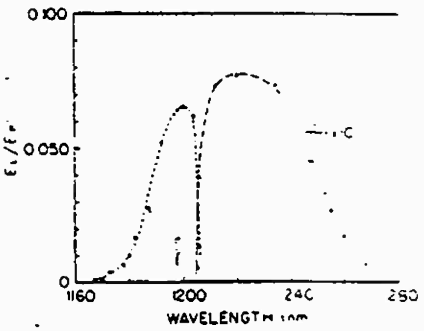

MH4 Fig. 2. Ratio of Cr:forsterite laser output E_L to the absorbed pump energy E_p as a function of wavelength. The two curves are obtained for two different output couplers.

The absorption and emission spectra shown in Fig. 1 contain contributions from both the Cr^{3+} and Cr^{4+} ions.

Pulsed laser action was obtained for both the 1064- and 532-nm excitations from a Q-switched Nd:YAG laser. The Cr:forsterite sample was longitudinally pumped at the center of a stable cavity formed by two 30-cm radius mirrors placed 20 cm apart. The free-running laser output was centered at 1235 nm and had a spectral FWHM of ~25 nm. The maximum output power slope efficiency measured to date is 21% and may be improved further.

The composite tuning curve obtained with two different output couplers for 1064-nm pulsed excitation is displayed in Fig. 2. With a birefringent single-crystal quartz plate at the Brewster angle as the intracavity dispersive element, continuous tuning over the 1167–1268-nm spectral range has been achieved.

Continuous-wave laser action of Cr:forsterite has also been achieved for longitudinal pumping by 1064-nm radiation from a cw Nd:YAG laser in a nearly concentric cavity formed by two 5-cm radius mirrors. The cw laser emission is centered at 1244 nm and has a spectral bandwidth of 12 nm. The effective emission cross section is estimated to be $\sim 1.1 \times 10^{-19}$ cm^2. Key spectroscopic and lasing properties of Cr:forsterite are summarized in Table I. (12 min)

1. V. Petricevic, S. K. Gayen, R. R. Alfano, K. Yamagishi, H. Anzai, and Y. Yamaguchi, Appl. Phys. Lett. **52**, 1040 (1988).
2. V. Petricevic, S. K. Gayen, and R. R. Alfano, Appl. Opt. **27**, 4162 (1988).

MH5 Solid state lasers on the basis of chromium-doped rare-earth scandium garnets

A. M. PROKHOROV, I. A. SHCHERBAKOV, Academy of Sciences of the U.S.S.R., Institute of General Physics, 38 Vavilov St., Moscow, U.S.S.R.

In certain crystal growing conditions for Cr^{3+}- and Nd^{3+}-doped garnets a portion of the trivalent chromium ions can be transferred into a tetravalent state. In the active medium they form phototropic centers with saturable absorption at the Nd laser wavelength. By doping with such phototropic centers, the active medium provides a Q-switched regime where each pump pulse has a fine structure containing a regular sequence of pulses, each with a duration of a few hundred nanoseconds. The peak repetition rate inside the pulses varies from tens to hundreds of kilohertz depending on the initial phototropic absorption. Peak generation power can reach 5×10^5 W. It is possible to obtain both high average and high peak power simultaneously in the same laser. This regime allows one to construct a small sized solid state laser capable of treating materials which cannot be cut in other pump regimes, i.e., in a cw mode.

Such a laser has been built in GSAG with chromium and neodymium concentrations of 2×10^{20} cm^{-3}. The laser rod was 6 mm in diameter and 75 mm in length. The initial phototropic absorption at the pump wavelength was 20%. Pulse pump duration was 0.8 ms with laser efficiency of 3.5%. The phototropic active element pump pulse had a peak structure with 100% depth of modulation. The duty factor of the pulse series was ~10 at a peak duration of 250 ns, which corresponds to a peak power of 10^5 W. This laser has also been studied in a high average power regime at pulse repetition rates of 100 and 20 Hz. The pulse duration for the first regime was 0.2 ms and for the second 0.8 ms. Average power was ~100 W. The thermooptical properties of the GSAG crystals are ~1.5 times better than those for YSGG. The limiting heat load for GSAG crystals is approximately twice as high as for GSGG crystals.

The lasing wavelength of YSGG Cr^{3+} Nd^{3+} is shorter than that for YAG and GGG and there is good agreement with the amplification profile of neodymium phosphate glass. It has been shown that the condition for amplification of pulses of the YSGG Cr^{3+} Nd^{3+} oscillator is very close to the condition for amplification of the YLF Nd^{3+} oscillator and neodymium phosphate glass oscillator itself.

It has been observed that the YSGG Cr^{3+} Nd^{3+} rod has very little influence on the YSGG Cr^{3+} Ho^{3+} Tm^{3+} rod when they are placed in the same resonator. Thus, we have built a laser which operates simultaneously at 2.08 and 1.06 μm.

In conclusion we point out that this laser is very successful for material processing and medical applications. (12 min)

Monday MORNING

24 April 1989 MI

CONVENTION CENTER ROOM 317

10:30 AM Stimulated Brillouin Scattering Phase Conjugation

George C. Valley, Hughes Research Laboratories, Presider

MI1 Phase conjugate fidelity of an SBS oscillator/amplifier at the 1-J/pulse level

METIN S. MANGIR, DAVID A. ROCKWELL, Hughes Research Laboratories, Optical Physics Dept., Malibu, CA 90265.

Phase conjugation (PC) via stimulated Brillouin scattering (SBS) is a widely used technique. Until now most successful PC experiments have been done with pump energies of ~100 mJ. For higher energies, the conjugate fidelity degrades. While the exact cause of this fidelity degradation remains to be determined, it appears to represent a fundamental limit of the SBS PC process. From basic considerations it can be concluded that good fidelity requires that the SBS gain length be several times the diffraction length, thereby promoting thorough mixing of different parts of the beam and achieving high selectivity for the phase conjugate mode. Indeed, experiments in our laboratory have shown that above ~10 times the SBS threshold energy, the PC fidelity is reduced. Competing nonlinearities or specifics of the geometry employed can also affect the fidelity. This fidelity degradation presents a problem in high energy laser applications which require PC at energies > 1 J.

A possible way to scale SBS phase conjugate mirrors to higher energy employs an oscillator/amplifier combination, as shown schematically in Fig. 1. The essential idea is that the oscillator employs SBS at an energy level consistent with good PC fidelity to create a Brillouin shifted seed that is the conjugate of the incident pump beam. The backward propagating seed intensity increases in the Brillouin amplifier at the expense of the incoming pump. Attenuators placed between the two cells ensure that the depleted pump beam is of sufficiently low intensity as it enters the SBS oscillator. Analysis shows that the seed intensity needs to be 1–10% of the pump intensity to achieve high reflectivity. In this configuration the oscillator achieves the required conjugation fidelity while the amplifier produces the high reflection efficiency. In recent papers[1,2] good fidelity with ~70% reflectivity was reported. The present effort addresses the possibility that the amplifier can distort the (assumed) perfect fidelity of the seed.

In our experiments we used the frequency doubled output of a phase conjugate Nd:glass laser producing up to 2.5 J at 527 nm. The far field beam quality is 1.5–2 times diffraction limited; the near field has a slightly nonuniform intensity profile. Our experimental setup including diagnostic equipment is shown in Fig. 2. The amplifier cell length can be changed between 30 and 120 cm in 30-cm steps. We have monitored the energies and pulse shapes (<1-ns time resolution) at the input and output of both the oscillator and amplifier. Also, the near and far field beam shapes were monitored at the output of amplifier and oscillator using a CCD TV camera coupled to a video frame grabber and computer. We present our experimental measurements of the energies, pulse shapes, and near and far field PC fidelity as a function of several experimental parameters, such as the amplifier small signal SBS gain, the seed-to-pump energy ratio, the degree of aberration, and the acoustic decay time of the medium. (12 min)

1. N. F. Andreev, V. I. Bespalov, M. A. Dvoretskii, and G. A. Pasmanik, "Nonstationary Stimulated Mandelstahm-Brillouin Scattering of Focussed Light Beams under Saturation Conditions," Sov. Phys. JETP **58**, 688 (1983).
2. V. N. Alekseev *et al.*, "Investigation of Wavefront Reversal in a Phosphate Glass Laser Amplifier with a 12-cm Output Aperture," Sov. J. Quantum Electron. **17**, 455 (1987).

MI2 Phase conjugation of astigmatic aberrations by stimulated Brillouin scattering

C. HOEFER, H. INJEYAN, B. ZUKOWSKI, M. NGUYEN-VO, TRW Space & Technology Group, 1 Space Park, Redondo Beach, CA 90278

Astigmatic beams were phase conjugated and corrected using stimulated Brillouin scattering (SBS). Experiments have shown that conjugation fidelity is preserved for astigmatic aberrations up to six to eight waves even though threshold is increased. Both the input and output beam quality was measured interferometrically while input and output energies were also monitored.

Figure 1 shows a schematic layout of the apparatus. A Nd:YAG laser with output energies of up to 100 mJ, pulse width of 20 ns, and frequency bandwidth of 3 GHz was collimated and propagated through an aberrator before focusing into a methane SBS cell. Infrared Mach-Zehnder interferometers were used to look at the aberrated and corrected wavefronts. The interferograms were simultaneously observed on a CCD camera and recorded on tape. The aberrators used were either a cylindrical lens or a helium jet and ranged from a fraction of a wave to eight waves over a 1-cm beam. The beam energy was varied from 10, which was the SBS threshold, to 100 mJ. Joulemeters were used to monitor the SBS reflectivity, and all measurements were made on a single-shot basis. Figure 2 is a typical set of interferograms showing the input and corrected output. Excellent fidelity was obtained throughout the range of aberrations used.

The SBS reflectivity was decreased, and the SBS threshold increased with increasing aberration although fidelity was preserved. This effect was modeled using the 2-D (one longitudinal, one transverse) wave optic BRIWON code which treats the second transverse dimension using geometric optics. To accommodate astigmatism, the code was modified by decoupling focusing along the two transverse axes. The model predicted good phase conjugation fidelity, confirming the experimental results, and changes in reflectivity and SBS threshold were in good agreement with those observed experimentally (Fig. 3). (12 min)

7. V. Petričević, S. K. Gayen, and R. R. Alfano, "Chromium-Activated Forsterite Laser", presented at the Topical Meeting on Tunable Solid-State Lasers, Cape Cod, May 1-3, 1989.

A Chromium-Activated Forsterite Laser

V. Petričević, S. K. Gayen,* and R. R. Alfano

Institute for Ultrafast Spectroscopy and Lasers, Departments of Physics and Electrical Engineering, City College of New York, New York, NY 10031.

* Department of Physics and Engineering Physics, Stevens Institute of Technology, Hoboken, New Jersey 07030.

Summary

The chromium-doped forsterite ($Cr:Mg_2SiO_4$) laser, a new member in the family of chromium-based, room-temperature, near-infrared vibronic lasers.[1] is emerging as a practical and useful source of coherent radiation in the near-infrared spectral region.[2,3] The Cr:forsterite system is unique both for its desirable laser properties, as well as for its interesting and intriguing spectroscopic properties. While successfully operated Cr-based tunable solid-state lasers like alexandrite, emerald, Cr:GSGG, together with $Ti:Al_2O_3$ span quite a different spectral range of 660-1090 nm, Cr:forsterite emits in the 1167-1345 nm range, centered on 1268 nm, the so-called "wavelength of zero material dispersion". The material dispersion will be minimal in this spectral range, making Cr:forsterite an extremely valuable source for optical communications. The most interesting spectroscopic feature of the Cr:forsterite crystal is that it is the first Cr-based system known to date where the 'lasing center' is other than the Cr^{3+} ion, presumably the tetravalent chromium (Cr^{4+}). In this paper, the unique spectroscopic, and laser properties of Cr:forsterite will be described.

The room-temperature absorption and emission spectra of Cr:forsterite are shown in Fig. 1(a). The absorption spectrum is characterized by three broad absorption bands centered at 1050 nm, 750 nm, and 480 nm, respectively. The emission spectrum spans the 680-1400 nm spectral range with peak at 1100 nm. The 750-nm and 480-nm absorption bands are attributed to transitions within the states of Cr^{3+} ion. A careful study reveals that the near-infrared absorption band centered at 1050 nm, and its Stokes-shifted fluorescence, presented in Fig. 1(b), are responsible for laser action in Cr:forsterite. These absorption and emission originate in transitions between the states of a center other than Cr^{3+}. The spectroscopic and theoretical evidences leading to this conclusion and the identification of this new lasing center will be presented.

Various laser-pumped laser experiments on Cr:forsterite system have been completed and will be reviewed:

- Pulsed laser action has been obtained for longitudinal pumping in a stable cavity by both the 1064-nm and 532-nm radiation.
- Continuous-wave operation has been demonstrated for longitudinal pumping by cw 1064-nm radiation in a nearly concentric cavity.
- Continuous tuning over the 1167-1345 nm spectral range, displayed in Fig. 2. has been obtained by using three different output couplers, and a birefringent, single-crystal quartz plate at Brewster's angle as the intra-cavity dispersive element.

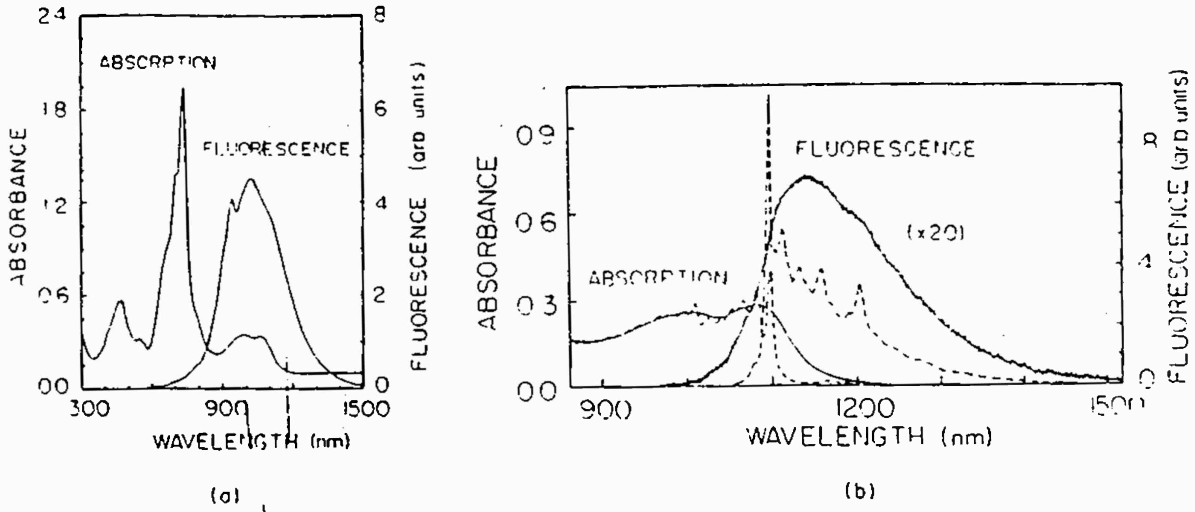

Fig. 1 Absorption and fluorescence spectra of Cr:forsterite: (a) room-temperature composite spectra showing contributions from both the optically-active centers present in the crystal (fluorescence excited by 488-nm radiation); (b) near-infrared spectra (fluorescence excited by 1064-nm radiation) attributed to transitions within the states of the 'lasing center' alone, presumed to be tetravalent chromium. All the spectra were taken for E⊥b axis of the crystal, and for excitation along the a axis. The dotted curves in (b) are taken at 77 K, while the solid curves are taken at 300 K.

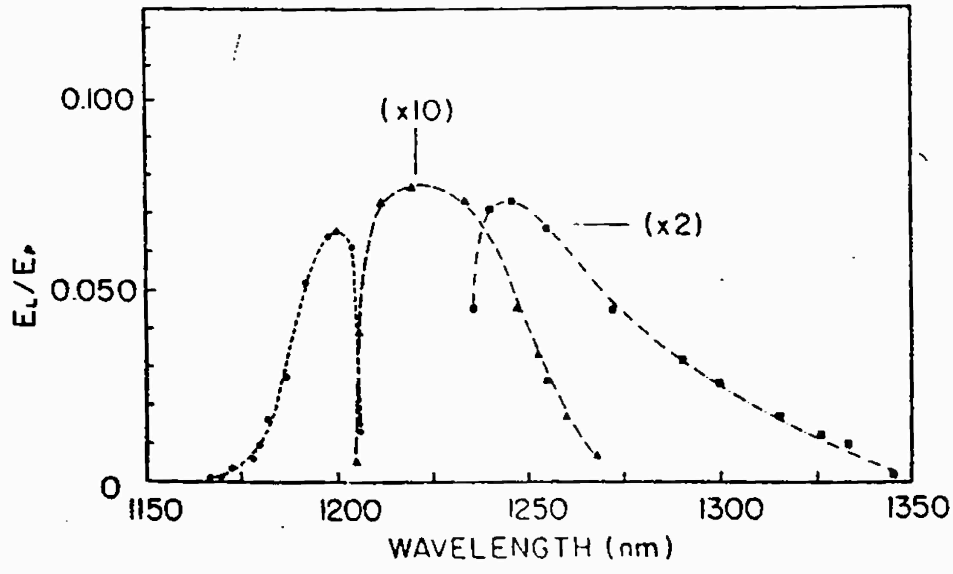

Fig. 2 The ratio of Cr:forsterite laser output (E_L) to the absorbed pump energy (E_P) as a function of wavelength. The three curves correspond to the three output couplers used in tuning measurement.

The successful cw operation and large fluorescence bandwidth of this system promise ultrashort pulse generation through mode-locked operation. Since large crystals may be readily grown, the system has the potential to be an amplifier medium in the infrared spectral region. Key spectroscopic and laser properties of Cr:forsterite are summarized in Table 1.

TABLE 1. Spectroscopic and laser properties of Cr-doped forsterite

Property	Value
Major pump bands	850-1200 nm, 600-850 nm, and 350-550 nm.
Fluorescence band	680-1400 nm
Room-temperature fluorescence lifetime	us
Cr-ion concentration	$\cdot 7 \times 10^{18}$ ions/cm^3
Lasing wavelength (center)	35 nm (pulsed)
	1.44 nm (cw)
Spectral bandwidth	~ 30 nm (pulsed)
	~ 12 nm (cw)
Slope efficiency	22% (pulsed)
	6.8% (cw)
Tuning range	1167-1345 nm
Effective emission cross section	1.1×10^{-19} cm^2

We would like to acknowledge K. Yamagishi, H. Anzai, and Y -hi of Mitsui Mining and Smelting Co., Japan for providing the crystals usc 'udy, and NASA and ARO for financial support.

References

1. J. A. Caird, S. A. Payne, P. R. Staver, A. J. Ramponi, L. L. Chase, and W. F. I. , IEEE J. Quantum Electron. 24, 1077 (1988), and references therein.
2. V. Petričević, S. K. Gayen, R. R. Alfano, K. Yamagishi, H. Anzai, and Y. Yamaguchi, Appl. Phys. Lett. 52, 1040 (1988).
3. V. Petričević, S. K. Gayen, and R. R. Alfano, Appl. Opt. 27, 4162 (1988); and Appl. Phys. Lett. 53, 2590 (1988).

8. V. Petričević, S. K. Gayen, and R. R. Alfano, "Tetravalent Chromium-Doped Forsterite Laser", **Invited** paper presented at the V International Conference on Tunable Lasers, Irkutsk, USSR, 20-23 September, 1989.

USSR ACADEMY OF SCIENCES

USSR PEOPLE EDUCATION GOVERNMENT COMMITTEE

V INTERNATIONAL CONFERENCE TUNABLE LASERS

PROGRAM

Irkutsk, USSR

September 20-22, 1989

Tetravalent Chromium-Doped Forsterite Laser

V. Petričević, S. K. Gayen*, and R. R. Alfano

Institute for Ultrafast Spectroscopy and Lasers
Departments of Physics and Electrical Engineering
The City College of New York
New York, New York 10031, U. S. A.

*Department of Physics and Engineering Physics, Stevens Institute of Technology
Hoboken, New Jersey 07030, U. S. A.

Abstract

Chromium-activated forsterite ($Cr:Mg_2SiO_4$) laser is continuously tunable over the 1167 - 1345 nm spectral range. The characteristics of laser operation and relevant spectroscopic and quantum electronic properties of the system will be reviewed.

Tetravalent Chromium-Doped Forsterite Laser

V. Petricevic, S. K. Gayen,* and R. R. Alfano

Institute for Ultrafast Spectroscopy and Lasers, Departments of Physics and Electrical Engineering
City College of New York, New York, NY 10031, U. S. A.
* Department of Physics and Engineering Physics, Stevens Institute of Technology
Hoboken, New Jersey 07030, U. S. A.

Summary

Chromium-activated forsterite ($Cr:Mg_2SiO_4$) is a new vibronic laser[1,2] with unique spectroscopic and laser properties. A number of chromium-based tunable solid state lasers[3], together with $Ti:Al_2O_3$ laser[4] span a spectral range of 660-1240 nm. $Cr:Mg_2SiO_4$ laser extends the tuning range further into the near-infrared to 1345 nm.[5] The most important feature of the tuning range of Cr:forsterite laser is that it lies in the wavelength region of zero material dispersion. This property makes Cr:forsterite very useful source for optical communications. The most interesting spectroscopic property of the Cr:forsterite crystal is that it is the first Cr-based system where the lasing center is tetravalent chromium (Cr^{4+}).

The room-temperature absorption and emission spectra of Cr:forsterite are shown in Fig. 1(a). The absorption spectrum is characterized by three broad absorption bands centered at 1050 nm, 750 nm, and 480 nm, respectively. The emission spectrum spans the 680-1400 nm spectral range. The 750-nm and 480-nm absorption bands are attributed to transitions within the states of Cr^{3+} ion. A careful study reveals that the near-infrared absorption band centered at 1050 nm, and the corresponding Stokes-shifted fluorescence, presented in Fig. 1(b), are responsible for laser action in Cr:forsterite. These absorption and emission are attributed to transitions in Cr^{4+} ion in a tetrahedrally coordinated site. The spectroscopic and theoretical evidences leading to this conclusion and the identification of this new lasing center will be presented.

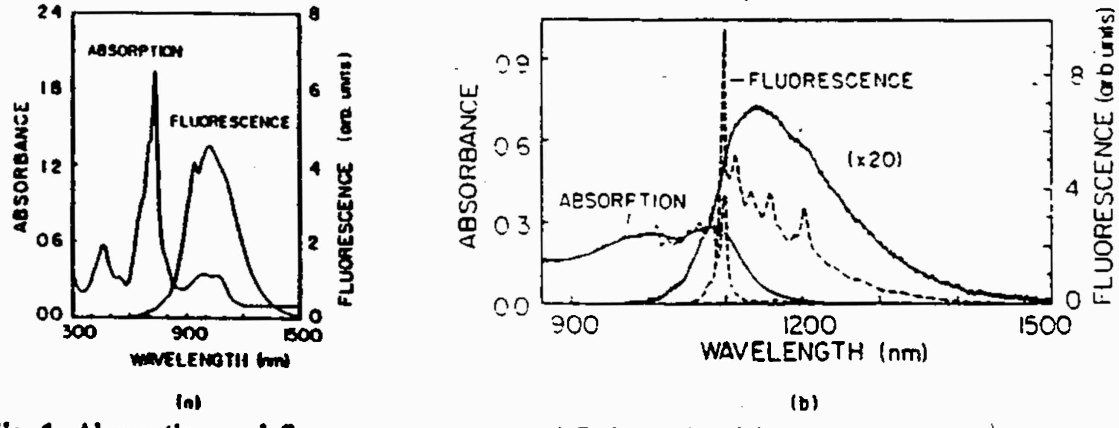

Fig. 1 Absorption and fluorescence spectra of Cr:forsterite: (a) room-temperature composite spectra showing contributions from both the optically-active centers present in the crystal (fluorescence excited by 488-nm radiation); (b) near-infrared spectra (fluorescence excited by 1064-nm radiation) attributed to transitions within the states of the Cr^{4+} ion. The dotted curves in (b) are taken at 77 K, while the solid curves are taken at room temperature.

Various modes of operation of the Cr:forsterite laser have been achieved. Room temperature pulsed laser operation for 532-nm, 630-nm, and 1064-nm pumping has been obtained[1,2] with maximum output slope efficiency of 22%. Continuous-wave operation has been demonstrated[6] for longitudinal pumping by cw 1064-nm radiation. Continuous tuning over the 1167 -1345 nm spectral range, shown in Fig. 2 has been obtained[5] by using three different output couplers and a birefringent, single crystal quartz plate at Brewster's angle as the intracavity dispersive element.

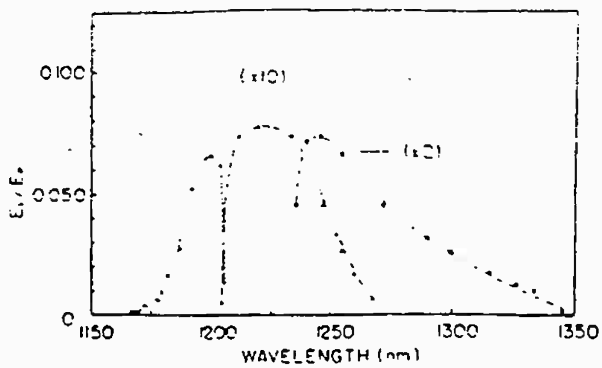

Fig. 2 The ratio of Cr:forsterite laser output (E_L) to the absorbed pump energy (Ep) as a function of wavelength. The three curves correspond to the three output couplers used in tuning measurement.

The most important spectroscopic and laser properties of chromium-activated forsterite are summarized in Table 1.

TABLE 1. Spectroscopic and laser properties of Cr-doped forsterite

Property	Value
Major pump bands	850-1200 nm, 600-850 nm, and 350-550 nm.
Fluorescence band	680-1400 nm
Room-temperature fluorescence lifetime	15 μs
Cr-ion concentration	~ 7×10^{18} ions/cm^3
Lasing wavelength (center)	1235 nm (pulsed) 1244 nm (cw)
Spectral bandwidth	~ 30 nm (pulsed) ~ 12 nm (cw)
Slope efficiency	22% (pulsed) 6.8% (cw)
Tuning range	1167-1345 nm
Effective emission cross section	1.1×10^{-19} cm^2

We would like to acknowledge K. Yamagishi, H. Anzai, and Y. Yamaguchi of Mitsui Mining and Smelting Co., Japan for providing the crystals used in this study, and NASA and ARO for financial support.

References

1. V. Petricevic, S. K. Gayen, R. R. Alfano, K. Yamagishi, H. Anzai, and Y. Yamaguchi, Appl. Phys. Lett. 52, 1040 (1988).
2. V. Petricevic, S. K. Gayen, and R. R. Alfano, Appl. Opt. 27, 4162 (1988); and Appl. Phys. Lett. 53, 2590 (1988).
3. For a list of tunable solid state lasers see J. A. Caird et. al., IEEE J. Quantum Electron. 24, 1077 (1988); For most recent results see Kaminskii et. al., Inorg. Mater., 23, 618 (1987), 23, 1700 (1988), and 24, 579 (1988).
4. P. F. Moulton, J. Opt. Soc. Am. B 3, 125 (1986).
5. V. Petricevic, S. K. Gayen, and R. R. Alfano, Appl. Opt., to be published.
6. V. Petricevic, S. K. Gayen, and R. R. Alfano, Opt. Lett., to be published.

9. R. R. Alfano, "A Chromium-Doped Forsterite Laser", **Plenary talk**, presented at the International Conference on Lasers '89, December 1989, New Orleans, Louisiana.

THE FORSTERITE LASER

R. R. Alfano

Institute for Ultrafast Spectroscopy and Lasers
Departments of Physics and Electrical Engineering
City College of New York
New York, NY 10031

Chromium-activated forsterite ($Cr:Mg_2SiO_4$) is a new chromium-based vibronic laser with unique spectroscopic and laser properties. Pulsed room temperature laser operation for 532-nm, 630-nm, and 1064-nm pumping has been obtained with output slope efficiency as high as 22 %. Free-running laser output is centered at 1235 nm and has spectral bandwidth of 30 nm. The large bandwidth promises generation of ultrashort pulses in the femtosecond range through mode-locked operation. With a single crystal quartz birefringent plate inserted in the laser cavity at Brewster's angle, and using different laser mirrors, smooth continuous tuning over the 1167-1345 nm spectral range has been achieved. This tuning range is of great technological importance for ranging, remote sensing and optical communications. Continuous-wave laser operation for longitudinal pumping by 1064-nm radiation from CW Nd:YAG laser has also been obtained. Spectroscopy of chromium-doped forsterite will be reviewed. These studies indicate that in Cr:forsterite a center other than Cr^{3+}, presumably tetravalent Cr^{4+} in a tetrahedrally coordinated site, is responsible for laser action.

This work was performed in collaboration with V. Petricevic and S. K. Gayen. The research is supported by NASA, ARO, Hamamatsu Photonics KK, and CCNY Organized Research.

Plenary talk, presented at the International Conference on Lasers '89, December 1989, New Orleans, Louisiana.

10. V. Petričević, A. Seas, S. K. Gayen, and R. R. Alfano, "Effective Gain Measurements in Chromium-Doped Forsterite", presented at the Topical Meeting on Advanced Solid-State Lasers, Salt Lake City, Utah, March 5-7, 1990.

Effective Gain Measurements in Chromium-Doped Forsterite

V. Petričević, A. Seas, S. K. Gayen* and R. R. Alfano

Institute for Ultrafast Spectroscopy and Lasers
Departments of Physics and Electrical Engineering
City College of New York, New York, NY10031
Telephone: (212) 690-6960, Fax: (212) 690-8185

*Department of Physics and Engineering Physics
Stevens Institute of Technology, Hoboken, New Jersey 07030

Summary

Chromium-doped forsterite is an important laser system for the near infrared spectral range. It operates in both pulsed[1-3] and continuous-wave[4] mode of operation. Its output can be tuned over the 1167-1345 nm range.[5]The most interesting feature that distinguishes this laser system from other chromium-based lasers is that the lasing ion is tetravalent chromium (Cr^{4+}) in a tetrahedrally coordinated site.[2,3,6]

In this work we present pump-and-probe measurements of the effective gain cross-section in chromium-doped forsterite. Results of these measurements show the effect of excited-state absorption (ESA) on laser performance of chromium-doped forsterite laser.

ESA is a critical process which impedes operation of tunable solid state lasers. It has been shown that it affects laser performance of V^{2+}-doped crystals,[7, 8] inhibits laser action in Mn^{2+}-doped crystals,[9] and limits the slope efficiency of Cr^{3+}:$Mg_3Ga_2Li_3F_{12}$ laser.[10] It is also present in alexandrite.[11] Absence of ESA is one of the most important advantages of Ti:Al_2O_3 laser.[12]

The experimental setup used to measure the effective gain cross section is shown in Fig. 1. The upper lasing level assigned to $^3T_2$ state of Cr^{4+} ion is populated by 1064-nm pump beam from the Q-switched Nd:YAG laser. The excited state is probed by a collinearly propagating probe beam. Probe beams were obtained from a tunable forsterite laser pumped by a Nd:YAG laser. Pump and probe beams were carefully overlapped and focused in the sample. The sample is a 38-mm long and 4-mm diameter rod with end faces anti-reflection coated for the 1.1-1.4 μm range. A gated boxcar integrator was used to measure the average ratio S_2/S_1, where S_2 is the signal proportional to the intensity of the transmitted probe beam and S_1 is proportional to the intensity of the probe beam before the sample.

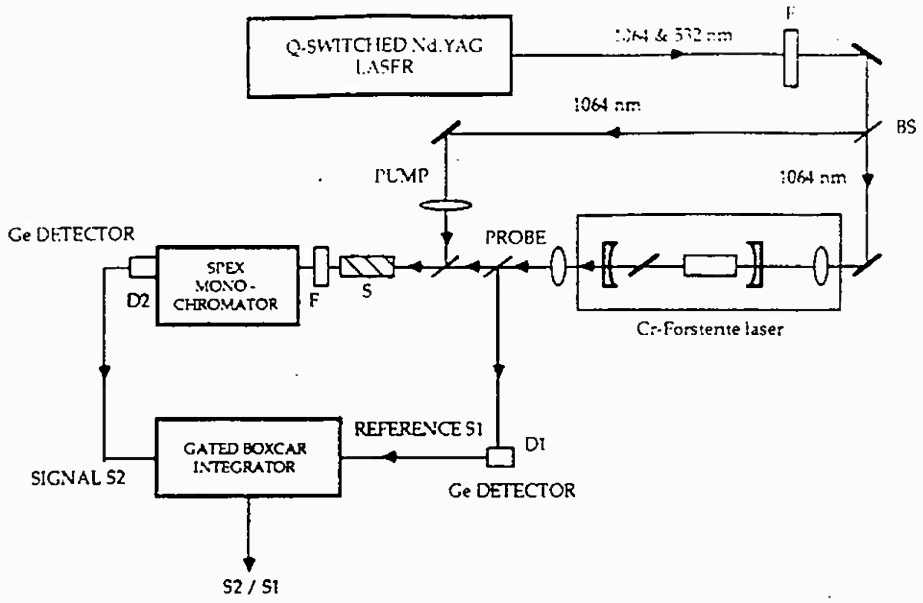

Figure 1. Experimental setup used to measure the effective gain cross-section in Chromium-doped forsterite.

The effective gain cross section is given by

$$\sigma_{EFF} = \sigma_E - \sigma_{ESA} - \sigma_G = -(1/N_E l)\ln R, \qquad (1)$$

where σ_E is the gain cross section, σ_{ESA} is the excited-state absorption cross section, σ_G is ground state absorption cross section at probe wavelength, N_E is population density of the excited state, l is length of the crystal and R is defined by

$$R = (S_2/S_1)_u/(S_2/S_1)_p. \qquad (2)$$

The subscripts u and p refer to unpumped and pumped cases, respectively. Excited-state population density (N_E) was estimated by measuring the pumped volume of the sample and the energy of the pump pulse absorbed, assuming that each pump photon absorbed creates one excited ion.

The measured effective (net) gain cross section as a function of wavelength in the 1180-1330 nm wavelength region is presented in Fig. 2 by triangles superimposed on the fluorescence spectrum. The measured values of the net gain cross section should be compared to the value of ~2 x 10^{-19} cm^2 for the peak gain cross section obtained from radiative lifetime and fluorescence lineshape measurements.[11] The close agreement between the measured effective gain cross section and the peak gain cross-section predicted using radiative lifetime and fluorescence linewidth indicates that ESA cross section is at least an order of magnitude smaller than the gain cross section.

This agreement implies that ESA is not a major loss mechanism in chromium-doped forsterite.

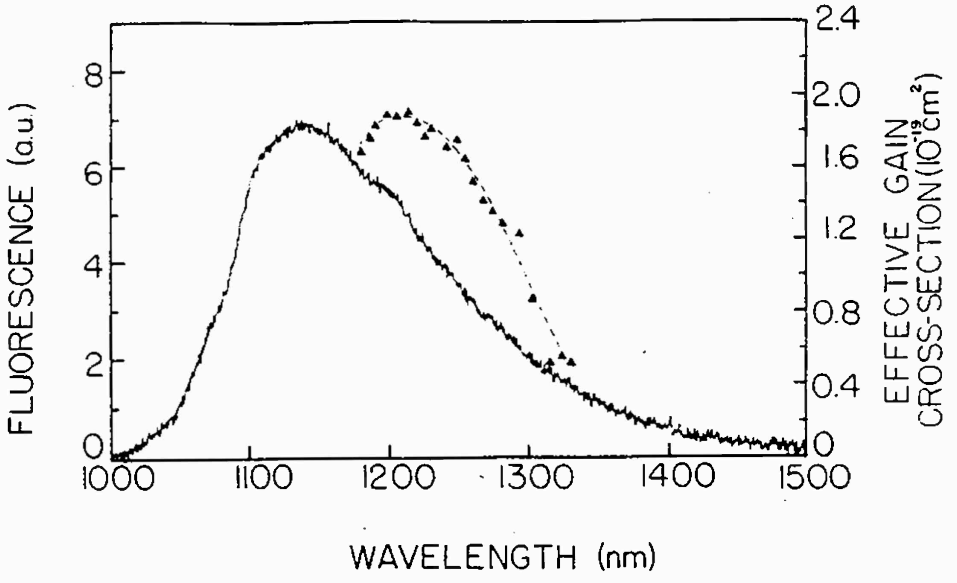

Figure 2. Fluorescence spectrum of chromium-doped forsterite for 1064-nm excitation (solid line) and effective gain cross-section (triangles and broken line).

Research is supported in part by ARO and NASA.

References:

1. Petričević, S. K. Gayen, R. R. Alfano, K. Yamagishi, H. Anzai, and Y. Yamaguchi, Appl. Phys. Lett. **52**, 1040 (1988).
2. V. Petričević, S. K. Gayen, and R. R. Alfano, Appl. Phys. Lett. **53**, 2590 (1988).
3. H. R. Verdun, L. M. Thomas, D. M. Andrauskas, T. M. Collum, and A. Pinto, Appl. Phys. Lett. **53**, 2593 (1988).
4. V. Petričević, S. K. Gayen, and R. R. Alfano, Opt. Lett. **14**, 612 (1989).
5. V. Petričević, S. K. Gayen, and R. R. Alfano, Appl. Opt. **28**, 1609 (1989).
6. V. Petričević, S. K. Gayen, and R. R. Alfano, to be published in the OSA Proceedings of the Topical Meeting on Tunable Solid-State Lasers, Cape Cod, Massachusets, May 1-3, 1989.
7. R. Moncorge and T. Benyattou, Phys. Rev. B **37**, 9177 (1988).
8. S. A. Payne, L. L. Chase, and G. D. Wilke, Phys. Rev. B **37**, 998 (1988).
9. R. Clausen and K. Petermann, IEEE J. Quantum Electron. **24**, 1114 (1988).
10. J. Caird, S. A. Payne, P. R. Staver, A. J. Ramponi, L. L. Chase, and W. E. Krupke, IEEE J. Quantum Electron. **24**, 1077 (1988).
11. M. L. Shand and J. C. Walling, IEEE J. Quantum Electron. **QE-18**, 1152 (1982).
12. P. F. Moulton, J. Opt. Soc. Am. B **3**, 125 (1986).

11. A. Seas, V. Petričević, and R. R. Alfano, "Transient Gain Measurements of Nonradiative Dynamics in Chromium-Doped Forsterite (Cr^{4+}:Mg_2SiO_4)", presented at the Optical Society of America 1990 Annual Meeting, Boston, Massachusetts, November 4-9, 1990.

1990

Optical Society of America Annual Meeting Technical Digest

Summaries of papers presented at the Annual Meeting of the Optical Society of America

November 4–9, 1990
Boston, Massachusetts

Conference Edition

Optical Society of America
2010 Massachusetts Ave., NW,
Washington, DC 20036
(202) 223-8130

TuXX

Tuesday AFTERNOON
November 6, 1990
4:45pm BALLROOM B

Symposium on Instrumentation

James C. Wyant, *Wyko Corporation, Presider*

4:45pm (Invited)

TuXX1 Acousto-optical spectrometers

V. I. Pustovoit
USSR State Committee for Product Quality Control and Standards, 9 Leninsky Prospect, Moscow 117049, USSR

We describe an acousto-optical spectrometer consisting of a Bragg cell made of single-crystal quartz. Spectral range of 420–780 nm and resolution of 0.2 nm is achieved. Applications in the monitoring of plasma-assisted material treatment are described.

5:15pm

TuXX2 Power-spectrum measurements using radial shearing interferometry

Ronald J. Sudol and Robert K. Jungquist
AMS Division, B-65 Research Laboratory, Eastman Kodak, Rochester, New York 14650-1813

A common-path radial-shearing interferometer is examined for its ability to measure the power spectrum of an object's intensity transmittance. For an object illuminated with spatially incoherent light, it is shown that the contrast of the intensity distribution observed at the interferometer's output contains a cosine transform of the object's intensity transmittance. From a coherence theory point of view, this manifestation is shown to be the result of a direct mapping between the object's frequency spectrum and the coherence properties of the interfering beams. Alternatively, when one considers the system impulse response, each point in the object is found to produce a set of cosinusoidal fringes whose frequency is directly related to that object point. The subsequent incoherent summation over the object results in an interference pattern that contains a bias term plus the transform of the object's intensity transmittance. Experimental results obtained for standard objects such as circular apertures and Ronchi rulings compare favorably with theoretical predictions.

5:30pm

TuXX3 A Fourier-transform spectrometer for the visible and UV region based on laser-diode interferometric control

Geert Wyntjes, James Engel, David Carlson, and Rick Dorval
OPTRA, 66 Cherry Hill Drive, Beverly, Massachusetts 01915

We describe the design and preliminary performance of a Fourier transform spectrometer (FTS) built to operate in both the visible and UV regions. Conventional FTS instruments have generally been restricted to use in the IR because of the difficulties in providing sufficiently precise control of the mirror velocity and alignment. We are building an FTS, which uses a laser-diode source, in which both mirror motion and alignment are dynamically controlled on the basis of interferometric signals. By using a multiphase detection technique, we are able to make interferometric measurements with /768 precision at a 5 MHz update rate. These data are used to servocontrol the mirror velocity and alignment to better than 0.01% and 1 radian respectively. This degree of control, combined with optics that are good to /40 in the visible-light spectrum, make it possible to attain spectral resolution in the visible and near-UV regions that is limited only by radiometric noise considerations.

5:45pm

TuXX4 Complex homodyne laser-diode velocimeter

Geert Wyntles and Michael Hercher
OPTRA, 66 Cherry Hill Drive, Beverly, Massachusetts 01915

We describe a laser Doppler velocimeter based on a single illuminating beam from a laser diode and employing a complex homodyne detection system. Conventional laser Doppler velocimeters are based on the detection of light scattered by particles that traverse a region illuminated by intersecting laser beams. Performance is generally improved, particularly in low-velocity applications, by means of heterodyne detection (the intersecting beams differ in optical frequency by the heterodyne frequency). The system we describe is compact and achieves precise and unambiguous measurements through the use of a complex homodyne technique. In this technique we make simultaneous measurements, updated at 5 MHz, of three interferometric signals whose phases differ by 120. These data are processed in real time to provide a linear output of unwrapped phase, whose derivative is proportional to velocity. The sample volume is illuminated by a single beam, and a complex spatial filter is used to generate the three, differently phased interferometric signals. We describe the theoretical basis for the measurement, the sensor design, and a variety of data obtained from both fluids and diffusely scattering surfaces.

TuYY

Tuesday AFTERNOON
November 6, 1990
5:00pm BALLROOM A

Ultrafast Spectroscopy

R. R. Alfano, *City College of New York, Presider*

5:00pm

TuYY1 Transient gain measurements of nonradiative dynamics in chromium doped forsterite (Cr^{4+}:Mg_2SiO_4)

A. Seas, V. Petricevic, and R. R. Alfano
Institute for Ultrafast Spectroscopy and Lasers, Departments of Physics and Electrical Engineering, City College of New York, New York 10031

The gain dynamics of photoexcited chromium-doped forsterite (Cr^{4+}:Mg_2SiO_4) were measured by means of a pulsed excite-and-probe technique. The nonradiative relaxation time within the 3T2 vibronic state was determined by measuring the change in the induced gain of the probe pulse as a function of the pumpprobe delay. A 30 ps, 1.064 m pulse from a mode-locked Nd:YAG laser was split into two beams. The first beam provided the pump pulse to populate the 3T2 manifold. The other beam was focused in a calcite crystal to generate a 1.2 m probe pulse by means of stimulated Raman scattering. The transient gain was determined from the measured ratio of the transmitted probe intensity for unpumped and pumped cases as a function of the pumpprobe delay. The rise time (time for growth of the gain from 10% to 90%) was calculated to be 50 ps. A rate-equation analysis of population in the various states was used to extract a value for the vibrational relaxation time from the experimental data under the assumption of Gaussian pump and probe pulses. The best fit to the experimental data of gain as a function of time yields a value of 10 5 ps for the intra-3T2-state vibrational relaxation time.

This research is supported by the Army Research Office.

5:15pm

TuYY2 Picosecond infrared spectroscopy using a regenerative amplifier

T. M. Jedju, I. Rothberg, and M. Roberson
AT&T Bell Laboratories, 600 Mountain Avenue, Murray Hill, New Jersey 07974

An apparatus for doing picosecond, narrowband infrared spectroscopy is presented. The procedure, based on a 540 Hz regenerative amplifier, uses a gated up-conversion technique. Spectral resolution of 1 cm^{-1} is achieved by difference-frequency mixing the output of a narrowband, sync-pumped, grating dye laser, which is pumped by residual light from the regenerative amplifier, with 532 nm laser light in $LiIO_3$. The output is nar-

12. S. G. Demos, J. Buchert, and R. R. Alfano, "Nonequilibrium Phonon Dynamics in Forsterite", presented at the Optical Society of America 1990 Annual Meeting, Boston, Massachusetts, November 4-9, 1990.

piezoelectric fields on the order of 10^4–10^5 V/cm.[1,2] These fields lead to interesting nonlinear optical effects, which can depend on the density of free carriers. At low carrier density, there is an effect of the piezoelectric fields on the nonlinear susceptibilities due to parity mixing of the levels: $[\chi^{(2)}]$, and due to piezoelectric field-driven changes in the carrier dispersion relations: $[\chi^{(3)}]$. In an SLS, grown on a buffer layer intermediate in concentration between the two active epilayers, we use a transfer matrix technique[3] to obtain dispersion relations for the superlattice and an exact superlattice wavefunction. This is done within a single band model with momentum mixing of the bands due to zone-folding considered. Using these results we calculate $\chi^{(2)}$ and $\chi^{(3)}$ for a CdTe/ZnTe SLS. We find $\chi^{(2)} \sim 10 \times$ bulk GaAs. A large $\chi^{(3)}$ results because of electric field modulated band nonparaboliticity in the SLS. We find $\chi^{(3)} \sim 60 \times$ bulk GaAs. The level broadening in the minibands demonstrates a strain-induced Franz–Keldysh effect in this system, whose explicit form varies with electric field. Finally, we consider the effect of screening on $\chi^{(3)}$ as a function of carrier density.

References

1. D. L. Smith, Sol. St. Communications 57, 919 (1986).
2. D. L. Smith and C. Mailhot, Phys. Rev. Lett. 58, 1264 (1987).
3. S. A. Jackson, to be published.

2:45pm

WJ6 Second-order optical susceptibilities in asymmetric quantum wells

S. J. B. Yoo, M. M. Fejer, R. L. Byer, and J. S. Harris, Jr.*

Edward L. Ginzton Laboratory, Stanford University, Stanford, California 94305

Recently, there have been extensive studies of intersubband transitions. The large oscillator strengths of transitions between subbands of quantum wells[1] have led to investigations of their application to lasers, detectors and nonlinear optical devices. In this paper, we discuss the extremely large second order optical susceptibility $[\chi^{(2)}]$ predicted and observed[2] in structures with inversion symmetry broken through external electric fields or compositional asymmetry. Second order susceptibility of the quantum well system is obtained by solving effective mass Hamiltonian in the conduction band. The large oscillator strengths and relatively narrow linewidths lead one to expect large . Experimental measurements of $\chi^{(2)}$ have been obtained for second harmonic generation over the tuning range of CO_2 laser in both electric field biased and compositionally asymmetric modulation doped structures, resulting in 28 nm/V and 100 nm/V near resonance, respectively. These are extremely large compared to $\chi^{(2)}$ of bulk GaAs, for example, which is 0.38 nm/V at similar wavelengths. In actual frequency conversion devices, the strong absorption at resonance adversely affects efficiency, which ultimately depends on the ratio of $\chi(2)$ to absorption. We discuss the design of quantum well devices for large conversion efficiency.

Stanford Electronics Laboratory, Stanford University.

References

1. L. C. West and S. J. Eglash, App. Phys. Lett. 46, 1156 (1985).
2. M. K. Gurnick and T. A. DeTemple, IEEE J. Quantum Electron. QE-19, 791 (1983); M. M. Fejer, S. J. B. Yoo, R. L. Byer, A. Harwit, and J. S. Harris, Jr., Phys. Rev. Lett. 62, 1041 91989).

3:00pm

WJ7 Optically induced and charge-transport-assisted electroabsorptive and electro-optic nonlinearity in cadmium telluride

Mehrdad Ziari and William H. Steier

Center for Photonic Technology, Department of Electrical Engineering, University of Southern California, Los Angeles, California 90089-0483

We have observed the optically triggered formation of a high electric field region underneath the negative electrode. The optical control of the magnitude and the position of this field build-up, typically 10 to 20 times the applied field, combined with the electro-optic or the Franz–Keldysh effect, provides a novel large optical nonlinearity. The high field region (0.1–0.2 mm wide) forms in few microseconds upon illumination by below bandgap light (860–900 nm) and persist in the dark with a latch time of 2–5 s. This effect is highly sensitive, requiring approximately 10 nJ/cm^2 absorbed fluence, and exhibits an intensity and applied voltage dependent response time. Furthermore, this high field can be erased by illuminating the region through ITO electrodes with near bandgap light (835-nm GaAs laser diode). This field buildup and erasure can be used in a variety of device configurations (one- or two- dimensional arrays, self switching or two wavelength schemes) for opto-optical switching and spatial light modulation applications. These devices can benefit from the large electro-optic coefficient of CdTe (5–6 pV/m) for high contrast polarization switching, or taking advantage of the high electric fields, use the observed Franz–Keldysh electro-absorption which provides large absorption and the associated refractive index changes.

WK Wednesday AFTERNOON, November 7, 1990, 1:30pm, BALLROOM B

Ultrafast Optical Phenomena: 1

Arthur Smirl, *University of Iowa, Presider*

1:30pm

WK1 Ultrafast opto-optic switching

Sushrut Mehta, Philippe Fauchet, and Kais Gzara

Department of Electrical Engineering, Princeton University, Princeton, New Jersey 08544

We present a design for an ultrafast optically driven optical switch capable of subpicosecond switching and recovery times. The switch essentially consists of a phased array in which the phase of the light emitted by each element of the array is optically controlled. The distribution of the far field diffraction pattern from such an array can be varied considerably by altering the phase distribution of the array. The extremely short switching times are obtained by utilizing the optical Stark effect, which involves only virtual transitions, and there are no real carriers to restrict recovery times. The switch is also found to be extremely robust against noise as well as partial failure.

1:45pm

WK2 Nonequilibrium phonon dynamics in forsterite

S. G. Demos, J. M. Buchert, and R. R. Alfano

Institute for Ultrafast Spectroscopy and Lasers, City College of New York, Convent Avenue at 138 Street, New York, New York 10031

Phonon dynamics in photoexcited Forsterite—a new tunable solid state laser—has been studied by time resolved spontaneous Raman scattering following absorption in $^3T_2$ electronic state. High rate of photoexcitation by 400 fs pulses are responsible for creation of nonequilibrium phonon population in the excited state. Phonons are generated by relaxation of the photoexcited electrons in the excited state. The finite relaxation time of phonons and strength of electron-phonon interactions produces the observed high nonequilibrium distribution during the short time after excitation. The short pulse measures the hot phonons while the longer pulses measure overall phonon population. These measurements give direct information on which nonradiative process and which phonons are involved in the relaxation of photoexcited ions in electronic state. For shortest pulse of 400 fs the 220-cm^{-1} mode appears to be coupled with photoexcited tetravalent chromium Cr^{4+} showing the nonequilibrium distribution.

This work is supported by the Army Research Office.